Differential proteomics and early neuronal differentiation of MEHMO patient-derived iPSCs

Dissertation

zur Erlangung des Grades eines

Doktors der Naturwissenschaften

der Mathematisch-Naturwissenschaftlichen Fakultät

und

der Medizinischen Fakultät

der Eberhard-Karls-Universität Tübingen

vorgelegt

von

Maíra Bertolessi Lourenço

aus São Paulo, Brasilien

Oktober - 2016

Tag der mündlichen Prüfung: 10.03.2017

Dekan der Math.-Nat. Fakultät: Prof. Dr. W. Rosenstiel

Dekan der Medizinischen Fakultät: Prof. Dr. I. B. Autenrieth

1. Berichterstatter: Prof. Dr. Stefan Liebau

2. Berichterstatter: Prof. Emeritus Dr. H.-J. Wagner

Prüfungskommission: Prof. Emeritus Dr. H.-J. Wagner

Prof. Dr. Stefan Liebau

Prof. Dr. Guntram Borck

PD Dr. Meltem Avci-Adali

Declaration

I hereby declare that I have produced the work entitled “Differential proteomics and early neuronal differentiation of MEHMO patient-derived iPSCs”, submitted for the award of a doctorate, on my own (without external help), have used only the sources and aids indicated and have marked passages included from other works, whether verbatim or in content, as such. I swear upon oath that these statements are true and that I have not concealed anything. I am aware that making a false declaration under oath is punishable by a term of imprisonment of up to three years or by a fine.

Tübingen, ...

Date Signature

Acknowledgements

I would like to express my special appreciation and admiration to Prof. Dr. Stefan Liebau, a dream supervisor, who always supported and guided me, trusting my judgment and allowing me the freedom to pursue any aspect I considered relevant in this research project. My sincere thanks to my journey friends Jasmin Haderspeck, Kevin Achberger, Moritz Klingenstein and Stefanie Raab who were always supportive and patient, especially when life or lab wanted to drag down my mood. I need to thank the generous supervision of Dr. Leonhard Linta, who tirelessly support me with brilliant insights and discussions throughout these years. To all advisory board members: Prof. Emeritus Dr. H.-J. Wagner and Dr. Johannes Gloeckner, I want to express my appreciation for their accessibility and fruitful discussions. The whole process of sample preparation and analysis for SILAC was just possible thanks to the kind assistance and guidance of Felix von-Zweydorf and Dr. Johannes Gloeckner. I also want to show my gratitude to Sabine Conrad, whose experience and advices were fundamental to accomplish the high-throughput gene expression analysis. I need to thank my friend and technical assistant Clara Misbah, who makes daily life in lab easy-going and always brings along a smile and an atmosphere of kindness. My thanks to Prof. Dr. Guntram Borck (Ulm University – Germany) and Dr. Thomas Dever (National Institutes of Health - USA) who gave me the opportunity to work with this intriguing and fascinating topic, which they master. I am deeply indebted to the generosity of all those who donated plucked hair samples, and without whom this research would not be possible. At last, but not least, my sincere gratitude and love to my husband Thomas and his family, to my beloved family and friends by their support and understanding of being so far away from home.

Summary

The eukaryotic initiation factor 2 (eIF2) is a protein complex which is part of the cellular translation machinery. eIF2 comprises three subunits (α, β, γ), the γ subunit being the one which contains a GTP-binding domain and binding sites for the other two subunits α and β to interact. eIF2 acts in the initial part of the protein synthesis, forming a complex with GTP and Met-tRNA$^{Met}_{i}$. This ternary complex associates itself with the 40S subunit of the ribosome and, in a cap-dependent manner, scans the mRNA with the help of other factors. The recognition of the first AUG codon leads to the final assembly of the ribosome and the translation of the protein. Due to eIF2 importance, mutations in highly conserved regions of their genes might be lethal; however, a *EIF2S3* mutation was recently found to be responsible for intellectual disability in male patients. In those patients, signs of problems in nervous system development are accompanied by a broad spectrum of other symptoms such as obesity, microgenitalism and ataxia gait, a syndrome known as MEHMO. This finding has motivated the present study in investigating why function disruption in a central player of protein translation mainly impacts on nervous system development. Patient-derived iPS cells were generated, and served as the model to learn more about eIF2, its impact on the cell proteome and its function in early neuronal development. The global translation profile from the iPSCs was obtained by SILAC-based LC-MSMS analysis, and the expression of candidate genes was assessed in a high-throughput manner at different time points of neuronal differentiation. A specific increase in APOE and CRABP1 (retinoic acid related proteins) translation and transcription was observed in patient cells, whereas CBS and TKT protein levels were decreased. Interestingly, other genes correlated to translation regulatory mechanisms were also differentially expressed. All this data indicates an imbalance of survival/apoptotic pathways activation due to translational impairment. Although the present results need further confirmation, this alteration on translation rates (iPSCs) suggests a very early embryonic development effect of the mutation. The findings on altered candidate proteins/mRNAs might open new avenues for future research. This hopefully will contribute to the understanding of both, the eIF2S3 roles so far not described and the exact functional consequences of the mutation.

Contents

1. Background

1.1. Protein synthesis

1.1.1. Importance of protein synthesis regulation

Apart from non-coding RNA (e.g. ribosomal RNA, tRNA and miRNA), proteins are the ultimate product of gene expression. On the one hand, proteins delineate the broadly variable cell shape by forming the membrane, the cytoskeleton and the extracellular matrix. On the other hand, they act on intra and extra-cellular communication through diverse signaling pathways coordinating countless processes, such as biosynthesis, cellular growth, division, differentiation, catabolism and apoptosis. Thus, the cellular proteome pattern is constantly being adjusted in response to intrinsic and extrinsic signals to maintain homeostasis and activate various cellular processes. This continuous control of protein levels is accomplished by several regulatory mechanisms that range from epigenetic gene silencing to multiple transcription factor networks, thereby regulating gene expression. Moreover, protein levels are determined by its degradation rates that, in mammals, occurs mainly via ubiquitin and lysosomal-mediated proteolysis.

A cell proteome is finally governed by controlled transcript translation. Due to the importance of protein balance and to the high energy consumption involved in protein synthesis, it is logical that mRNA translation is tightly regulated and can be aborted, especially in its initial phase to avoid energy misuse.

Localized translation is a good example of the protein translation regulation significance for certain cellular needs. The long distance transport of mRNA in highly polarized cells (e.g. neurons) enables a localized, and rapid translation in response to distinct stimuli. In this way, on-site translation is able to avoid protein degradation during its transport and unintended signaling modulation, since the same protein can fulfil different functions in different cellular regions. Besides that, the localized protein translation permits a finer spatial control of its concentration. Another recent and interesting example of the importance of regulation during translation is the finding that protein levels during mitosis are mainly governed by changes in translation, rather than changes in transcription (Tanenbaum et al.,

2015).

1.1.2. Eukaryotic translation initiation modes

The first proposed mechanism for eukaryotic translation initiation refers to the scanning feature of the ribosome, and to a gain in mRNA ribosomal recognition through the 7-methylguanosine bound to mRNA 5´end (5´cap structure) (Kozak, 1978). This mechanism, later known as cap-dependent initiation (canonical initiation), was probably first identified due to its expressive efficiency, when compared to other mechanisms so far described. Although the canonical initiation mechanism elucidated many issues, such as higher translation rates for mRNA presenting cap structures, it could not cover many other concerns that started to be unveiled with the development of the field, now provided with mass spectrometry and high-throughput sequencing technology, for instance.

The classical view of a mature eukaryotic mRNA having one unique coding sequence (CDS), and being therefore monocistronic, has been recently challenged (Mouilleron et al., 2016). The substantial number of evidences collected by the authors also raises the question whether the usual 100 codons cut-off, which classifies an ORF (open reading frame) as CDS, would not exclude physiological relevant “short” coding alternative ORFs located upstream and/or downstream to the CDS, or even overlapping with it.

The canonical model for initiation would be incompatible with polycistronic eukaryotic mRNAs, as the scanning ribosome would preferentially start at the first alternative coding ORF translation over the CDS. Therefore, as a result of the diversity of transcripts, which can encode more than one polypeptide, several efforts have been made in order to explain this apparent incongruity, and new translation initiation mechanisms have been described.

Leak scanning, for example, clarifies how a second start codon (from CDS) is preferred to the first start codon from an upstream open reading frame (uORF). In principle, a transcript comprising a weak Kozak sequence context around the first uORF start codon allows the ribosome to bypass the first uORF (Kozak, 2002).

Another version of translation initiation (also called reinitiation), which likewise refers to the presence of uORF, interferes in the efficiency of downstream CDS

translation inasmuch as it can hamper new formation of the translation machinery following uORF termination. This CDS translation regulation performed by reinitiation depends, among other aspects, on uORF length, its position in relation to CDS start codon and the availability of activated ternary complexes to reinitiate the translation process. Factors such as the particular/specific secondary structure of each transcript, might also play important roles for uORF regulation. Thus, to define a unique formula for reinitiation in different transcripts is, so far, unrealistic (Wethmar, 2014).

An additional intricate example of a translation mechanism is the one proposed for the human core histone 4 (H4) (Martin et al., 2011). Extremely relevant for chromatin replication and gene regulatory processes, the eukaryotic canonical histone genes are replication dependent, intronless and their transcripts lack polyadenylation (Marzluff, 2005). The absence of polyadenylation at the transcript 3´end and the presence of a short 5`UTR would, in principle, hinder formation of the mRNA closed loop, thereby avoiding the described canonical scanning mechanism. However, H4 mRNA presents secondary structures which, resembling internal ribosome entry sites (IRESs), attracts the ribosome to the 5´AUG.

Also part of the translation initiation mechanisms repertoire is the cap-independent translation. In this process, the very mRNA nucleotide sequence itself is determinant for the formation of secondary structures capable of attracting the translational machinery, the previously mentioned IRESs.

Although in both, IRES-mediated and H4 mechanisms, secondary structures recruit the ribosome in a cap-independent way, H4 elongation further demands binding of eIF4E and the cap-structure (Martin et al., 2011). Additionally, the IRES-mediated translation mode, also called internal initiation, does not require an eIF4F complex and therefore its efficiency, normally low, is increased in conditions where eIF4F is down regulated (e.g. infection, inflammation and other processes triggered by stress) (Johannes et al., 1999). It is still worth mentioning that this mechanism is focus of much debate, and unlike it happens with viral mRNA, the existence of IRES in cellular mRNA is not a consensus (Merrick, 2004).

Finally, the diversity in mature mRNA along with the absence of a universal mode

for translation initiation illustrates the complexity of the regulatory mechanisms coordinating protein synthesis in eukaryotic cells. Although cellular mechanisms for regulation of protein synthesis has being studied for decades, many aspects of translation in different cell types and physiological states are still to be uncovered.

1.1.3. Canonical eukaryotic translation initiation

The eukaryotic translation is classically divided into three phases; namely: initiation, elongation and termination. Initiation is the phase in which most of the factors participate, probably because it is in this stage that protein synthesis can be regulated, in an energy saving mode, avoiding unnecessary translation initiation and proteolysis.

The canonical translation initiation is characterized by 43S pre-initiation complex assembly, in which the 40S ribosomal subunit binds activated eIF2 (GTP-bound) carrying methionylated initiator tRNA (Met-tRNA$^{Met}_i$) and several other eukaryotic factors (eIF3, eIF1A, eIF1, eIF5) that support both complex stability and start codon fidelity (Maag et al., 2006; Nanda et al., 2013; Sokabe and Fraser, 2014).

In the 1970s, the necessity for assembling ternary complex (eIF2-GTP- Met-tRNA$^{Met}_i$) and other factors to 40S ribosomal subunit before binding the transcript, was already recognized (Safer et al., 1978). Still, in the same study, the authors observed that the recruitment of the ribosome to mRNA must be the rate-limiting step of translation (Safer et al., 1978), evoking the regulatory role this step should have in controlling levels of protein synthesis, as mentioned earlier.

Following pre-initiation complex formation, its attachment to mRNA 5´-end is guided by another set of initiation factors (eIF4F, eIF4B, eIF3 and PABP) that fulfil new functions, such as cap-binding, unwinding of mRNA secondary structures, and bridging of transcript 5´-end to poly-(A) tail in order to form a “closed loop”. PABP is still believed to contribute to ribosome recycling and tethering of eIF4F to the cap structure (Jackson et al., 2010). Once the 43S pre-initiation complex is bond to the transcript, the Met-tRNA$^{Met}_i$ anticodon, present in the peptidyl-tRNA binding site of the small ribosomal subunit, is consecutively inspecting the mRNA sequence, scanning for the start codon (AUG). AUG recognition triggers GTP (eIF2-bond) hydrolysis in a reaction promoted by eIF5. The subsequent

displacement of initiation factors succeed and binding of the larger ribosomal subunit (60S) takes place to form the 80S functional ribosome machinery (Figure 1).

A ribosome harbors the catalytic center, wherein protein synthesis effectively occurs. Its structure consists of three t-RNA sites or EPA, abbreviation of: Exit, Peptidyl-tRNA binding and Aminoacyl-tRNA binding sites. The A-site accommodates the next codon to be paired with the selected charged tRNA anticodon. The peptide bond formation occurs between A-site located amino group and the ester group placed on P-site. Posteriorly to peptide bond formation, the growing peptide chain, before attached on peptidyl-tRNA, moves to the A-site tRNA and the ribosome translocates. Thereby, discharged t-RNA moves to the E-site, from where it exits the ribosome.

The amino acid polymerization, or elongation phase, described above proceeds towards the 3´end of the transcript. Translation termination is marked by stop codon (UAA, UAG, and UGA) recognition, when release factors bind to the ribosomal A-site, releasing the new synthetized protein and disassembling the ribosome subunits. Dever and Green, 2012 provide a detailed discussion about elongation and termination mechanisms, as well as about involved factors and recycling aspects of translation (Dever and Green, 2012).

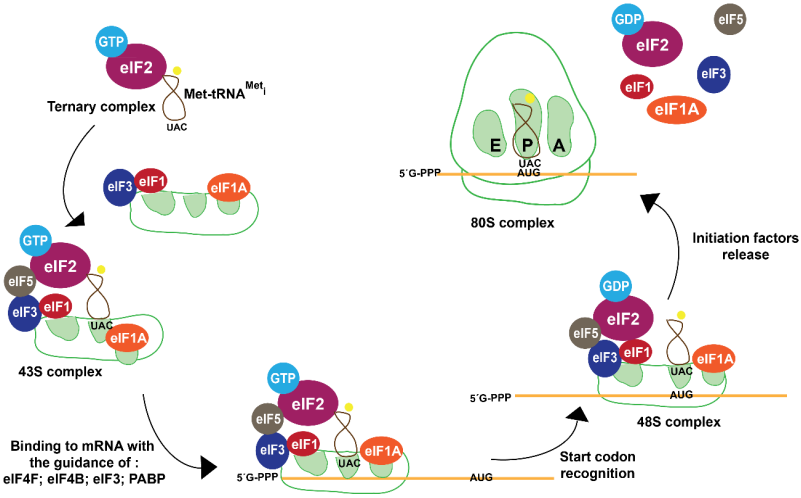

Figure 1. Canonical Eukaryotic Translation Initiation. Simplified scheme of the canonical eukaryotic translation initiation steps: Translation is initiated by activation of eIF2 (GTP-bound). The formation of the ternary complex is completed by binding of Met-tRNA$^{Met}_{i}$, which is then able to bind to 40S ribosome subunit together with eIF1, eIF1A, eIF3 and eIF5 to form the 43S pre-initiation complex. Attachment of the 43S complex to the transcript is accomplished as a result of binding of the eIF4 complex, eIF4B, eIF3 and PABP. Thus, the formed complex is able to scan for the start codon, and the latter recognition triggers binding of 60S ribosome subunit, thereby constituting an elongation competent machinery.

1.1.4. eIF2 heterotrimeric complex

Purified over 40 years ago, eIF2 was identified together with Met-tRNA$^{Met}_{i}$ and GTP as being part of a pre-initiation complex, later termed ternary complex (Gupta et al., 1973; Levin et al., 1973), and over all those years various aspects of eIF2, such as partners interactions, activity regulation and targeted pathways have been deeply investigated.

Consisting of three distinct subunits; i.e., eIF2S1 (eIF2α), eIF2S2 (eIF2β) and eIF2S3 (eIF2γ), the eukaryotic initiation factor 2 has been conserved throughout evolution, fact that supports its relevance in translation. Furthermore, presence of eIF2S1 and eIF2S2 subunits has been shown to be essential for life, while particular mutations on eIF2S3 generate infertile mice and a mental retardation syndrome in humans (Borck et al., 2012; Heaney et al., 2009; Matsubara et al.,

2015; Scheuner et al., 2001). It is noteworthy to mention that mice carry two eIF2S3 homologues and that the X homologue can apparently compensate for the absence of Y chromosome encoded eIF2S3, by generating fertile mice (Yamauchi et al., 2016). Thus, if a more aberrant phenotype, such as embryonic lethality and neuronal impairment, was not observed in mice (Matsubara et al., 2015), does not necessarily mean that a complete deletion (of both X and Y gene homologues) or a double mutation would not cause severe consequences.

The solved crystallographic structure of an eIF2 homologous factor, the archaeal aIF2 complex (Stolboushkina et al., 2008; Yatime et al., 2007) revealed for its subunit 3 a structure-function relation which elucidates previous findings of biochemical assays. Considered to be the complex core, subunit 3 of aIF2 interacts with the other two subunits, which do not seem to bind themselves (Schmitt et al., 2002; Yatime et al., 2006). Nevertheless, human eukaryotic binding assays (Rajesh et al., 2008; Suragani et al., 2005) show that all the three subunits interact with each other, revealing a more complex regulatory network for human factors in comparison to its orthologue.

Playing a central role in the canonical translation initiation, eIF2 subunits possess interesting features which confer them the ability to both promote and restrict canonical translation initiation, depending on environmental conditions. eIF2S3 is a guanine nucleotide binding protein, cycling from inactive (GDP-bound) to active (GTP-bound) states. In its active state, eIF2 is able to anchor Met-tRNA$^{Met}_{i}$, forming this way the ternary complex (Figure 2) (Kapp and Lorsch, 2004). This activation is therefore expected to be regulated, due to its consequential role in protein synthesis control.

The GDP-GTP switch is catalyzed by another translation factor, named eIF2B, and the control of this catalysis is done by a group of eIF2S1 kinases. The mammalian kinases HRI, PKR, PERK, and GCN2 are able to phosphorylate Ser51 residue of eIF2S1 in response to heme deficiency, viral infections, ER stress and amino acid deprivation, respectively (Donnelly et al., 2013). This phosphorylation produces a significant increase in affinity between the eIF2S1 and the eIF2B regulatory subcomplex (α, β and δ subunits). The phosphorylated eIF2S1 Ser51 (phospho-eIF2S1) acts as a competitive inhibitor for eIF2B, impairing the latter guanine nucleotide exchange factor role, thereby precluding

protein synthesis (Figure 2) (Krishnamoorthy et al., 2001; Nika et al., 2001).

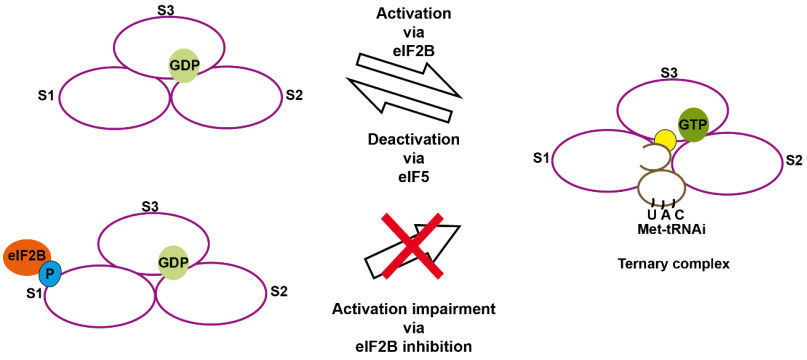

Figure 2. Ternary complex formation. eIF2 activation switches from GDP to GTP binding mode, by the action of a GTP exchange factor (eIF2B). Upon start codon recognition, GTP hydrolysis takes place via eIF5, deactivating and recycling eIF2. Regulation of eIF2-GTP levels is accomplished by eIF2S1 phosphorylation, which in this form, has a higher affinity to eIF2B, hampering its GTP exchange role.

For the purpose of investigating additional eIF2 post-translational modification sites, aside from eIF2S1 Ser51, that could act as regulatory sites, a recent mass spectrometry study evaluated the three eIF2 subunits and encountered highly phosphorylated N-terminal in eIF2S2 (Beilsten-Edmands et al., 2015). This post-translational modification could be the key to explain a regulation in the GTP hydrolysis process, since eIF2S2 is interacting with GTP, as well as with eIF5 (GTPase-activating factor) and eIF2B (GTP exchange factor) (Asano et al., 1999; Chakrabarti and Maitra, 1992; Kimball et al., 1998).

Besides presenting a binding interface with GTP, eIF2S2 also plays a role in mRNA and Met-tRNA$^{Met}_{i}$ binding. However, the G-protein eIF2S3 is considered the major binding site for Met-tRNA$^{Met}_{i}$ (Bommer and Kurzchalia, 1989; Flynn et al., 1994; Gaspar et al., 1994; Gonsky et al., 1992; Laurino et al., 1999; Naveau et al., 2013; Nika et al., 2001; Roll-Mecak et al., 2004; Schmitt et al., 2010).

A point mutation in the backside of the eIF2S3 GTP-binding domain was the first *EIF2S3* human described mutation (Borck et al., 2012). The iPS patient cells developed in the present study originate from a somatic cell line presenting a frameshift mutation, predicted to cause a truncation at the C-terminus of eIF2S3.

While archaeal eIF2S3 N-terminus (G domain) together with domain II are known to be required for Met-tRNA$^{Met}_{i}$ binding, mutation on domain III (C-terminal) impairs binding to ribosomal 40S (Roll-Mecak et al., 2004; Shin et al., 2011).
To conclude, being eIF2S3 central for translation in all cell types, the gene mutations broad phenotype is intriguing. Therefore, we believe the human *EIF2S3* mutation iPSC line to definitely provide an invaluable model to unveil pathophysiological aspects of this translation machinery element.

1.2. Embryonic neuronal development and disease

1.2.1. Neuronal differentiation during embryogenesis

Subsequent to fertilization, a series of cellular divisions give rise to the blastocyst, a structure characterized by its polarized arrangement and its two different cell populations, an outer cell mass or trophoblast, and an inner cell mass composed by two lineages; i.e. epiblast and primitive endoderm (or hypoblast). Both trophoblast and hypoblast are responsible for the formation of extra-embryonic structures, whereas the epiblast is mainly committed to embryonic development itself.
Following embryonic implantation into the endometrium, cells reorder to form the primitive streak. This cellular reorganization marks a critical event, the gastrulation, which converts the epiblast into three embryonic germ layers (endoderm, mesoderm and ectoderm).
The ectoderm is the layer originating all structures of the nervous system (central and peripheral). Considered to initiate even earlier in development (sixteen-blastomere stage) (Gaur et al., 2016; Streit et al., 2000), the neural specification is just observed on the third gestational week, when ectoderm underlying structures (notochord and mesoderm) release morphogens that contribute to the neural plate emergence within the ectoderm. The neural plate invaginates producing neural folds, which in turn fuse into a neural tube. This tubular structure is ultimately responsible for the formation of the brain, spinal cord and posterior pituitary gland. The surface ectoderm (external ectoderm), which merges again after detachment of the neural tube, is deriving among other structures skin and the anterior pituitary gland.

The lateral edges of the neural plate form the so called neural crest, which differentiates from the neural tube and overlying ectoderm by its capacity of migration to populate diverse tissues, such as autonomic ganglia that innervates many organs. Thus, the neural crest is the origin of the peripheral nervous system. Finally, the neural tube lumen give rise to the adult ventricular system. Ventricles walls are lined by ependymal cells and in distinct locations by choroid plexus, major responsible for cerebrospinal fluid (CSF) production, and that constitute part of the blood-brain barrier. Furthermore, ventricles walls accommodate a population of neural stem cells and therefore the subventricular zone is recognized as the bulk of adult neurogenesis (Fuentealba et al., 2012).

During the fourth developmental week, the neural tube folds to form the primary brain vesicles; namely: prosencephalon (forebrain), mesencephalon (midbrain) and rhombencephalon (hindbrain), which will in addition to the spinal cord form the adult central nervous system.

As exposed here, the sequential events that determine vertebrate development are highly complex, and governed by multiple signaling pathways. Several patterning molecules that have been focus of extensive studies, are known to act during the very early neuronal commitment. WNT (Bielen and Houart, 2014), NOTCH (Louvi and Artavanis-Tsakonas, 2006), BMP (Liu and Niswander, 2005) and SHH (Fuccillo et al., 2006; Komada, 2012) are examples of crucial regulators, controlling cellular self-renewal, proliferation and fate determination.

In addition to influence in embryonic development rate, retinoic acid levels has an impact on the formation of fore-, mid- and hindbrain (Okada et al., 2004) and level variations can even be the cause of death in post-implantation embryos (Huang et al., 2005; Niederreither et al., 1999). Retinoic acid is another essential molecule that presents a broad range of actions, modulating diverse gene expression in combination with co-factors. Lack or loss of function of proteins related to retinoic acid homeostasis resulted in a wide variety of neurological disorders (Rhinn and Dolle, 2012).

1.2.2. Neurodevelopmental disorders and translation

The maintenance of approximately 86 billion healthy and functional neurons, and the same number of healthy and functional glial cells (Azevedo et al., 2009) is

energetically very costly for humans. Keeping both ionic balance and neurotransmitters homeostasis is essential and enables a neuron to fire and send diverse signals into its network of synapses. Processes such as; neurotransmitters synthesis, uptake, and catabolism, in addition to ionic traffic across membranes are essentially costing considerable amount of energy (Du et al., 2008). Therefore, the energy consumed by the brain is mainly used to re-establish ionic gradients. The protein synthesis, which is generally considered to be a major energy-demanding cellular process, does not have a great effect on brain energy consumption (Engl and Attwell, 2015).

Although translation is not among the highly energy costing process in the brain, its control has been identified as an important mechanism regulating neuronal plasticity (Zukin et al., 2009), and its disruption has been associated to various neurodevelopment and neurodegenerative disorders (Jung et al., 2014). The impact that protein levels can have on the nervous system is possibly mediated due to the rapid molecular response required for synaptic signaling changes. Supporting this idea, axonal and dendritic local protein synthesis has been described (Jung et al., 2012; Sutton and Schuman, 2005) along with mechanisms of translational activation by neuronal stimuli triggering microRNA degradation (Fu et al., 2016). This demonstrates the importance to maintain dynamic regulation of protein levels in neuronal compartments. Despite of being essential for all tissues, it is not unwise to assume that proteome regulation in the brain is far more refined, and responsive to environmental changes, exhibiting therefore, a much faster phenotypic change in comparison to other organs. Corroborating with this, mutations known to affect the translational machinery have been associated to both neurodevelopmental and neurodegenerative disorders. The molecular mechanisms underlying these pathologies are focus of recent interest but are still poorly understood.

Neurodegenerative disorders, as Alzheimer, Parkinson, and autism spectrum disorder (ASD) are linked to a global decrease of translation via phosphorylation of eIF2S1 (Jung et al., 2014). Neurodevelopmental syndromes, such as Fragile X (FXS), Prader-Willi (PWS), Angelman (AS), Vanishing White Matter (VWM), besides the newly described PPP1R15B and MEHMO, have being assigned as consequences of mutation in genes directly related to translation.

Translation effect	Syndrome Gene	Components affected	Disease features
Global translation OFF	MEHMO *EIF2S3*	Impaired ternary complexes and decresase of start codon fidelity	Intellectual disability, epileptic seizures, microcephaly, enlarged ventricular system, delayed myelination, ataxia gait, panhypopituitarism, hypogonadism, short stature, dyslipidaemia. Borck et al., 2012
	PPP1R15B	Increased levels of phospho-eIF2S1	Intellectual disability, microcephaly, diabetes, short stature, delayed myelination, enlarged ventricular system, ataxia gait. Harding et al., 2008; Kernohan et al., 2015; Abdulkarim et al., 2015
	Vanishing White Matter *EIF2B*	Reduced levels of eIF2-GTP	Myelin degeneration, ataxia gait, enlarged ventricular system, early onset (microcephaly and growth failure). Bugiani et al., 2010
	PACT/RAX	Increased levels of phospho-eIF2S1	Reproductive and developmental defects, reduced body size, craniofacial defects, anterior pituitary hypoplasia. Dickerman et al. 2015
Target mRNA translation OFF	Fragile X *FMR1*	Reduction levels of phospho-eIF4E	Intellectual disability, seizures, behaviour deficits, craniofacial efects, macroorchidism. Bhakar et al., 2012
	Prader-Willi & Angelman *CYFIP1*	Reduction levels of phospho-eIF4E	Intellectual disability, behaviour deficits, growth retardation, obesity. Chung et al., 2015
Global translation ON	Wolcott-Rallison *PERK*	Reduced levels of phospho-eIF2S1	Early-onset of insulin-dependent diabetes, hepatic dysfunction, short stature. Julier & Nicolino, 2010; Harding et al., 2001

Figure 3. MEHMO and other syndromes affecting translation initiation.

The guanine nucleotide exchange factor eIF2B is a key translation regulatory protein, and it is normally present in much lower levels when compared with eIF2, therefore a small fluctuation on levels of active eIF2B can substantially affect the amount of active eIF2-GTP and thus global translation initiation (Singh et al., 2007). As described before, an effective inhibition of eIF2B is done by the phosphorylated form of eIF2S1 that is in higher concentrations in the absence of PPP1R15B. PPP1R15B is known to be an eIF2S1 phosphorylation repressor due to its role of recruiting a phosphatase to eIF2S1. A missense mutation on this gene is causing a series of symptoms which highly remember MEHMO syndrome (Abdulkarim et al., 2015; Harding et al., 2009; Kernohan et al., 2015).

PPP1R15B mutation is not the only causing eIF2S1 phosphorylation imbalance. Although mice lacking eIF2S1 kinases GCN2 or PKR, or expressing a non-phosphorylatable form of eIF2S1 have altered synaptic plasticity and memory (Costa-Mattioli et al., 2005; Costa-Mattioli et al., 2007; Zhu et al., 2011), the consequent decrease of phospho-eIF2S1 is mainly associated with early-onset of diabetes and obesity or death per hypoglycemia. This contradicting glycemic effects (either hypo or hyperglycemia) seem to be highly dependent on phospho-

eIF2S1 availability (Harding et al., 2001; Julier and Nicolino, 2010; Scheuner et al., 2001; Scheuner et al., 2005). On the other hand, and in line with the features presented by *PPP1R15B* mutation, lack of a PACT/RAX (causing increase in phospho-eIF2S1) leads to anterior pituitary hypoplasia and growth restriction, MEHMO syndrome symptoms. It is interesting to note that anterior pituitary cells are expressing high levels of RAX, indicating a possible relevance on the control of phosphorylated eIF2S1 levels in this tissue (Dickerman et al., 2015).

Similarly to what is observed in proteins regulating phospho-eIF2S1 levels, mutation in any of the eIF2B subunits genes is also affecting global translation rates causing the so-called Vanishing White Matter disease (Leegwater et al., 2001; Pavitt and Proud, 2009). Characterized by myelin loss and cerebellar ataxia, this disease affects mainly astrocytes and oligodendrocytes, but its molecular basis is still unknown. Interestingly, the disease is not considered developmental, but to have a progressive nature, as its onset can be precipitated by major stress episodes, also in adulthood. Thus, it has been proposed that symptoms emergence it is not due to a continuous and preponderant decrease of global translation rates, but due to a cellular response to stress, by increasing certain mRNA translation, such as e.g. ATF4 (Kantor et al., 2005). However, might be important to notice that in the early-onset of the disease, two common features in global translation impairment disorders are observed, microcephaly and growth failure (Figure 3) (Bugiani et al., 2010).

Among the neurodevelopmental diseases disturbing translation, particular intellectual disability (ID) disorders, namely: Fragile X (FXS), Prader-Willi (PWS), Angelman (AS) have been intensively studied and, although they had their molecular determinants scrutinized, a lot is still to be unveiled. The basis of these syndromes is the ability of their affected proteins to mediate translational control by binding target mRNAs (Ashley et al., 1993; Napoli et al., 2008; Schenck et al., 2001). This regulation takes place mainly on neuronal tissue, a site where these syndrome-causing genes are normally highly expressed (Hinds et al., 1993; Pathania et al., 2014).

FXS patients exhibit ID and other neurological symptoms, such as seizures and behavioral disorders, besides growth problems and macroorchidism. The disease genetic background is commonly the silencing of the *FMR1* gene, caused by

hypermethylation of an inherited 5´UTR repeat expansion (CGG). FMRP (*FMR1*-encoded protein) is participating in neuronal translational control by different means, impairing both initiation and elongation phases of protein synthesis. The first two involved pathways are related to the inhibition of eIF4E- mRNA binding, via FMRP-CYFIP1 interaction (Napoli et al., 2008; Schenck et al., 2001). As previously described, along with other factors, eIF4E forms a eIF4F complex to bind the 5´cap structure of the mRNA and to attract the 40S ribosomal subunit to it. For proper binding to occur, eIF4E needs to be phosphorylated by mitogen-activated protein kinase (MAPK)-interacting kinase (MNK). Besides MNK, activation of the MTORC pathway is also increasing translation rates, through eIF4E binding proteins (4E-BP) phosphorylation that, in this form, are not able to immobilize eIF4E, thereby allowing cap-dependent translation. Synaptic activity, via either BDNF or mGluR stimulation activates the above-mentioned pathways and regulates specific mRNA translation (FMRP targets) by induction of CYFP1-eIF4E dissociation, thus promoting FMRP target mRNA translation (Figure 4). The third mechanism, by which translation is regulated is the FMRP interaction with the mRNA coding region, blocking ribosome transit and consequently stalling elongation. (Bhakar et al., 2012; Richter et al., 2015).

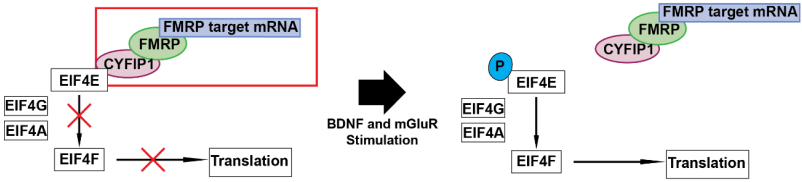

Figure 4. Neuronal control of FMRP target mRNAs translation. Simplified scheme showing CYFIP1 binding to eIF4E and impairing translation of FMRP target mRNAs. CYFIP1 affinity to eIF4E diminishes upon eIF4E phosphorylation via BDNF and mGluR stimulation and results in eIF4E binding to eIF4G and eIF4A to form the cap-mRNA binding complex (eIF4F). The consequent release of CYFIP1 enables translation activation of FMRP target mRNAs (Based on (Bassell and Warren, 2008; Bhakar et al., 2012; Napoli et al., 2008)).

PWS and AS are neurodevelopment disorders characterized mainly by ID. These syndromes are caused by deletion of a region on chromosome 15 (15q11-q13), which when of paternal origin leads to PWS, and when from maternal

chromosome leads to AS. The *CYFIP1* gene is located in the previously mentioned region and its absence, in both syndromes, is related to a more severe form of ID (Bittel et al., 2006; Chung et al., 2015).

Besides coupling of CYFIP1 and FMRP to control translation by the principle exposed before, CYFIP1 is very important for actin cytoskeleton arrangements, for it is also a member of the WAVE complex (Bogdan et al., 2004; Kunda et al., 2003). Coordinating spine morphology changes, BDNF signaling was found to shift CYFIP1 from the translation inhibitory complex to the WAVE complex, repressing actin polymerization. Therefore mature spine formation depends on BDNF signaling combining translation and actin remodeling roles via CYFIP1 (Chen et al., 2010; De Rubeis et al., 2013).

Much similar to what is seen in MEHMO, besides ID, PWS is featured by hypogonadism, obesity and hypotonia, while epilepsy and absence of speech characterize mainly AS.

Augmenting the list of essential components for proper translation, there are some other ribosome-related proteins that have a major impact on brain development. For instance, mutations on *EIF4A3* (Favaro et al., 2014), *RPL10* (Brooks et al., 2014), *EMG1* (Armistead et al., 2015) and *PHF6* (Todd et al., 2016; Wang et al., 2013a) greatly affect neurodevelopment, causing syndromic ID and developmental disorders.

Finally, delving into the sophisticated embryonic and neuronal translation pathways will certainly reveal the overlapping pathogenic mechanisms underlying the diseases considered here, and will provide a comprehensive view on the role of eIF2S3 in the intricate controlling mechanisms governing physiological translation on brain development, and in the disturbed pathways during disease.

1.2.3. MEHMO syndrome and eIF2S3

MEHMO is the acronym formed from the syndrome characteristics; namely, Mental retardation, Epileptic seizures, Hypogenitalism, Microcephaly and Obesity. This disorder was first clinically described in late 1980s (DeLozier-Blanchet et al., 1999; Delozier-Blanchet et al., 1989) and it had its genetic background partially identified a decade later, when Steinmüller and colleagues assigned the disease locus to the short arm of the X-chromosome and proposed

a recessive inheritance based on pedigrees of affected families (Steinmuller et al., 1998).

Besides the frameshift mutation that leads to a C-terminus truncation of eIF2S3 in the patient considered here, a large scale X-chromosome exome sequencing considering 208 families presenting X-linked intellectual disability was realized. From those 208 evaluated families, 9 showed *EIF2S3* point mutations (p.V151L and p.K125R) (Tarpey et al., 2009). Another family was reported by Borck and colleagues (Borck et al., 2012) to present an *EIF2S3* mutation in its pedigree genealogical tree. This was the first investigation that raised the possibility that the *EIF2S3* mutation was actually the genetic cause of MEHMO syndrome. The authors concluded that the specific single nucleotide mutation (p.I222T) on the GTP binding site of eIF2S3 was ultimately affecting the start codon fidelity on yeast studies.

The same study still (Borck et al., 2012) points out the symptomatic variability found in patients having the very same mutation, and expose the difficulty in concluding whether MEHMO-associated manifestations constitute reduced penetrance or variable expressivity, since even a hallmark symptom, such as epilepsy, seems to present significant variance in severity (DeLozier-Blanchet et al., 1999). Contrarily, movement disorders, facial dysmorphisms and growth retardation are features present in all MEHMO reported cases (Table 1). It is also necessary to emphasize that more profound biochemical and anatomical analysis of the first patients described were not possible. Brain magnetic resonance imaging of the most recent patients could show calcifications in choroid plexus, thin corpus callosum and enlargement of lateral ventricles and subarachnoid frontotemporal space, characterizing a developmental problem during ventricular system formation. The ventricles cavities form, together with the spinal cord canal and the subarachnoid space, a communicating network area wherein CSF circulates (Lun et al., 2015). Choroid plexus and corpus callosum are structures that could be easily compromised by abnormal development of the ventricular system (Del Re et al., 2015; Lowery and Sive, 2009; Lyoo et al., 1996)

Table 1 Collection of all MEHMO patient features from the different publications.

Reference	Symptoms
(DeLozier-Blanchet et al., 1999; Delozier-Blanchet et al., 1989)	**Movement disorder- Hypertonia**
	Facial dysmorphisms
	Growth retardation
	Hyperglycemia
	Behavior impairment
	Speech impairment
(Steinmuller et al., 1998)	**Movement disorder**
	Facial dysmorphisms
	Growth retardation
	Diabetes diagnosed at age 6 months
	Increased levels of fatty acids
	Fatty liver
	Small thyroid
(Borck et al., 2012)	**Movement disorder - Ataxia gait**
	Facial dysmorphisms
	Growth retardation
	Low GH levels
	Behavioral impairment
	Speech impairment
	Enlarged lateral ventricles
	Thin corpus callosum
(Stanik, J., Skopkova, M., Stanikova, D., Brennerova, K., Ukropec, J., Danis, D., Kurdiova, T., Ukropcova, B., Ticha, T., Klimes, I., Gasperikova, D. (2015). Genotype and phenotype characterization in two patients with MEHMO syndrome. Abstract published in Hormone Research in Paediatrics 82, Supplement 1)	**Movement disorder – Hypotonia**
	Facial dysmorphisms
	Panhypopituitarism (low levels of GH, TSH, ACTH)
	Diabetes (hypoglycemia in the first 6 months of life)
	Elevated hepatic enzymes
	Severe combined dyslipidemia
	Lactose intolerance
	Enlarged subarachnoid space; calcifications in choroid plexus
	Myelination delay
	VCC-atrial septal defect

1.3. iPSCs as a neurological disease model system

Human induced pluripotent stem cells (hiPSCs) are reprogrammed somatic cells which acquire the pluripotency characteristics comparable to cells of the embryonic inner cell mass, the human embryonic stem cells- hESCs.

Pluripotency, or cell capacity of generating all three germ layers and self-renew, can be assessed by the most stringent test, the tetraploid complementary assay, which was shown to be positive also for artificially reprogrammed cells (Zhao et al., 2009).

Being embryogenesis undoubtedly a very delicate ethical issue, much of the current knowledge available is derived from mice and other vertebrate models. Thus, detailed signaling pathways imperative during embryogenesis and their peculiarities in human development are still poorly understood.

As the hiPSCs transcriptome resembles that of morula blastomeres and epiblast cells of the embryo, the limitation to study human neuronal systems can now be overcome by the generation of hiPSCs and their differentiation into several neuronal types. This turns the hiPSC model into a powerful and attractive tool to explore human particularities, which could not be assessed otherwise.

On the other hand, human developmental processes are challenging to model and iPSCs also present their disadvantages, such as differences in epigenetics which produces a background that could interfere in a particular gene expression. In an attempt to compare gene expression profiles from *in vitro* and *in vivo* pluripotent cells, Yan and colleagues (Yan et al., 2013) applied single-cell RNA sequencing to both human epiblast cells and *in vitro* hESCs. The analysis showed substantial differences in cells´ transcriptomes. However, it is important to consider that there are differences in gene expression even among hESC lines (Abeyta et al., 2004). The gene expression contrast observed between hESC lines is equally found among hiPSCs lines, and also when comparing hiPSCs with hESCs. This variance, though, could be explained by the aforementioned diverse epigenetic influences but also by non-standardized culture conditions, and non-standardized protocols among laboratories worldwide - reviewed by (Sullivan et al., 2010) -. In addition, a standardized global genome study showed no significant differences between lines derived from different sources (Galan et al., 2013).

Thus, although the field of embryogenesis has a lot to profit from stem cells, caution has to be taken when designing and evaluating the experiments. The expansion of techniques using iPSCs will definitely contribute to better understand the complexity involving the interactions of eIF2S3 in pathways of translation regulation, and accordingly, affecting transcriptional and post-transcriptional cellular mechanisms. The latter being explained by the likely ER stress, caused by an accumulation of unfolded proteins derived from a deregulated translational process.

2. Aim

To have a more comprehensive view about gene expression and translational pattern in patients with mutation in *EIF2S3* gene, patient-derived iPS cells were generated. iPS cells served as a model in the identification of candidate genes/proteins which are regulated or affected by eIF2S3. Patients with such a mutation present mainly neurological abnormalities. To understand how the neuronal activity is impaired in the affected individuals, different stages of neuronal differentiation were analyzed via expression of neuronal markers, together with genes of interest, which were selected in the course of the study.
All the data generated here will hopefully give us hints to better assess the role of eIF2S3 in brain development.

3. Material and Methods

3.1. Chemicals, enzymes and commercially available kits

For the preparation of culture media and all other solutions and buffers, chemicals from Merck (Darmstadt, Germany), Sigma-Aldrich® (Darmstadt, Germany) and Carl Roth® (Karlsruhe, Germany) were used, when not otherwise indicated. All enzymes and corresponding buffers needed were provided by Thermo Fisher Scientific™ (Waltham, USA). mRNA extraction and qRT-PCR were performed employing QIAGEN (Hilden, Germany) kits (RNeasy Mini® kit; QuantiTect® primer assays; QuantiFast® SYBR® Green RT-PCR kit). Plasmid DNA was extracted by using JetQuick Gel extraction, PCR purification and Plasmid Miniprep Spin kits (GENOMED GmbH - Löhne, Germany) or NucleoBond® Xtra Maxi EF (Macherey-Nagel - Düren, Germany), for larger amounts of plasmid DNA.

3.2. Plasmids, primers and antibodies

All plasmids used for cloning, transfection and viruses production (Table 2) as well as the oligonucleotides used for cloning and sequencing (Table 3) are grouped below. Table 4 contains a list of all QuantiTect® primers (QIAGEN) used during quantitative RT-PCR. Immunostaining and western blot required the primary and secondary antibodies listed in Table 5.

Table 2. Plasmid constructs used in this study.

Plasmid	Description	Source
eIF2		
pC4291	pcDNA4/TO/myc-His A (EcoRI-XhoI)+*EIF2S3*	(Borck et al., 2012) Kindly provided by Dr. Thomas Dever, NIH
pC4292	Derived from pC4291 (I222T mutation on *EIF2S3*)	(Borck et al., 2012) Kindly provided by Dr. Thomas Dever, NIH
Competent strain and Lentiviral plasmids		
Electrocompetent *E. coli*	DH5α derivative	(Hanahan, 1983)
pLVX-Tet3G	Neo^R; Lenti-X™ Tet-On® 3G Inducible Expression System	Clontech Laboratories, Inc
pLVX-TRE3G	$Puro^R$; Lenti-X™ Tet-On® 3G Inducible Expression System	Clontech Laboratories, Inc
pLVX-TRE3G-4291	Derived from pLVX-TRE3G and pC4291	This study
pLVX-TRE3G-4292	Derived from pLVX-TRE3G and pC4292	This study
Codon-optimized OKSM red	Multicistronic reprogramming vector	(Warlich et al., 2011)
pSPAX2	GAG/Pol-Vector (lentiviral packaging plasmid) Plasmid #12260	Addgene (Cambridge - USA)
pMD2.G	VSVg-Vector (envelope expressing plasmid) Plasmid #12259	Addgene

Table 3. Oligonucleotides used in this study

Primer	Sequence (5´→ 3´)	$T_{melting}$ (°C)	Use
D_Not_I_fw	ATAGCGGCCGCCGTTTAAACTTAA	61	Amplification of 1509bp *EIF2S3* WT gene from pc4291
D_NdeI_rev	CGCCATATGATGAGTTTTTGTTCGA	59	Amplification of 1509bp *EIF2S3* WT gene from pc4291
S3 2f	ATGTAGCTCATGGGAAATCCAC	52	Identification of *EIF2S3*
S3 3f	TGTTGACTGTCCTGGCCA	50	Identification of *EIF2S3*
S3 4f	GCAGAGGGAGCTCCCATTAT	52	Identification of *EIF2S3*
S3 6f	AGGTGTACGCACTGAAGGAGA	51	Identification of *EIF2S3*
S3 1 rev	ATAACTTCGTGTGAAAGTGGCG	54	Identification of *EIF2S3*
S3 2 rev	TGGATTTCCCATGAGCTACAT	51	Identification of *EIF2S3*

Table 4. Human QuantiTect® primers (QIAGEN) used in this study.

Primer (Gene symbol)	Gene full name
ACHE	Acetylcholinesterase (Yt blood group)
AFP	Alpha-Fetoprotein
APOE	Apolipoprotein E.
ATF4	Activating Transcription Factor 4
ATF5	Activating transcription factor 5

Primer (Gene symbol)	Gene full name
BCL2	B-Cell CLL/Lymphoma 2
CAMKII (CAMK2G)	Calcium/calmodulin-dependent protein kinase II gamma
CBS	Cystathionine beta-synthase
CHAT	Choline O-acetyltransferase
CRABP1	Cellular retinoic acid-binding protein 1
CRABP2	Cellular retinoic acid-binding protein 2
CYFIP1	Cytoplasmic FMR1 interacting protein 1
CYP26A1	Cytochrome P450, family 26, subfamily A, polypeptide 1
DDIT3 (CHOP)	DNA Damage Inducible Transcript 3
DLX2	Distal-Less Homeobox 2
EIF1 (EIF1A)	Eukaryotic translation initiation factor 1
EIF2S1	Eukaryotic initiation factor 2 S1
EIF2S2	Eukaryotic initiation factor 2 S2
EIF2S3	Eukaryotic initiation factor 2 S3
EIF2B1	Eukaryotic translation initiation factor 2B, subunit 1
EIF2B2	Eukaryotic translation initiation factor 2B, subunit 2
EIF2B3	Eukaryotic translation initiation factor 2B, subunit 3
EIF2B4	Eukaryotic translation initiation factor 2B, subunit 4
EIF2B5	Eukaryotic translation initiation factor 2B, subunit 5
EIF3A	Eukaryotic translation initiation factor 3, subunit A
EIF3B	Eukaryotic translation initiation factor 3, subunit B
EIF3C	Eukaryotic translation initiation factor 3, subunit C
EIF4A2	Eukaryotic translation initiation factor 4A2
EIF4E	Eukaryotic translation initiation factor 4E

Primer (Gene symbol)	Gene full name
EIF4G1	Eukaryotic translation initiation factor 4 gamma
EIF5	Eukaryotic translation initiation factor 5
EOMES (TBR2)	T-box brain 2
EMX1	Empty spiracles homeobox 1
FMR1	Fragile X mental retardation 1
FABP4	Fatty acid binding protein 4
FABP5	Fatty acid-binding protein, epidermal
FOXA2	Forkhead-Box-Protein A2
FOXJ3	Forkhead transcription factor
G6PD	Glucose-6-Phosphate Dehydrogenase
GABBR1	Gamma-aminobutyric acid (GABA) B receptor, 1
GABRA1	Gamma-aminobutyric acid (GABA) A receptor, alpha 1
GAPDH	Glyceraldehyde-3-Phosphate Dehydrogenase
GRM1 (MGLUR1)	Glutamate Receptor, Metabotropic 1
GRM5 (MGLUR5)	Glutamate Receptor, Metabotropic 5
GSK3B	Glycogen synthase kinase-3
H2AFX	H2A Histone Family Member X
HMBS	Hydroxymethylbilane synthase
HOMER1	Homer1
HOXA2	Homeobox A2
HOXC4	Homeobox C4
HOXC8	Homeobox C8
KRT1	Keratin 1, Type II
KRT18	Keratin, type I cytoskeletal 18

Primer (Gene symbol)	**Gene full name**
LRAT	Lecithin retinol acyltransferase
LRP8 (APOER2)	Low Density Lipoprotein Receptor-Related Protein 8 (Apolipoprotein E Receptor)
MAP2	Microtubule-associated protein 2
MTOR	Mechanistic Target Of Rapamycin (Serine/Threonine Kinase)
MYH6	Myosin, Heavy Chain 6, Cardiac Muscle, alpha
NANOG	Nanog
NES	Nestin
NRXN1	Neurexin-1-alpha
NR1H3 (LXRA)	Nuclear receptor subfamily 1 group H member 3
OCT4A	Octamer binding transcription factor 4
OTX2	Orthodenticle Homeobox 2
PAX6	Paired Box 6
PET1 (FEV)	FEV (ETS oncogene family)
PITX3	Paired-Like Homeodomain 3
PPARD	Peroxisome proliferator-activated receptor delta
PPP1R15A	Protein Phosphatase 1, Regulatory Subunit 15A
PPP1R15B	Protein Phosphatase 1, Regulatory Subunit 15B
RALDH2 (ALDH1A2)	Aldehyde dehydrogenase 1 family, member A2
RARB	Retinoic acid receptor, beta
RBP1	Retinol binding protein 1, cellular
RDH10	Retinol dehydrogenase 10 (all-trans)
RELN	Reelin
RXRA	Retinoid X receptor, alpha
SLC2A14	Solute carrier family 2, facilitated glucose transporter member 14

Primer (Gene symbol)	Gene full name
SOX1	Sox1, SRY (sex determining region Y)-box 1
SOX2	Sox2, SRY (sex determining region Y)-box 2
STRA6	Stimulated by retinoic acid 6
SYP	Synaptophysin
T	T Brachyury Transcription Factor
TBR1	T-box brain 1
TBX6	T-Box 6
TH	Tyrosine hydroxylase
TKT	Transketolase
TUBB3	Tubulin, Beta 3 Class III

Table 5. Antibodies used in this study

Primary Antibody	Description	Source
Pluripotency		
OCT-4-A	Rabbit IgG Monoclonal	StemLight™ Pluripotency Antibody Kit - Cell Signaling Technology®
SOX2	Rabbit IgG Monoclonal	
NANOG	Rabbit IgG Monoclonal	
SSEA4	Mouse IgG3 Monoclonal	
TRA-1-60	Mouse IgM Monoclonal	
TRA-1-81	Mouse IgM Monoclonal	

Three Germ Layers		
β- 3 TUBULIN	Chicken	Millipore
DESMIN	Mouse	Dako
SOX17	Goat	R&D Systems
Western Blot		
β- Actin	Chicken	Abcam
EIF2S3	Rabbit Polyclonal. N-terminal region.	Aviva; Abcam
APOE	IgG1 Mouse	Novus Bio
Second Antibodies	**Description**	**Source**
Anti-Mouse IgM	Alexa Fluor® Donkey 568nm	Abcam
Anti-Mouse, Rabbit, Chicken, Goat and Sheep IgG	Alexa Fluor® Donkey and Goat 488, 568 and 647 nm	Abcam
Anti-Chicken	HRP conjugated	Abcam
Anti-Mouse; Rabbit	800 CW and 680RD	LiCOR

3.3. Cell lines

The cell lines donated and generated for this study are listed in the Table 6. MH stands for MEHMO patient, whereas C refers to clonal line. All MH1 lines belong to the same MEHMO patient.

Table 6. Cell lines used in this study

Cell line	Genotype, Phenotype	Organism
REF	Rat Embryonic Fibroblast - isolated from Day E14 Sprague Dawley rat embryos as described in (Takahashi and Yamanaka, 2006)	Rat
MEF	CD-1 Mouse Embryonic Fibroblasts, Day E12.5 (StemCell™ Technologies - Vancouver, Canada)	Mouse
HEK 293T	Human Embryonic Kidney 293T for Lentiviral Packaging (Takara - Mountain View, CA, USA)	Human
HFF	Human Foreskin Fibroblasts (System Biosciences – Palo Alto, CA, USA)	Human
hiPSC Control lines		
K1	Control Male	Human
K3	Control Male	Human
K5	Control Male	Human
hiPSC Patient lines (from same patient)		
MH1	Mixed lines	Human
MH1C1	Clone 1	Human
MH1C3	Clone 3	Human

3.4. Media and other solutions

3.4.1. Bacterial media

Generally, Luria Bertani Miller Broth (LB) was used for cultivation of *E. coli*. Super Optimal broth with Catabolic repressor (SOC) was used to cultivate *E. coli*. following electroporation. For preparation of agar plates, agar in a concentration

of 15 g/L was added to LB medium. Media were prepared with deionized water and autoclaved for 20 minutes at 121°C, whereas thermo-sensitive solutions were sterilized by filtration with 0.2 µm pore size filters (Millipore - Darmstadt, Germany). All bacterial media used in this study are listed in Table 7.

Table 7. Media used for cultivation of E. coli strains

Medium	Composition
LB	1% Tryptone
	0.5% Yeast extract
	1% NaCl
SOC	2% Peptone
	0.5% Yeast extract
	10mM NaCl
	2.5mM KCl
	10mM $MgCl_2$
	10mM $MgSO_4$
	20mM Glucose

For selection of resistant bacteria, Ampicillin (Ap) was added to the media to a final concentration of 100 µg/mL. Antibiotic was dissolved in deionized water and sterilized by filtration with 0.2 µm pore size filters (Millipore).

3.4.2. Mammalian cell culture media

All media supplements that required previous dilution were sterilized by filtration with 0.2 µm pore size filters (Millipore). All mammalian cell media and supplements used in this study are listed in Table 8 and Table 9.

Table 8. Media used for cultivation of mammalian cell lines.

Medium	Composition
MEF/REF/HEK293T	Dulbecco's Modified Eagle Medium (DMEM) - Life Technologies
	15% Fetal Bovine Serum (FBS) - Life Technologies
	1% Antibiotic-Antimycotic - Gibco™
	2 mM GlutaMAX™ - Life Technologies
	100 µM Nonessential amino acids (NEAA) - Life Technologies
HFF	Dulbecco's Modified Eagle Medium (DMEM) - Life Technologies
	10% Fetal Bovine Serum (FBS) - Life Technologies
	1% Antibiotic-Antimycotic - Gibco™
	2 mM GlutaMAX™ - Life Technologies
	100 µM Nonessential amino acids (NEAA) - Life Technologies
Keratinocytes	EpiLife® Medium, with 60 µM calcium - Gibco™
	1X Human Keratinocyte Growth Supplement (HKGS) - Gibco™
	10µM ROCK Inhibitor (Ascent Scientific, Avonmouth, BS, UK)
Reprogramming	EpiLife® Medium, with 60 µM calcium - Gibco™
	1X Human Keratinocyte Growth Supplement (HKGS) - Gibco™
	8 µg/mL Polybrene (Sigma-Aldrich®)
	10µM ROCK Inhibitor - Ascent Scientific
	Codon-optimized OKSM red virus suspension
hiPSC	Knockout™ DMEM - Gibco™
	1% Antibiotic-Antimycotic - Gibco™
	20% KnockOut™ Serum Replacement - Gibco™
	2 mM GlutaMAX™ - Life Technologies
	100 µM Nonessential amino acids (NEAA) - Life Technologies
	100 µM Beta-mercaptoethanol - Gibco™

hiPSC (cont.)	50µg/mL L(+)-Ascorbic acid - Carl Roth®
	10µM ROCK Inhibitor - Ascent Scientific
	10 ng/mL Recombinant Human FGF-2 - Cell Guidance Systems (Cambridge, UK)
FTDA (based on (Frank et al., 2012))	DMEM/F-12, GlutaMAX™ supplement - Gibco™
	1% Antibiotic-Antimycotic - Gibco™
	0.1% Human Serum Albumin (HSA) - Biological Industries (Kibbutz Beit-Haemek, Israel)
	1:100 Chemically Defined Lipid Concentrate - Life Technologies
	5ug/mL Insulin, 5ug/mL Transferrin, and 5ng/mL Selenious Acid (ITS Premix) - Corning® (NY, USA)
	5 ng/mL Activin A- Cell Guidance Systems
	10 ng/mL Recombinant Human FGF-2 - Cell Guidance Systems
	0.5 ng/mL Recombinant Human TGF-β1 - Peprotech (Rocky Hill, NJ, United States)
	50 nM Dorsomorphin (Compound C) – Abcam (Cambridge, UK)
SILAC base medium (FTDA adapted for SILAC)	DMEM:F12 (1:1) Media for SILAC – Thermo Fisher Scientific™
	1% Antibiotic-Antimycotic - Gibco™
	0.1% Human Serum Albumin (HSA) - Biological Industries
	1:100 Chemically Defined Lipid Concentrate - Life Technologies
	1X GlutaMAX™ Supplement - Gibco™
	5ug/mL Insulin, 5ug/mL Transferrin, and 5ng/mL Selenious Acid (ITS Premix) - Corning®
	5 ng/mL Activin A- Cell Guidance Systems
	10 ng/mL Recombinant Human FGF-2 - Cell Guidance Systems
	0.5 ng/mL Recombinant Human TGF-β1 - Peprotech
	50 nM Dorsomorphin (Compound C) - Abcam
EB´s	PeproGrow hESC Embryonic Stem Cell Media - Peprotech
	10µM ROCK Inhibitor - Ascent Scientific
	10µM (±)-Blebbistatin - Abcam

hESC	DMEM/F-12, GlutaMAX™ supplement - Gibco™
	1% Antibiotic-Antimycotic - Gibco™
	20% KnockOut™ Serum Replacement - Gibco™
	100 µM Nonessential amino acids (NEAA) - Life Technologies
	100 µM Beta-mercaptoethanol - Gibco™
N1M	DMEM/F-12, GlutaMAX™ supplement - Gibco™
	1% Antibiotic-Antimycotic - Gibco™
	1X Hormonmix (Table 9)
	1X B-27® Supplement (50X), serum free - Gibco™
	2µM Dorsomorphin (Compound C) - Abcam
N2M	DMEM/F-12, GlutaMAX™ supplement - Gibco™
	1% Antibiotic-Antimycotic - Gibco™
	1X Hormonmix (Table 9)
	1X B-27® Supplement (50X), serum free - Gibco™
	2µM Dorsomorphin (Compound C) - Abcam
	10 ng/mL Recombinant Human FGF-2 - Cell Guidance Systems
N3M	DMEM/F-12, GlutaMAX™ supplement - Gibco™
	1% Antibiotic-Antimycotic - Gibco™
	1X Hormonmix (Table 9)
	1X B-27® Supplement (50X), serum free - Gibco™
	2µM Dorsomorphin (Compound C) - Abcam
	10 ng/mL Recombinant Human FGF-2 - Cell Guidance Systems
	10 ng/mL Recombinant Human Epidermal growth factor (EGF) - Cell Guidance Systems
N4M	50% DMEM/F-12, GlutaMAX™ supplement - Gibco™
	50% Neurobasal® Medium - Gibco™
	1% Antibiotic-Antimycotic - Gibco™
	1X Hormonmix (Table 9)

N4M (cont.)	1X B-27® Supplement (50X), serum free - Gibco™
	1mM Dibutyryl-cAMP - ENZO (Lörrach, Germany)
	200µM L(+)-Ascorbic acid - Carl Roth®
	10ng/mL Recombinant Human Glial-derived Neurotrophic Factor (GDNF) - Cell Guidance Systems
	10ng/mL Recombinant Human Brain-derived Neurotrophic Factor (BDNF) - Cell Guidance Systems

Table 9. Hormonmix supplement used for cultivation in neuronal differentiation.

Hormonmix Composition (50X)
24nM Sodium selenite
16nM Progesterone
80 µg/mL Holotransferrin
20 µg/mL Insulin
87.58µM Putrescin

Antibiotics were added to media to the final concentration described in Table 10. For selection of resistant cell lines, Puromycin (Puro) and Geneticin (G418) from Thermo Fisher Scientific™ were applied, while Doxycycline (DOX) from Sigma-Aldrich® was used in case of inducible gene expression system application.

Table 10. Antibiotics used in this study.

Antibiotics	Final concentration
Puromycin	1µg/mL
Geneticin	800µg/mL
Doxycycline	1µg/mL

3.5. Mammalian cell culture

All cell lines were incubated at 37°C, 5%O_2; 5% CO_2 and 95% relative air humidity (Heracell™ 240iCO_2 Incubator). If not otherwise indicated, cells were centrifuged at room temperature and 400xg for 2 min (Thermo Fisher Scientific™ Heraeus™ Megafuge™ 16R Centrifuge).

Thawing of frozen cell cryogenic vials, as well as media warming were performed on a water bath (Thermo Fisher Scientific™) at 37°C. For cells washing steps Dulbecco's phosphate-buffered saline (PBS) no calcium, no magnesium (Gibco™) was used. If not otherwise mentioned, all flasks and plates used to cultivate the cells were tissue culture treated and purchased by Corning®.

Cell lines were frozen using specific media and deposited on cryogenic vials (Corning® cryogenic vials, internal thread). Cryogenic vials were gradually frozen in Cryo-Safe™ -1°C Freeze Controller containers (SP Scienceware™) at -80°C overnight, to be further stored in liquid N_2 tank (CryoPlus2 - Thermo Fisher Scientific™).

3.5.1. MEF/REF/HEK293T/HFF culture

MEF (Mouse Embryonic Fibroblasts); REF (Rat Embryonic Fibroblasts), HEK 293T (Human Embryonic Kidney 293T) and HFF (Human Foreskin Fibroblasts) sources are described on Table 6 .For their culture, a vial of frozen cells was rapidly thawed and immediately transferred into 10 mL of medium (see Table 8). Cells were centrifuge and pellet was resuspended in 15mL medium, which was plated on a T75 flask and incubated. Medium was changed every second day.

3.5.1.1. MEF conditioned medium

In order to prepare MEF conditioned medium, MEF cells were cultivated as described on previous section to 100% confluence and split 1:3. Two days after splitting, medium (see Table 8) was collected (at this stage cells should be approximately 60% confluent), filtered using a 0.2µm sterile filter (Millipore) and stored at -20°C (long term) or at 4°C.

3.5.1.2. Lentivirus production

For lentivirus production, a number of 4-5 x 10^6 low passage HEK293T cells was plated in a 10 cm^2 dish (Cell Star®) using 10 mL HEK medium (Table 8), one day before transfection. At the day of transfection, a mixture of plasmid DNA was prepared with 400µL Opti-MEM® (Life Technologies), 8µg vector with gene of interest, 5.5µg pSPAX2, 2µg pMD2.G and 70µg Linear polyethylenimine (Polysciences, Inc.). The mixture was incubated at RT for 10min, then 1mL of DMEM was added. Cells medium was replaced by 6.5mL DMEM (Life Technologies) and the mixture preparation was drop wise added, promoting an even distribution. Cells were incubated for 4h and medium was replaced with 8mL HEK medium. At the second day after transfection medium was collected and stored at 4°C. New 8mL HEK medium was once more given to the cells, which were incubate again. Medium was collected in the fourth day after transfection, and mixed with the previously collected medium to be centrifuged (RT;400xg; 2min). In order to separate the remaining cells, the supernatant was filtered using a 0.45µm sterile filter (Millipore). Concentration was made by mixing the virus solution and Lenti-X™ Concentrator (Clontech Laboratories, Inc - Mountain View, CA, USA) in a ratio of 1:3 by volume. The mixture was incubated at 4°C overnight and centrifuged the day after (4°C; 1,500xg; 45min). Supernatant was discarded and virus was resuspended with 1mL of appropriate medium (DMEM/F-12, GlutaMAX™ supplement - Gibco™ or EpiLife® Medium, with 60 µM calcium - Gibco™). Virus 100µL aliquots (5x10^8 proviral copies) were stored at -80°C for later usage.

3.5.2. Keratinocytes generation and culture

Keratinocytes were isolated from donated patient and control plucked hairs presenting a healthy outer root sheath. Those hair roots were either kept on DMEM (Life Technologies) at RT for transportation or immediately used for plating. For plating of hair roots, T25 flasks were coated using Matrigel® Basement Membrane Matrix, LDEV-Free, (Corning®) diluted 1:5 in EpiLife® Medium, with 60 µM calcium (Gibco™) supplemented by 1X HKGS (Gibco™). Flasks were incubated for 1h. Hair roots were placed on the top of the coated

flask surface and one drop of the same matrigel used to coat was carefully given to the root in a 1:10 dilution. The flask was again incubated for 2h. After the incubation time, 1mL of MEF conditioned medium (see sections 3.5.1.1 and 3.5.1.2) supplemented by 10ng/mL FGF2 (Peprotech), 10μM ROCK Inhibitor (Ascent Scientific) and 50 μg/mL ascorbic acid (Sigma-Aldrich®) was carefully added to the hair and the flask incubated. MEF conditioned medium supplemented was daily changed and when the first keratinocytes emerging out of the outer root sheath were observed, the medium was changed to keratinocytes medium (see Table 8).

Once the keratinocytes flask was confluent, 400 μL of Dispase (Corning®) was given to the flask and incubated for 10 min. Cells were collected with PBS and centrifuged.

To freeze keratinocytes, Synth-a-Freeze® Cryopreservation Medium (Gibco™) was used.

In case of further culture, keratinocytes pellet was resuspended in keratinocytes medium (see Table 8) and plated on a previously coated 6-well format plate. For coating, collagen from human placenta Type IV (Sigma-Aldrich®) was diluted in PBS to a final concentration of 20μg/mL and plate was incubated for 1h.

3.5.3. Human induced pluripotent stem cells generation

The patient lines MH1, MH1C1 and MH1C3 were generated thanks to the kindly patient hair sample donation. Control cell lines K1, K3 and K5 originate from hair (keratinocytes) provided by healthy donors. All lines were generated at the Institute of Neuroanatomy and Developmental Biology of the Eberhard Karls University Tübingen.

3.5.3.1. Keratinocytes reprogramming preparation

For keratinocytes reprogramming, keratinocytes were cultivated as described in section 3.5.2 to a confluence of 70% (~ $3x10^5$ cells). At least one day before starting the transduction, mitotic inactivated REF cells were prepared to serve as feeder layer for the reprogramming.

3.5.3.2. REF cells mitotic inactivation

REF cells mitotic inactivation was initiated when the culture achieved a confluence of 90-100% (see section 3.5.1). Old medium was discarded and cells were treated with 7.5 µg/mL mitomycin C (Biomol - Hamburg, Germany) in fresh REF medium (see Table 8). Posteriorly, cells were incubated for 2.5h. After treatment, cells were washed three times in PBS and detached using 1X TrypLE™ Express Enzyme (Gibco™), as usual.

For reprograming, 3 wells (6-well format plate) were plated with 1.5 x 10^5 treated REF cells per well.

3.5.3.3. Reprogramming and culture of hiPSCs

At the day of reprogramming, keratinocytes well was washed with PBS and medium was changed to reprogramming medium (see Table 8). Cells were incubated overnight and the same procedure was repeated on the following day. On the third day of reprogramming, keratinocytes were detached with 1X TrypLE™ Express Enzyme (Gibco™), centrifuged, resuspended on hiPSC medium (see Table 8) and split 1:3. Cells were plated on the three previously prepared REF feeder wells (see section 3.5.3.2). hiPSC medium was daily changed.

After approximately 10 days, hiPSCs-like colonies normally arise from the transduced keratinocytes. At this stage the colonies were transferred into a feeder-free system. To transfer the colonies, wells (6-well format plate) were coated using Matrigel® hESC-Qualified Matrix, LDEV-Free (Corning®) diluted according to manufacturer's instructions and incubated for 1h. With the help of a pipette, colonies were scratched and carefully transferred into the previously coated well with 1.5mL FTDA medium (see Table 8). For clonal lines, a single small colony was separately transferred.

In order to further culture and expand cells, they were washed in PBS and incubated for 2 minutes in Dispase in Hank's Balanced Salt Solution Modified (StemCell™ Technologies) diluted 1:5 in DMEM/F-12, GlutaMAX™ supplement (Gibco™) for splitting. After incubation, cells were washed in PBS and FTDA medium was given to them. Cells were detached with the help of a cell spatula

(TPP® - Trasadingen, Switzerland) and small colony clumps were plated in previously coated wells, as described before.

3.5.3.4. Freezing and thawing hiPSCs

To freeze, cell colonies were detached as for splitting (see section 3.5.3.3). Scratched colonies were centrifuged and cell pellet was resuspended in CryoStem™ Freezing Medium (Biological Industries) to be frozen.
Thawing of the frozen cryogenic vial was performed by incubation in water bath and immediate resuspention in 10mL FTDA medium. Cells were centrifuged, supernatant discarded and pellet was ressuspended in fresh FTDA for plating in a previously coated well (see section 3.5.3.3).

3.6. Generation of overexpression HFF cell lines

Generation of *EIF2S3* wild-type and mutant (I222T mutation on *EIF2S3*) HFF overexpression lines, required cloning of the gene of interest into a lentiviral vector (pLVX-TRE3G), as described in sections 3.11 and 4.4.1. Lentivirus production was accomplished by using pSPAX2 and pMD2.G (Table 2), as it is described in the previous section 3.5.1.2.
Two days prior to HFF (Table 6) infection, cells were usually split (section 3.5.1). At the day of infection, cells were washed twice with PBS and 5mL of HFF medium (Table 8) supplemented with 10μM ROCK Inhibitor (Ascent Scientific), 8 μg/mL Polybrene (Sigma-Aldrich®) and virus suspension of interest was given to each well. Cell plate was centrifuged (RT; 1,000xg; 30 min) and incubated for 4h. Following incubation period, medium was discarded and fresh HFF medium was given. The infection process was equally repeated at the following day and cells were normally culture and further selected. Infected cells were selected by addition of either Puromycin or Geneticin (Table 10) to the culture for 3 to 4 days. Cells infection with Lenti-X™ Tet-On® 3G Inducible Expression System (Clontech Laboratories, Inc) required a double infection with virus originated from the response plasmid (pLVX-TRE3G-4291 or pLVX-TRE3G-4292) and from the regulator plasmid (pLVX-Tet3G). The control line was infected with the regulator plasmid and an empty response plasmid.

3.7. Generation of knock-down HFF cell lines

Generation of *EIF2S3* knock-down HFF line, required lentivirus production (section 3.5.1.2) using pSPAX2 and pMD2.G (Table 2) and a pTRIPZ lentiviral inducible shRNA (Clone ID: V3THS_395443) expression vector (Open Biosystems).

Two days prior to HFF (Table 6) infection, cells were, as usually, split (section 3.5.1). At the day of infection, cells were washed twice with PBS and 5mL of HFF medium (Table 8) supplemented with 10μM ROCK Inhibitor (Ascent Scientific), 8 μg/mL Polybrene (Sigma-Aldrich®) and virus suspension of interest was given to each well. Cell plate was centrifuged (RT; 1,000xg; 30 min) and incubated for 4h. Following incubation period, medium was discarded and fresh HFF medium was given. The infection process was equally repeated at the following day and cells were normally culture and further selected. Infected cells were selected by addition of Puromycin (Table 10) to the culture for 3 to 4 days. The control line did not present any construct.

3.8. Three germ layers differentiation

In order to demonstrate hiPSC lines pluripotency, three germ layers differentiation was carried out. At first day of differentiation a confluent plate (6-well format) of the hiPSCs was washed with PBS and FTDA medium was given to them. Cells were collected, centrifuged and ressuspended in 10mL hESC medium (Table 8) supplemented by 10μM ROCK Inhibitor (Ascent Scientific). Cells were transferred into a T25 flask to form Embryoid Bodies (EB´s), and medium was partially changed every two days with 8mL hESC medium without Rock Inhibitor for 10 days. At the eleventh day both 12-well and 24-well format plates were coated with Matrigel® hESC-Qualified Matrix, LDEV-Free (Corning®), diluted according to manufacturer's instructions, and incubated for 1h. Being the 24-well format plated for staining purposes, coverslips Ø 13mm, thickness I (Neolab - Heidelberg, Germany) were placed inside the wells previously to the coating. After the incubation period, 2 to 4 EB´s were plated using 1 mL hESC medium. Medium was daily changed and cells were cultivated for 10 more days. Thereafter cells were either harvested for RNA isolation or forwarded for immunostaining.

3.9. Undirected neuronal differentiation

Based on Kim et al. 2011 (Kim et al., 2011), undirected neuronal differentiation started with treatment of hiPSCs with 1X TrypLE™ Express Enzyme (Gibco™) for about 5 minutes on incubator to create a single cell suspension. After incubation, some FTDA medium (see Table 8) was given to the cells. At this point, cells were counted for a total of 20.000 cells per well (96-well format plate). Medium was discarded and EB´s medium (see Table 8) was added, according to the calculated volume. Cells were plated on a 96-well conical bottom plate (Sarstedt - Nümbrecht, Germany) and incubated for two consecutive days. On the third day, medium was changed to N1M (see Table 8) and cells were once more incubated for two consecutive days. To plate the formed EB´s on the fifth day, a 6-well format plate was coated with Matrigel® hESC-Qualified Matrix, LDEV-Free (Corning®), diluted according to manufacturer's instructions, and incubated for 1h.

Most of the matrigel was discarded and the EB´s were plated using N2M medium (Table 8). EB´s were further cultivated until the formation of neural "rosettes". This step usually lasted from 2 to 7 days and N2M was daily changed. Once the neural "rosettes" were formed, the old medium was discarded and fresh N3M (Table 8) was added. Cells were detached mechanically by carefully pipetting medium on them. All neural "rosettes" were transferred into an ultra-low attachment 25cm^2 flask (Corning®) in a total volume of 10mL N3M. Medium was changed each second day during eleven days.

Thereafter, the formed neurospheres of neural stem cells (NSCs) were plated in coated wells using N4M medium (Table 8). Coating had two phases, each 1h in the incubator. The first phase required covering of the surface with enough volume of 10 µg/mL Poly-L-ornithine (Sigma-Aldrich®). In the second step, Poly-L-ornithine solution was discarded, well was washed in PBS twice and coated with enough volume of 5 µg/mL Laminin (Roche - Basel, Switzerland). Occasionally, when neurospheres were remarkably large, a previous treatment with StemPro Accutase Cell Dissociation Reagent (Life Technologies) for 5 minutes was appropriate. 50% of the medium volume was carefully changed every second day. Cells were cultivated for three or four weeks, when they were used for further analysis.

3.10. Bacterial cells manipulation

3.10.1. Bacterial culture conditions

Inoculum of *E.Coli* strains of interest were cultivated either in tubes containing 4mL of LB medium or in 1L baffled flasks containing 300 mL of LB medium (see Table 7). In both cases the culture was supplemented by 100 µg/mL ampicillin, if appropriate. The cultures were incubated overnight at 37°C and 160rpm (Shaking Incubator with orbital motion, GFL - Hannover, Germany). Cultivation on solid medium (LB with agar and, if appropriate, 100 µg/mL ampicillin) was carried out after transformation of *E. coli* (see section 3.10.4) and was also incubated overnight at 37°C.

3.10.2. Conservation of *E.Coli* strains

In order to preserve bacterial strains, glycerol cultures were prepared giving 400µL liquid culture to 600µL glycerol (87%). Cultures were stored at -80°C and to cultivate them again, the glycerol stock was thawed on ice and 10µL of the stock was inoculated into a new LB culture flask.

3.10.3. Preparation of electrocompetent *E. coli*

The preparation of competent cells started with an initial culture of 5mL of LB medium (see Table 7) from a glycerol stock of *E. coli* DH5α (Table 2). The culture was incubated overnight at 37°C and 125rpm (Shaking Incubator with orbital motion, GFL), and on the following day it was used to inoculate 300mL of LB medium to an OD_{600} of 0.1. Bacteria were left growing at 37°C and 160rpm (Shaking Incubator with orbital motion, GFL) to reach an OD_{600} of 0.35-0.4. At this point, culture was placed on ice for 30 minutes. Thereafter, cell culture was centrifuged (1,000xg, 4°C, 20 min) and supernatant discarded. Cell pellet was resuspended in 240mL of cold H_2O_{dest} and cells were harvested again by centrifugation (1,000xg, 4°C, 20 min). Cells were once more rinsed in 120mL of cold H_2O_{dest} and centrifuged as described before. In the last washing step, cells were rinsed on 24mL of cold 10%glycerol solution. After centrifugation, pellet was

finally resuspended in 600µL of cold 10% glycerol solution and aliquots of 100µL were stored at -80°C.

3.10.4. Transformation of electrocompetent *E. coli*

To transform *E. coli*, 1-2µg of the plasmid of interest was added to an aliquot of 100µL competent *E. coli* (see section 3.10.3) previously thawed on ice. Thereafter, bacterial suspension was transferred into a pre-chilled electroporation cuvette (PeqLab – Erlangen, Germany) and pulsed using a Gene-Pulser II (Bio-Rad – Munich, Germany). The expected pulse length was close to 5 ms and the settings applied: 1.8kV, 25µF and 600Ω. Immediately after electroporation, 800µL SOC medium (see Table 7) was given to the bacteria, which was incubated at 37°C, 500rpm for 1hour (Thermomixer pro - Cell Media - Elsteraue, Germany). Following incubation, bacteria was harvest by centrifugation (3 minutes at 1,000xg) and plated on a LB plate (supplemented with antibiotic, if necessary – see section 3.10.1) and incubated overnight at 37°C.

3.11. DNA techniques

All centrifugation steps were performed in a microcentrifuge (Thermo Fisher Scientific™ Heraeus™ Fresco™) and, if not otherwise indicated, incubations took place in an orbital shaker (Thermomixer pro - Cell Media).

3.11.1. Plasmid isolation from *E. coli.*

For amplification and isolation of plasmid DNA, transformed *E.Coli* cells were cultivated (see section 3.10.1). Cells were harvested by centrifugation (1 min, 11,000xg) and plasmid isolation was carried out, as recommended by the supplier, using either JetQuick Plasmid Miniprep Spin kits (GENOMED GmbH) or NucleoBond® Xtra Maxi EF (Macherey-Nagel). The isolation kit was chosen according to the amount of plasmid required.

3.11.2. Polymerase chain reaction (PCR)

Polymerase chain reaction (PCR) was performed in a thermocycler (PERKIN ELMER DNA Thermal Cycler 480) according to the protocol described below.

Primers (Table 3) were provided by biomers.net GmbH and diluted in $H_2O_{dest.}$ to a final concentration of 100 pmol/µL. The melting temperature (Table 3), temperature at which 50% of the oligonucleotides form double strand, was calculated by the manufacturer, considering salt concentration, oligonucleotides composition and concentration.

For a PCR reaction assay, 5ng of template DNA was mixed to 10µL 5x Prime STAR GXL Buffer, 4µL 2.5 mM dNTP mixture (Takara), 1.5µL 10µM primer forward, 1.5µL 10µM primer reverse and 1µL Prime STAR GXL DNA Polymerase (Takara). $H_2O_{dest.}$ was added, if necessary, to complete 50µL of reaction volume. All reaction parameters were set according to the enzyme supplier´s recommendations. PCR conditions consisted of 30 successive cycles of denaturation (98°C for 10 seconds), annealing (60°C for 15 seconds) and elongation (68°C for 90 seconds). PCR products were analyzed by agarose gel electrophoresis (see section 3.11.3).

3.11.3. Gel electrophoresis

As a mean of separating different sizes of DNA fragments, electrophoresis gels were prepared with 1% agarose diluted in 1X TAE buffer (Table 11) and supplemented with 1X GelGreen™ Nucleic Acid Gel Stain, 10,000X in DMSO (Biotium - Fremont, CA, USA). DNA samples were mixed with 6x DNA loading buffer and applied on the gels, always besides a MassRuler Express Forward DNA Ladder Mix 10kb (Thermo Fisher Scientific™), used as DNA size reference. Electrophoresis was performed in an Bio Rad apparatus (Bio-Rad) set to 100V.

Table 11. Gel electrophoresis buffers

Solution	Composition
50 X TAE Buffer (1L)	2M Tris
	50 mM EDTA
	57.1mL acetic acid, pH 8.5
1 X TAE Buffer	50 x TAE buffer diluted in $H_2O_{dest.}$

Solution	Composition
6X DNA loading buffer	0.25% (w/v) bromphenol blue
	0.25% (w/v) xylene cyanol FF
	40% (w/v) sucrose

3.11.4. DNA extraction from agarose gels

Agarose gel containing GelGreen™ (Biotium) allowed the visualization of DNA by UV radiation (366nm). The fragments of interest were excised with a scalpel, and DNA extraction from the gel was carried out with JetQuick Gel Extraction Spin kit (Genomed GmbH) according to the supplier´s instructions. DNA concentrations were determined in the NanoPhotometer® P-Class 330 (IMPLEN - Munich, Germany). Purity was accessed by determination of the quotient of A_{260} / A_{280}, which ranges between 1.8 and 2.0 for pure DNA.

3.11.5. Restriction of DNA

Cloning of DNA fragments into vectors requires compatible ligation sites created by restriction of specific sequence in both fragment and vector. Therefore, treatment with one or two restriction enzymes, as recommended by the supplier, was accomplished. To avoid re-ligation of vectors during the first restriction, FastAP alkaline phosphatase (Thermo Fisher Scientific™) was added to the reaction. A general restriction protocol included up to 1µg chromosomal or plasmid DNA, 1X FastDigest buffer, 1µL restriction enzyme I, 1µL restriction enzyme II (optional) and $H_2O_{dest.}$, if necessary, to complete 20µL of reaction volume. The reaction volume was scaled up appropriately according to the needs.

For following ligation, DNA was purified after restriction by gel electrophoresis and extraction (sections 3.11.3 and 3.11.4). For control restriction, DNA was further analyzed by gel electrophoresis (section 3.11.3).

3.11.6. Ligation (Cloning of restriction enzyme generated fragments)

The last step in cloning required the ligation of the restricted DNA fragment and

vector by T4 DNA Ligase enzyme. The reaction was composed by a 3:1 insert fragment molar ratio over vector, 1x T4 DNA Ligase buffer, 1µL T4 DNA Ligase and $H_2O_{dest.}$, if necessary, to complete 20µL of reaction volume. Ligation reaction was carried out for 1 hour at 22°C and either frozen at -20°C for further use or directly used for *E.Coli* transformation (see section 3.10.4).

3.11.7. DNA Sequencing

All cloned vectors were sent to GATC Biotech (Konstanz, Germany), together with the appropriated sequencing primer (Table 3). To verify the fidelity of the cloning process, FinchTV software (Geospiza, Inc., Seattle, USA) was used for genomic comparison.

3.12. RNA techniques

All centrifugation steps, if not otherwise indicated, were performed in a microcentrifuge (Thermo Fisher Scientific™ Heraeus™ Fresco™).

3.12.1. RNA isolation from mammalian cells.

RNA extraction was performed using RNeasy Mini® kit (QIAGEN). For this purpose, cells were washed in PBS and harvested by centrifugation (2min, RT; 400xg) (Thermo Fisher Scientific™ Heraeus™ Megafuge™ 16R Centrifuge). Cell pellet was ressuspended in RLT buffer according to cell number, and isolation was performed following supplier´s instructions. RNA was eluted in up to 60µL RNAse-free H_2O and concentrations were determined in the NanoPhotometer® P-Class 330 (IMPLEN). Purity was accessed by determination of the quotient A_{260}/A_{280}, which is 2.0 for pure RNA.

3.12.2. Quantitative real-time PCR (qRT-PCR)

Quantitative analysis of gene expression was possible by the real-time polymerase chain reaction of RNA samples. Initial RNA reverse transcription was followed by PCR, allowing quantification to be accomplished in one step. Quantification of different targets was done by binding of SYBR Green I fluorescent dye to double-stranded DNA molecules, emitting a fluorescent signal.

This way, target RNA amounts can be measured in a real-time modus, as the DNA copies are being produced.

The reaction made use of QuantiTect® primers (QIAGEN) (Table 4) and QuantiFast® SYBR® Green RT-PCR kit (QIAGEN), according to manufacturer's instructions.

Reference genes *HMBS*, *GAPDH* and *G6PD* were empirically found to be the best for the cell types analyzed, due to their constant transcription considering the experimental conditions.

Experiment was run in the Applied Biosystems StepOne™ Real-Time PCR System and StepOne™ Software v2.3 was the software of choice to obtain the raw data in cycle threshold (Ct) values, which were used to calculate the amount of initial mRNA, as described by Livak and Schmittgen, 2001 (Livak and Schmittgen, 2001).

3.12.3. qRT-PCR array - FLUIDIGM®

Besides the usual qRT-PCR, high throughput gene expression analysis was accomplished by a special cycler, the BioMark™ HD (Fluidigm® - South San Francisco, CA, USA), in which smaller amounts of samples are needed and many different genes are analyzed simultaneously.

Preparation started by reverse transcription of RNA samples into cDNA. DNA impurity was removed by treatment of 320ng RNA (sample volume of 9µL) with 0.25µL DNaseI (Sigma-Aldrich®) and 1µL DNaseI Reaction Buffer (Sigma-Aldrich®) for 15minutes at room temperature. Following incubation, enzyme was inactivated by the adding of 1µLStop solution (Sigma-Aldrich®) to the reaction. For cDNA synthesis, 2.75µL of the previous reaction (80ng) was mixed with 1µLof 5XRT Buffer (Promega - Wisconsin, USA), 0.25µL of dNTPs (GE Healthcare Life Sciences), 0.313µL Hexanucleotides mix (Roche), 0.25µL MMLV RT (Promega) and 0.438µL RNase free H_2O. The reaction tube was incubated at 37°C for 60 minutes and at 85°C for 10 minutes. cDNA was stored at 4°C or already used for preamplification. The preamplification step was useful to increase number of DNA copies and facilitate detection of low-expression genes.

Preamplification was prepared employing PreAmp Master Mix (Fluidigm®) according to manufacturer's instructions, but applying a different assay, the

QuantiTect® primer assays (QIAGEN) in a final concentration of 500nM and the 80ng of previously synthetized cDNA. After this step, samples were treated to remove unincorporated primers by using Exonuclease I (New England BioLabs - Ipswich, Massachusetts, USA). To this purpose the final 5μL volume preamplification assay was mixed with an earlier prepared solution containing 1.4 μL PCR certified H_2O (TEKnova - Hollister, CA, USA), 0.2μL Exonuclease I Reaction Buffer and 0.4μL Exonuclease I at 20Units/μL. The reaction was incubated at 37°C for 30min and enzyme inactivated by further 15min incubation at 80°C. To the 7μL samples, 43μL TE Buffer (TEKnova) was added and stored at -20°C for later usage.

At the following day, 2.7μL of the stored treated samples were well mixed to 3μL 2XSsoFast EvaGreen Supermix with Low ROX (Bio-Rad) and 0.3μL 20XDNA Binding Dye Sample Loading Reagent (Fluidigm®). Sample mixture was centrifuged for 30 seconds and temporarily stored at 4°C. A second mix was prepared by adding 2.5μL 2XAssay Loading Reagent (Fluidigm®) to 2.5μL of the specific QuantiTect® primer assay (QIAGEN), so that assay concentration in this mixture was 1000nM. Assay solution was well mixed and centrifuged for 30 seconds. After both assays and samples mixtures were prepared the 96.96 Dynamic Array™ IFC was loaded (Fluidigm®) following manufacturer's instructions. The loaded chip was placed into the BioMark™HD (Fluidigm®) reader and the thermal cycling protocol for 96.96 Array was selected. After run, reaction specificity was evaluated and raw data in cycle threshold (Ct) values collected to calculate the amount of initial mRNA, as described by Livak and Schmittgen, 2001 (Livak and Schmittgen, 2001). The software programs chosen for analysis were Fluidigm Real-Time PCR Analysis Software v.3.0.2 and Python software.

3.13. Protein techniques

All centrifugation steps were performed in a microcentrifuge (Thermo Fisher Scientific™ Heraeus™ Fresco™) and, if not otherwise indicated, incubations took place in an orbital shaker (Thermomixer pro - Cell Media).

3.13.1. Western Blot

3.13.1.1 Protein extraction for Western Blot

For lysis, cells were placed on ice, washed in cold PBS and scratched. After centrifugation (2min, 4°C; 400xg), cell pellet was diluted in RIPA Lysis Buffer (Table 12). For approximately $2x10^6$-$1x10^7$ cells, 60 to 80µL of lysis buffer was used. The solubilized cells were transferred into a pre-chilled 1.5mL reaction tube and the content was vortexed for few seconds. Thereafter, tubes were moved into ultrasonic bath (Transsonic T460/H - ELMA) containing cold water and sonicated for 1 minute. Samples were centrifuged for 10 minutes (10,000xg; 4°C) and protein supernatant was carefully collected. Protein concentration was determined by Pierce BCA Protein Assay Kit (Thermo Fisher Scientific™) according to supplier´s instructions. Samples were measured at 562nm in NanoPhotometer® P-Class 330 (IMPLEN).

Table 12. RIPA Lysis Buffer

Solution	Composition
RIPA Lysis Buffer	150mM NaCl
	5mM EDTA, pH8.0
	50mM Tris pH8.0
	1% IGEPAL® CA-630 (SIGMA)
	0.5% sodium deoxycholate
	0.1% SDS
	1X Halt™ Protease and Phosphatase Inhibitor Cocktail, EDTA-Free (Thermo Fisher Scientific™)

3.13.1.2 Western Blot

A qualitative and quantitative analysis of specific proteins in different cell lines was performed by western blot. Therefore, the three classical steps for protein immunoblot were performed, namely electrophoresis, blotting and protein labelling.

The first step aims a separation by molecular mass of a protein pool, which can be further identified by the use of specific antibodies. For the separation to occur, the 3D protein structures were unfolded, and equally negatively charged in a denaturation process carried out by the addition of a commonly used surfactant agent, SDS. Protein samples were prepared by mixing 50µg protein lysate with 6X SDS loading buffer (Table 13) and $H_2O_{dest.}$ for a total volume of 18µL. Samples were next incubated for 3 minutes at 95°C.

Following samples denaturation, a sodium dodecyl sulfate-polyacrylamide gel electrophoresis (SDS-PAGE) was performed. The mentioned gel consists of two phases, an upper region (stacking gel) which stacks the proteins to improve resolution separation, and a lower region (resolving gel) where the proteins separation itself takes place. Samples were applied in the gel (12% Polyacrylamide Mini-PROTEAN® TGX™ Precast Protein Gels – Bio-Rad) and next to them, 5µL of a protein molecular weight marker (Chameleon™ Duo - LiCOR-928-60000), so that the different protein bands could have their size identified. Electrophoresis was carried out in a Mini-PROTEAN Tetra Cell apparatus (Bio-Rad) and chamber was filled with 1X Running buffer (Table 13). An electrical potential difference of 90V was applied to the samples in order to get them stacked in a line and the voltage was increased to 120V to resolve the gel.

After electrophoresis run, separated proteins were blotted in a nitrocellulose membrane (Protran BA85 Nitrocellulose Blotting Membrane, 0.45 µm) in wet conditions. Therefore, blotting cassette was prepared with gel lying on the membrane, ensuring no air bubbles had formed between them. Gel and membrane were then sandwiched by a blotting cassette externally sheltered by foam pads and internally by two sheets of pre-wetted Whatman® paper (Sigma-Aldrich®). The blot cassette was clamped tightly together and submerged in

blotting chamber containing 1X Wet Transfer buffer (Table 13). Blotting was performed by applying 6V/200mA overnight and at 4°C.

Once blotting was finished, a series of incubations and washing steps were performed to stain the protein of interest with specific antibody. To do that, membrane was always kept in a petri dish with enough volume to ensure it was evenly covered. In all those steps, membrane was placed on a shaker for gentle and uniform agitation (IKA® VXR basic Vibrax® - ALDRICH). In order to avoid nonspecific binding of antibody, membrane was incubated in blocking solution (Table 13) for 2h at room temperature. Blocking solution was discarded and membrane was incubated overnight at 4°C with first antibody diluted in blocking solution according to supplier´s dilution recommendation.

On the following day, membrane was washed three times in 1XTBS buffer with 0.05%Tween20 (Table 13) and incubated in the dark for 1h30min in second antibody diluted as recommended by the supplier in blocking solution (Table 5 and Table 13). After incubation time, second antibody solution was discarded and membrane rinsed three times in 1x TBS buffer with 0.05%Tween20 (Table 13). The last washing was done using only 1X TBS (Table 13) to remove excess of Tween20.

Membrane was scanned using a near-infrared fluorescence two-color detection system, Odyssey® FC (LI-COR), and results analyzed using Image Studio Lite version software (LI-COR). After capturing blot image on LiCOR detection system, membrane was washed three times with 1x TBS buffer with 0.05%Tween20 (Table 13), in case of further staining with HRP conjugated second antibodies. Therefore, membrane is incubated, as before with blocking solution, primary and second antibodies and finally developed using Amersham ECL Western Blotting kit (GE Healthcare) according to manufacturer's instructions. Protein bands were once more visualized using Image Studio Lite version software (LI-COR). For comparison, the amounts of protein loaded in each slot were normalized to those of β-Actin.

Table 13. Western Blot buffers and solutions

Solution	Composition
6X SDS loading buffer (pH 6.8)	62mM Tris-HCl; pH6.8
	10% Glycerol
	2% (w/v) SDS
	5% β-mercaptoethanol
	0.00125% Bromphenol blue
10x Running buffer (pH 8.3)	0.25 M Tris
	1.92 M Glycin
	1% (w/v) SDS
1x Running buffer	1 part of 10x Running buffer and 9 parts of H_2Odest
10x Wet Transfer buffer	250 mM Tris
	1.92M Glycine
1x Wet Transfer buffer	1 part of 10x Wet Transfer buffer, 2 parts of Methanol and 8 parts of H_2Odest
10x TBS Buffer (pH 7.5)	500 mM Tris
	1.5M NaCl
1x TBS Buffer (pH 7.5)	1 part of 10x TBS Buffer and 9 parts of H_2Odest
1x TBS buffer with Tween20	1x TBS buffer
	0.05%Tween20
Blocking solution	6% porcine serum (PAA) in 1x TBS buffer

3.13.2. Stable isotope labelling by amino acid in culture (SILAC)

3.13.2.1. Protein extraction for SILAC

hiPSCs were cultivated as usual (section 3.5.3.3), but using SILAC medium (see Table 8 and Table 14). Light proline was supplemented in the three different SILAC media due to the metabolic conversion of labelled arginine to labelled proline, affecting the final peptides quantification (Lossner et al., 2011).

After cultivation of hiPSCs for 2 weeks in SILAC medium supplemented by light amino acids, cells were split so that wells would be 70% confluent in 48h. The splitting was planned to generate one sample out of 2 wells (6-well format). At the programed time point, medium was changed into medium labelled and heavy labelled medium (Table 8 and Table 14) and cells were incubated for 24h, 16h and 6h. After this period, protein was extracted, simultaneously for all samples. To that end, 700µL of Lysis Buffer (Table 15) per sample was prepared and placed on ice. Cells were placed on ice and washed twice with cold PBS. To scratch the cells, Lysis Buffer was added and cells were detached with a cell spatula (TPP®). Cells in Lysis Buffer were collected into a 1.5mL reaction tube and kept on ice. The tubes were lying on ice, and the ice container was placed in an orbital shaker (IKA® VXR basic Vibrax® - Sigma-Aldrich®) at 40rpm for 40 minutes. Tubes were centrifuged (4°C; 10,000xg; 10 min) and supernatant was collected into new pre-chilled tubes. The protein extract concentration was then measured in the NanoPhotometer® P-Class 330 (IMPLEN). The pre-selected samples were mixed in a 1:1 ratio to proceed with the protein precipitation step. Each precipitate sample had a total protein amount of 20µg.

Table 14. Amino acid mixtures supplements to SILAC base medium (see Table 8)

Medium	Composition
Light	0.5M L- proline (Silantes - Munich, Germany)
	0.4M L- arginine (Silantes)
	0.55M L-lysine (Silantes)

Medium	Composition
Medium labelled	0.5M L- proline (Silantes)
	0.4M $^{13}C_6$ –arginine (Silantes)
	0.55M $^{2}H_4$ –lysine (Silantes)
Heavy labelled	0.5M L- proline (Silantes)
	0.4M $^{13}C_6$ $^{15}N_4$ - L –arginine (Silantes)
	0.55M $^{13}C_6$ $^{15}N_2$ - L –lysine (Silantes)

Table 15. Buffers for protein extraction in SILAC experiment

Solution	Composition
10XTBS	1.5 M NaCl
	300 mM Tris
	pH7.4 (adjusted using HCl)
Lysis Buffer	1X TBS
	0.55% NP-40 Substitute (Sigma-Aldrich®)
	1X Protease Inhibitor Complexe Complete (Roche)

3.13.2.2. Protein precipitation for SILAC

After samples were mixed according to the designed experiment, the precipitation was executed at room temperature.

From the protein mix, an aliquot of 200µL was separated. To that aliquot, 800µL methanol p.a. v/v=100% (Merck) was added and the tube was vortexed and centrifuged at 9,000xg for 30seconds. Next, 200µL chloroform p.a. v/v=100% (Merck) was added and the mixture was likewise vortexed and centrifuged. After centrifugation, 600 µL HPLC water (Merck) was added, the mixture was vortexed, but this time the centrifugation lasted 1minute and revealed both organic and aqueous phases. The upper phase was discarded by pipetting the content out

and making sure not to touch the interphase with the pipette tip. To the lower phase, 600µL methanol p.a. v/v=100% (Merck) was added and the mix was smoothly pipetted up and down for two to three times. Thereafter, the tube was centrifuged for 5minutes at 16,000xg. Supernatant was carefully discarded and protein precipitate was dried under a laminar flow for 5 to 10minutes. Reaction tubes containing the pellets were snap-frozen by immersion in liquid nitrogen and immediately stored at -80 °C.

Precipitate samples were sent to German Center for Neurodegenerative Diseases (DZNE) within the Helmholtz Association (Tübingen, Germany) for further treatment and analysis.

3.13.2.3. Protein digestion and peptides enrichment

Protein pellet (20µg per sample) was resuspended in 30µL ABC (Table 16), and 4 µL Rapi Gest (Table 16) was added to it. Sample was strongly vortexed and content was spun down shortly. To the mix, 1µL DTT (Table 16) was added and sample was incubated at 60°C for 10minutes. To initiate digestion, sample was once more spun down and 2 µL Trypsin Solution (Table 16) was given. Sample was then immediately incubated overnight at 37°C; 500rpm.

On the following day, sample was centrifuged for 1 minute at room temperature; 9,000xg and the enzymatic reaction was interrupted by adding TFA (Merck) to a final concentration of 5%. The solution was transferred into a Polypropylen Insert with Bottom Spring; 200µL (SUPELCO - Sigma-Aldrich®), previously placed in a 1.5mL reaction tube. The tube was incubated for 10 minutes at room temperature and subsequently centrifuged at 22°C; 16,000xg for 15 minutes.

Samples were purified using C18-StageTips (Thermo Fisher Scientific™). To that end, the matrix was equilibrated with 20µL 80/5 Solution (Table 16). Matrix was next rinsed with 20µL 0/5 Solution (Table 16) and samples were applied. Matrix was washed with 20µL 0/5 Solution (Table 16) and the peptides were eluted into a new tube, using 20µL 50/5 Solution (Table 16). The remaining peptides were eluted again in 20µL 80/5 Solution (Table 16). Eluted samples were concentrated to approximately 5µL using Speed Vac® (Savant SPD111V, Thermo Fisher Scientific™).

Table 16. Solutions used in protein digestion and peptides enrichment. HPLC water (Merck) was used in the preparation of all solutions

Solution	Composition
Amonium bicarbonate solution (ABC)	50mM Amonium bicarbonate (Sigma-Aldrich®)
RapiGest	20mg/mL RapiGest™ SF Surfactant (Waters - Massachusetts, USA)
Dithiothreitol Solution (DTT)	100mM 1,4-Dithiothreitol (Merck)
Iodacetamide Solution (IAA)	300mM 2-Iodacetamide (Sigma-Aldrich®)
Trypsin Solution	1µg/µL Trypsin, Proteomics Grade (Sigma-Aldrich®). Dissolved in 1mM HCl (Merck)
80/5 Solution	5% (v/v) Trifluoracteic acid (TFA) , protein sequencing grade (Merck)
	80% (v/v) Acetonitrile, hypergrade for LC/MS (Merck)
50/5 Solution	5% (v/v) Trifluoracteic acid (TFA) , protein sequencing grade; (Merck)
	50% (v/v) Acetonitrile, hypergrade for LC/MS (Merck)
0/5 Solution	5% (v/v)Trifluoracteic acid (TFA) , protein sequencing grade (Merck)

3.13.2.4. Peptides analysis by LC-MSMS

SpeedVac-dried SEC-Fractions were redissolved in 0.5% TFA and analyzed by LC-MSMS using a nano-flow HPLC system (Ultimate 3000 RSLC, Thermo Fisher Scientific™) coupled to an Orbitrap QExactive (Thermo Fisher Scientific™) tandem mass spectrometer. For identification, crosslinked peptides were separated on the nano HPLC by 180 minute gradients and analyzed by a data-dependent approach acquiring CID MSMS spectra of the 10 most intense peaks (TOP 10), excluding single charged ions. The analysis was performed at the

Medical Proteome Center Tübingen (University of Tübingen). The raw data were directly analyzed with the MaxQuant software v1.5.2.8 (Cox and Mann, 2008). Downstream analysis was performed using Perseus v1.5.0.31 (http://www.biochem.mpg.de/cox).

3.13.3. Immunostaining

To analyze cellular identification and distribution of specific proteins, immunostaining was utilized. This method employs the specificity of antibody-antigen recognition. For plating, coverslips Ø 13mm, thickness I (Neolab) were placed inside wells (24-well format) and the different cell types were plated as described for them (see the respective cell type section). After the appropriated time of cultivation, cells were carefully washed in DPBS (PBS+/+), calcium, magnesium (Gibco™) and fixed with 300µL fixation solution (see Table 17) for 15 to 20 minutes at room temperature. After incubation time, fixation solution was discarded and cells were washed for three times in PBS+/+. In case of staining of an intracellular protein, non-ionic surfactant was used to permeabilize cells. Therefore 300µL Triton X -100 (Table 17) was added to cells, which were incubated at room temperature for more five minutes. Cells were once more washed in PBS+/+. To avoid unspecific binding of first antibody, 10% donkey or goat serum (Abcam) diluted in PBS+/+ was carefully given to cover cells surface and this was incubated at room temperature for 1 h. After blocking time, cells were incubated with first antibody solution for either 2h at RT or at 4°C, overnight. Dilution was done in blocking solution following supplier´s recommendation (Table 5). Before incubation with the second antibody, cells were washed in PBS+/+ for 5 minutes. Second antibody was diluted in PBS+/+, also according to supplier´s recommendation (Table 5). PBS+/+ was discarded and cells were incubated with second antibody solution at room temperature in dark for 1h. Finally, cells were washed for 3 minutes in PBS+/+, 3 more minutes in PBS and 3 last minute in $H_2O_{dest.}$ Water was discarded and the coverslip embedded in Prolong Gold with DAPI (Life Technologies) for nuclear staining. Coverslip was turned upside down on a slide 76 x 26 mm, extra white cutted with matt rim (Neolab). After drying in dark at room temperature, slides were kept at 4°C until microscopy.

Table 17. Solution employed for immunostaining

Solution	Composition
Fixation	4% Paraformaldehyde (Carl Roth)
	10% Sucrose (Carl Roth)
	1X Dulbecco's phosphate-buffered saline no calcium, no magnesium (Gibco™)
	pH 7.4 (adjusted with 1M NaOH)
Triton X -100	0.1% Triton X -100 (Carl Roth) diluted in DPBS, calcium, magnesium (Gibco™)

All immunostaining pictures were acquired using Axio Imager M2 (Carl Zeiss - Oberkochen, Germany) microscope with a camera model Axiocam MRm (Carl Zeiss). Image was analyzed using the software provided by the microscope producer, Carl Zeiss AxioVision Rel. 4.7.2.

3.14. Statistical methods

3.14.1. Gene expression analysis

Quantitative real-time PCR results were always normalized against the most suitable housekeeping gene. Statistical data charts always show the error bars for the standard error of the mean (S.E.M.). The sample size for control and patient hiPSCs is 6 each (3 different cell lines and 2 replicates each). For other stages of neuronal differentiation (Days 5; 11 and 22), the sample size is 4 (2 different cell lines and 2 replicates each). Statistical significance was determined by applying unpaired t-test and depicted by asterisk symbols, with the following meaning for the p-values: P≤0.001****; P≤0.01***; P≤0.03**; P≤0.05*; P≤0.1 (*).

3.14.2. SILAC protein analysis

As previously stated, peptides derived from SILAC experiment were identified by analysis of their mass spectrometry spectra. The analysis was performed at the Medical Proteome Center Tübingen (University of Tübingen).

Statistical analysis was performed using Perseus v1.5.0.31 (http://www.biochem.mpg.de/cox). For this, unpaired t-test in combination with Significance B were simultaneously applied. This combination was thought to be more stringent, improving exclusion of false positives. Significance B determines outliers ratios based on normal distribution of median ratios.

Only patient-control expression ratio values above 1.2 and below 0.83 were considered significantly different and presented.

4. Results

4.1. Keratinocytes culture and generation of patient-derived iPS cell

After informed consent was provided, hair-root samples containing an outer root sheath from two clinically diagnosed MEHMO patients were collect. The first affected individual (coded MH1) was a 5-years old child having a *EIF2S3* frameshift mutation (I465S fs*4), predicted to cause C-terminus truncation. The second donor (coded MH2) was a 15-years old patient, presenting a missense mutation (I222T) on the GTP-binding domain of eIF2S3.

Keratinocytes, derived from the outer root sheath, were the somatic cell source of choice to be reprogrammed. Besides being originated from a tissue, which does not require invasive acquisition, keratinocytes are also simple to isolate and possess a high reprogramming efficiency (Raab et al., 2014). Therefore, hair samples from the two MEHMO patients were collect and keratinocytes were cultivated according to Aasen and Izpisua Belmonte, 2010 (Aasen and Izpisua Belmonte, 2010).

Reprogramming (Figure 5) of these keratinocytes was successfully conducted using a multicistronic lentiviral vector carrying the four Yamanaka factors genes; namely: *c-Myc, Oct4, Sox2* and *Klf4* (Takahashi and Yamanaka, 2006). The reprogramming system still contained a fused red fluorescence marker that allowed the monitoring of exogenous Yamanaka factors expression and their posterior silencing, subsequent to pluripotency establishment (Warlich et al., 2011).

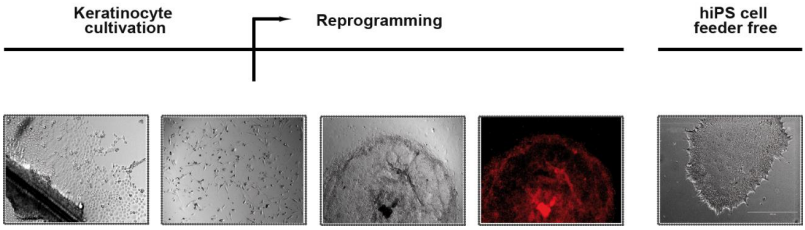

Figure 5. Scheme showing the different stages of keratinocytes reprogramming process. The first step shows hair roots plating and keratinocytes culture. This is followed by their reprogramming on a REF feeder layer, with formation of stem cell-like colonies

expressing Yamanaka factors (visualized also by the concomitant expression of red fluorescent marker). The later phase presents the induced pluripotent stem cell culture, in a feeder free system.

In order to check whether protein localization changed with the mutation, immunostaining using control and patient keratinocytes/iPSCs was conducted (Figure 6). As expected, eIF2S3 protein is distributed all over the cell cytoplasm but also, in a less extended way, in the nucleus of keratinocytes. Although, no evident morphological difference was found between patient and control cells, and no nuclear eIF2S3 localization was observed in iPSCs from both groups. This raises the possibility of a nuclear role in certain cell types and/or cell cycle period that has not yet been described for this translation factor.

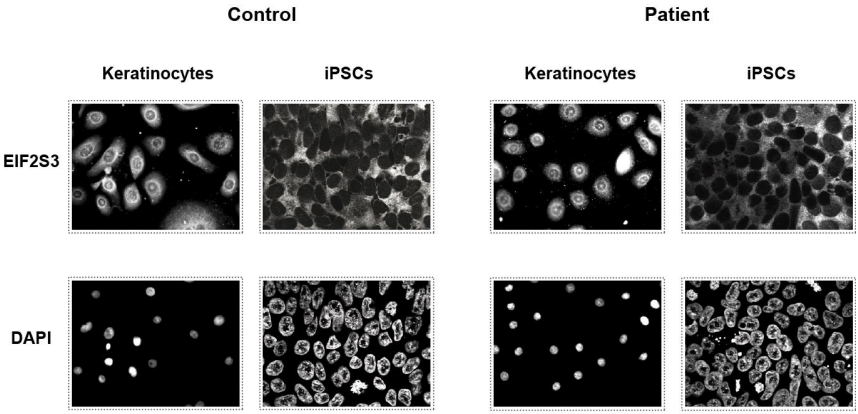

Figure 6. eIF2S3 immunostaining of control and patient keratinocytes (40X objective) and iPS cells (63X objective).

It has been shown though that other eukaryotic translation factors, such as eIF2S1, eIF4A and eIF4E can be highly localized in nucleus. eIF4E, for example, is responsible to increase cell cycle-related mRNAs export to the cytoplasm (Andersen et al., 2002; Culjkovic et al., 2007; Lobo et al., 1997; Tejada et al., 2009). eIF2 subunits nuclear roles are therefore open to speculation, as their possible requirement in the still much debated process of nuclear translation (Bohnsack et al., 2002; Iborra et al., 2001).

4.2. Patient iPS cells characterization

The generated human induced pluripotent stem cell (hiPSC) lines MH1, MH1C1 and MH1C3 were characterized according to their pluripotency state and their capacity of differentiating into all three germ layers. Patient MH2 keratinocytes unfortunately did not undergo successful reprograming. All the other control cell lines generated for this study were equally evaluated (not shown here).

4.2.1. Patient iPS cells pluripotency analysis

As already mentioned in the introductory section, the pluripotency state of a cell is measured by its capacity of generating tissue from any cellular lineage when exposed to particular environmental cues. Moreover, stem cells possess a self-renewal competence, being theoretically capable of infinite division cycles.

In nature, stem cells exist temporarily and are formed during embryogenesis. Following maternal and paternal pronuclei fusion that gives rise to a totipotent zygote, the embryo undergoes a global DNA demethylation up to ICM formation (Guo et al., 2014; Smith et al., 2012). Cells at this stage have the so called naïve pluripotency identity, presenting a specific epigenetic landscape, which promotes expression of pluripotency genes and repression of those related to cell fate specification.

As it is observed during embryogenesis, the epigenetic landscape is massively changed in the reprogramming process, and along with global transcriptional changes, it is an indispensable condition for pluripotency establishment. An intricate network for pluripotency maintenance is activated by a series of transcription factors (e.g. OCT4, NANOG and SOX2) known to have important downstream pluripotency targets. Therefore, standard analysis of gene expression were performed and endogenous *OCT4*, *NANOG* and *SOX2* expression showed at least 20-fold increase in comparison to parental keratinocytes for the MH1 hiPSC line, as showed by Figure 7.

The presence of the same transcription factors proteins was evaluated by immunostaining. They were all positive stained, along with other surface markers, known to be present in the membrane of pluripotent cells (Figure 8).

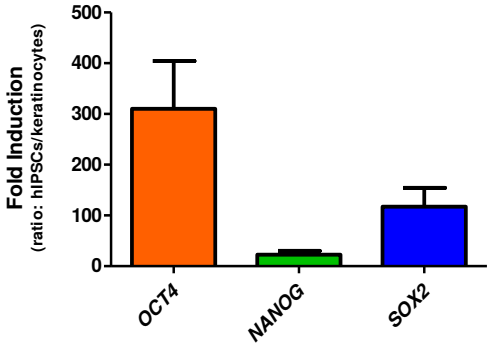

Figure 7. Pluripotency genes expression in MH1 hiPSC line. The graph shows the change in pluripotency gene expression level upon reprogramming. hiPSCs expression levels are compared to levels of parental keratinocytes cells. mRNA levels are relative to *HMBS* expression (Error bar is represented by S.E.M. of 3 technical replicates).

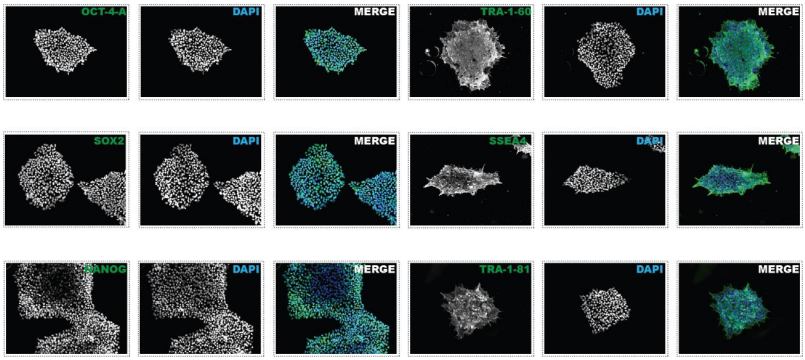

Figure 8. Immunostaining of pluripotency markers for MH1 hiPSC colonies (10X objective).

4.2.2. Differentiation of patient iPS cells into all three germ layers

In order to assess if generated hiPSC lines were able to differentiate into the three germ layers, transcript levels of some important layers markers were analyzed by q-RT PCR (Figure 9). The analysis indicated a successful differentiation into all three embryonic germ layers, as represented by the highly expression of

endodermal (*AFP* and *FOXA2*), mesodermal (*MYH6* and *T*) and ectoderm markers (*PAX6* and *TUBB3*) when compared to undifferentiated hiPSCs.

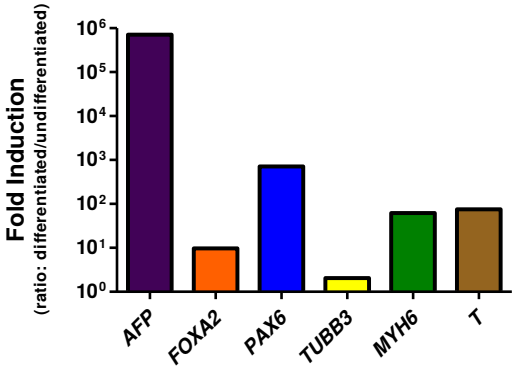

Figure 9. Endoderm, mesoderm and ectoderm-related genes expression in MH1 three germ layer differentiation. The graph shows the ratio of gene expression levels in differentiated MH1 cells in comparison to MH1 hiPSCs (on logarithmic scale). mRNA levels are relative to *HMBS* expression.

Besides gene expression, translation of SOX17 (endoderm), DESMIN (mesoderm) and TUBB3 (ectoderm) was verified by immunostaining, confirming cell line pluripotency (Figure 10).

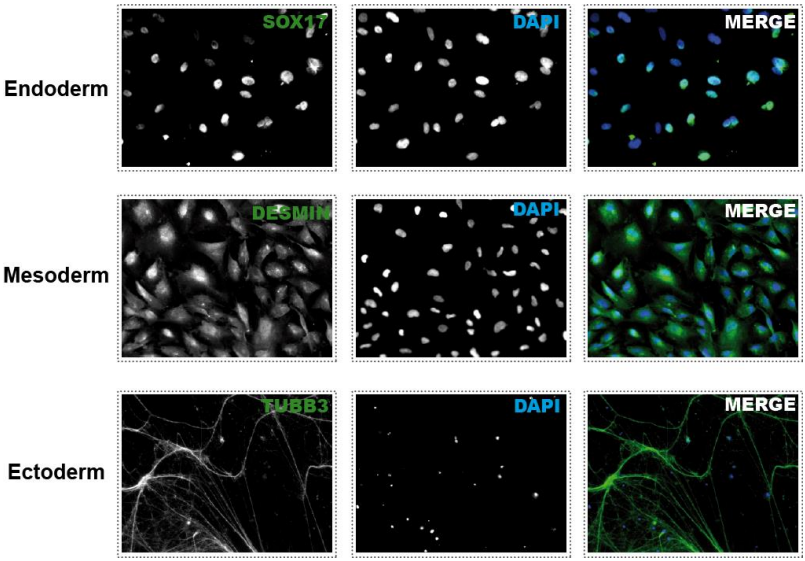

Figure 10. Immunostaining of endodermal, mesodermal and ectodermal markers for MH1 three germ layer differentiation (20X objective).

4.3. Gene expression analysis of patient derived iPSC lines

In a first step evaluating patient specific alterations in gene expression patterns already at the iPSC state, we performed high-throughput qPCR to gain a global view on deregulated mRNA expression, investigating candidate genes related to the patient's symptoms as well as genes related to eIF function.

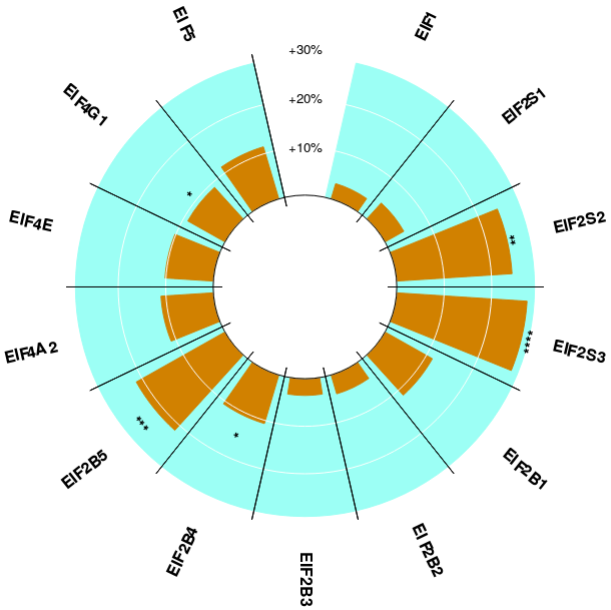

Figure 11. Gene expression ratio between patient and control hiPSC lines. mRNA levels are relative to *G6PD* expression (P≤0.001****; P≤0.01***; P≤0.03**; P≤0.05*; P≤0.1 (*)).

Notably, *EIF2S3* gene expression was highly increased in patient hiPSCs along with the eIF2 β subunit (*EIF2S2*), while *EIF2S1* presented no relevant change in expression. Moreover, two subunits of eIF2B, the guanine nucleotide exchange factor, which activates eIF2, were differentially expressed: EIF2B4 (δ subunit) and EIF2B5 (ε subunit). Still, among the eukaryotic translation initiation factors analyzed, eIF4G1, a member of the cap structure-guiding factor (eIF4F), presented a small increase in mRNA levels.

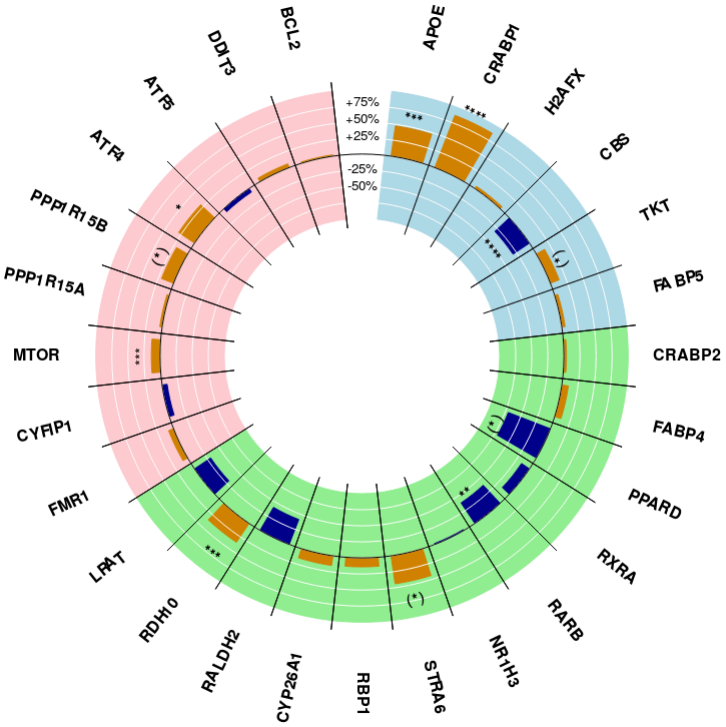

Figure 12. Gene expression ratio between patient and control hiPSC lines. mRNA levels are relative to G6PD expression (P≤0.001****; P≤0.01***; P≤0.03**; P≤0.05*; P≤0.1 (*)).

Correlating with protein levels (Table 18), significant higher expression of APOE and CRABP1, as well as lower CBS expression was detected in patient iPSC lines. TKT, however, presented conflicting levels of protein and mRNA, in which patients had lower levels of protein and higher gene expression, when compared to control. Moreover, different retinoic acid-related genes, as well as genes associated to translation control, as *ATF4* and *MTOR* were differently expressed in patients (Figure 12).

4.4. Generation of wild-type and mutated *EIF2S3* overexpression HFF cell lines

4.4.1. Creation of pLVX-TRE3G-4291 and pLVX-TRE3G-4292 overexpression constructs

To evaluate the effects that overexpression of *EIF2S3* has on the expression of *APOE*, we developed two lentiviral plasmids (Figure 13 (b)). For this purpose, both pC4291 and pC4292 (Figure 13 (a)) (Borck et al., 2012) were object of cloning in a lentiviral system (Clontech Laboratories, Inc) based on co-transduction of two vectors (Figure 13 (b) and (c)) that together can induce overexpression of the gene of interest (GOI).

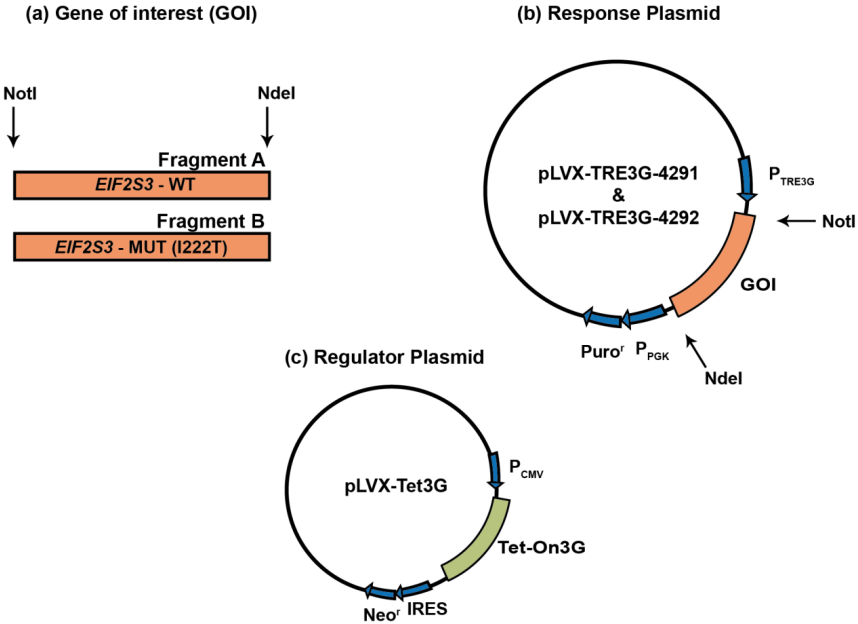

Figure 13. Schematic of the inducible expression system used and of the cloning strategy used to generate pLVX-TRE3G-4291 and pLVX-TRE3G-4292. (a) Gene of interest (GOI) was obtained by PCR from pC4291 and pC4292 templates using primers (D_Not_I_fw and D_NdeI_rev) that enabled the insertion of NotI and NdeI restriction sites in

the PCR products. Restriction of the amplified GOI´s generated the fragments A and B depicted. (b) Digestion of the multiple cloning site of pLVX-TRE3G using the same enzymes allowed GOI´s ligation downstream the inducible PTRE3G promoter. (c) Regulator plasmid is expressing Tet-On 3G transactivator protein, which undergoes a conformational change upon interaction with doxycycline, thus activating GOI expression.

4.4.2. Gene and protein expression of HFF lines overexpressing WT and MUT *EIF2S3*

Two different HFF lines were generated, one carrying the overexpression construct of *EIF2S3* wild-type (WT), and another the mutated *EIF2S3* form (MUT). Co-transduction of both the response and regulator derived viruses (sections 3.5.1.2 and 4.4.1) with further selection of infected cells using puromycin and geneticin gave rise to the two HFF lines named OE-WT and OE-MUT. Moreover, a control cell line for the overexpression (CTRL) experiment was derived also by co-transduction of the viruses, but this time using a response plasmid lacking a GOI.

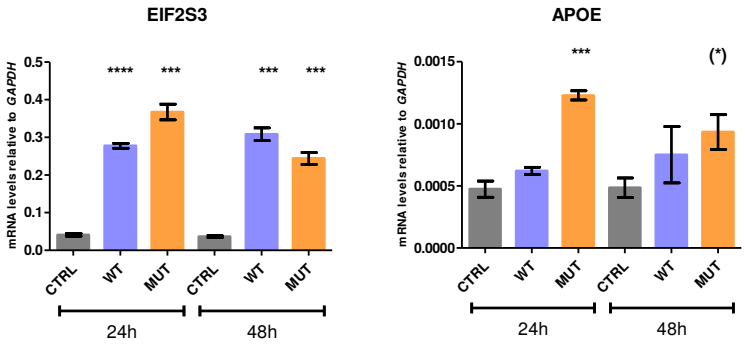

Figure 14. *EIF2S3* and *APOE* gene expression in HFF lines overexpressing wild-type (OE-WT) and mutant (OE-MUT) *EIF2S3* and in control HFF line (CTRL). The graph (left) shows EIF2S3 mRNA levels after 24 and 48h of doxycycline treatment and the right hand graph presents the increase in *APOE* expression when *EIF2S3* mutant is overexpressed. mRNA levels are relative to *GAPDH* expression (Error bar is represented by S.E.M. of 3 technical replicates; P≤0.001****; P≤0.01***; P≤0.03**; P≤0.05*; P≤0.1 (*)).

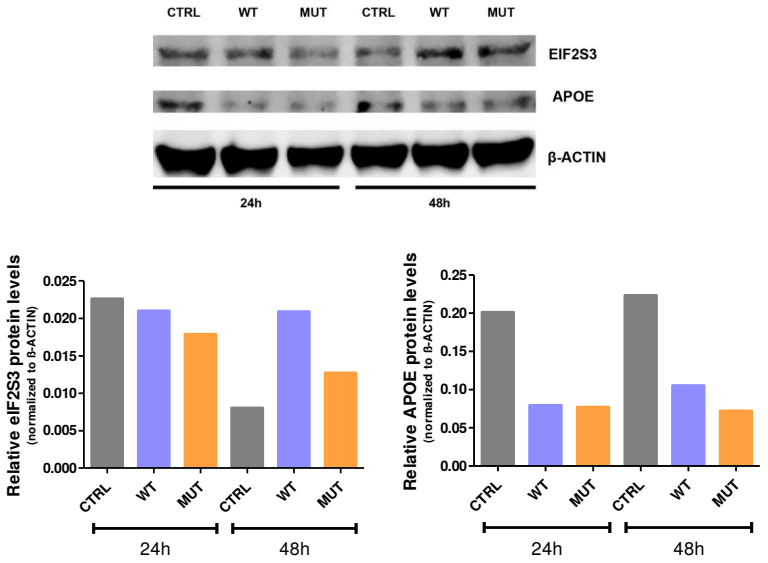

Figure 15. EIF2S3 and APOE protein levels in HFF lines overexpressing wild-type (OE-WT) and mutant (OE-MUT) *EIF2S3* and in control HFF line (CTRL). Western blot reveals eIF2S3 increased levels after 48h of DOX treatment and decreased levels of APOE protein after 24 and 48h of DOX treatment. All values are normalized to β-ACTIN levels.

For induction of GOI expression, activation of P_{TRE3G} promoter by Tet-On 3G transactivator protein were accomplished by treatment with doxycycline (DOX) for 24 and 48h. Cells were analyzed by q-RT-PCR and western blot. *EIF2S3* overexpression was successfully achieved at mRNA levels already after 24h of DOX treatment, and at protein levels increased only after 48h DOX treatment. On transcription levels, APOE is increased only when the mutated form of *EIF2S3* is overexpressed, while APOE translation is down-regulated in all cases of overexpression, after 24 and 48h of DOX treatment (Figure 14 and Figure 15).

4.5. Generation of an HFF cell line with the inducible *EIF2S3* knock-down system

In order to investigate whether APOE up-regulation seen here for MEHMO patients could be correlated with a partial eIF2S3 loss of function, we employed a knock-down cell model (see section 3.7) by the use of a pTRIPZ lentiviral inducible shRNA expression vector (Open Biosystems). *EIF2S3* silencing was induced by doxycycline (DOX) treatment for 1 to 8 days. The transduced cells expressing shRNA could be monitored by the concomitantly expression of a red fluorescent protein.

4.5.1. Gene and protein expression of *EIF2S3* knock-down in HFF cells

Treatment with doxycycline (DOX) for up to 8 days induced transcription of shRNA, which successfully promoted *EIF2S3* knock-down on mRNA and protein levels. Similar to *EIF2S3*, *APOE* expression decreased significantly upon *EIF2S3* silencing. On the other hand, APOE protein levels did not correlate with gene expression and presented a biphasic regulation, in which after 1 day of DOX treatment its levels were decreased, while prolonged knock-down favored its translation (Figure 16 and Figure 17).

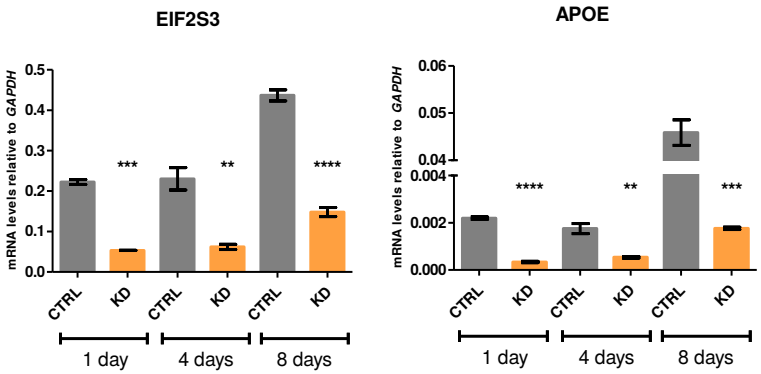

Figure 16. EIF2S3 and APOE gene expression in HFF control (CTRL) and EIF2S3 knock-down (KD) lines after induction of shRNA expression using DOX for 1 to 8 days. The graph (left) shows the decrease in EIF2S3 mRNA levels after 1, 4 and 8 days of DOX treatment and the right hand graph presents the same effect on APOE expression upon

EIF2S3 silencing. mRNA levels are relative to GAPDH expression (Error bar is represented by S.E.M. of 3 technical replicates; P≤0.001****; P≤0.01***; P≤0.03**; P≤0.05*; P≤0.1 (*)).

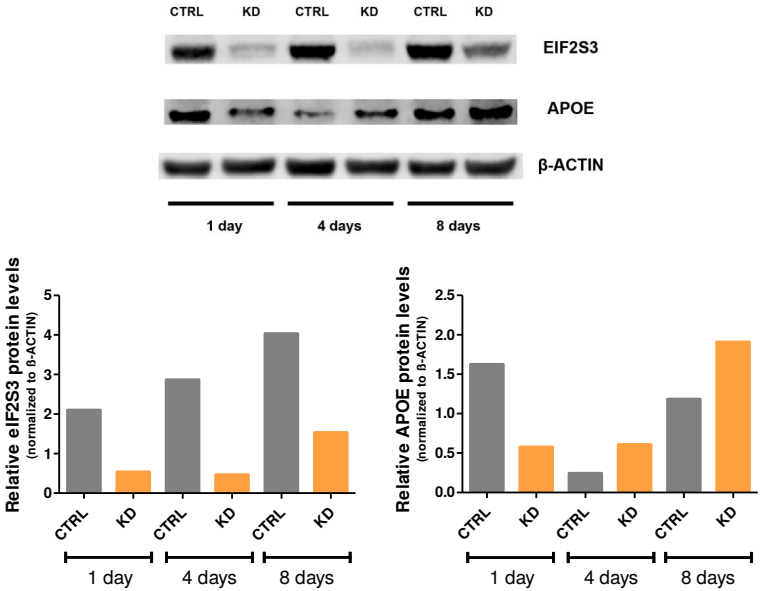

Figure 17. EIF2S3 and APOE protein levels in HFF control (CTRL) and *EIF2S3* knock-down (KD) lines after induction of shRNA expression using DOX for 1 to 8 days. Western blot reveals successful EIF2S3 knock-down at protein levels already after 1 day of DOX treatment and a biphasic effect for APOE levels, in which decreased levels are observed after 1 day of DOX treatment and an increase after 4 days of treatment. All values are normalized to β-ACTIN levels.

4.6. Stable isotope labelling by amino acid in culture (SILAC) of patient iPS cell lines

Mutations in *EIF2S3* were just recently found to be the genetic cause of MEHMO syndrome (G.Borck, personal communication). Besides a detailed phenotypic characterization of patients, nothing is known about the molecular basis of the disease. Therefore, a global protein analysis approach was chosen to guide our investigation into a more specific way, indicating proteins which have their translational rate affected by the mutation and, which could elucidate some of the

disease clinical features.

The mentioned proteome- wide analysis, SILAC, employs culture of two different cell lines in distinct labelled amino acids media, and aims to compare the cell lines, with respect to their global translational rates.

Figure 18 illustrates all the steps in a SILAC experiment, from cell culture in labelled amino acids media to mass spectrometry (MS) measurements. As previously described in section 3.13.2, patient-generated hiPSCs and healthy donor-generated hiPSCs were cultivated in SILAC medium supplied by normal light amino acids. Differences in protein turnover could be obtained by comparing the translational rate between patient and control samples, when medium was changed to labelled amino acids supplement media.

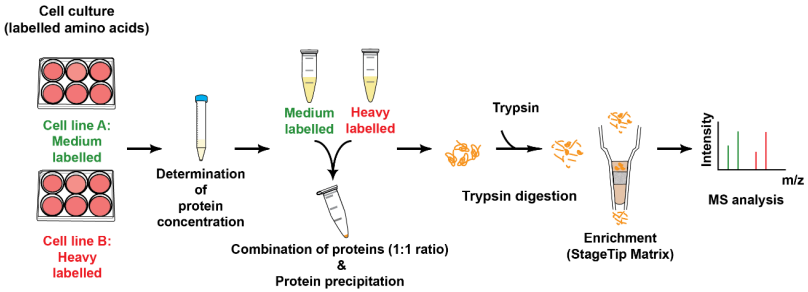

Figure 18. Schematic diagram of SILAC experiment. Patient and control cells lines were fed with differently labelled amino acids (medium and heavy) and their derived proteins were mixed in a 1:1 ratio, digested and enriched for MS analysis.

Two independent experiments were performed (Appendix B - Table B). In the first one the MH1C3 hiPS cell line was compared to the K5 hiPS cell line, while in the second the MH1C1 hiPS cell line was compared again to the K5 hiPS cell line.

After MS analysis, data was calculated using both the MaxQuant software v1.5.2.8 (Cox and Mann 2008) and Perseus v1.5.0.31 (http://www.biochem.mpg.de/cox). A combination of Student's t-test of the mean and Significance B was applied in both experiments. All the proteins overlapping in both experiments and of which ratio values were out of the methodological variation (Median: 0.83-1.2) were considered and all those that presented significant difference in translation ($P \leq 0.05$) are listed in Table 18.

Table 18. Proteins with deregulated translational rate in MEHMO patient-derived hiPSCs. Data summarizes results of two independent experiments. Each patient cell line indicated was compared with a control hiPS cell line.

Gene Name	Protein Name	Patient iPSC line	Median	Comparison of protein levels
APOE	Apolipoprotein E	MH1C1	1,609	Patient level higher than control
		MH1C3	1,768	
CRABP1	Cellular retinoic acid-binding protein 1	MH1C1	1,542	
		MH1C3	1,499	
H2AFX	H2A Histone Family Member X	MH1C1	1,481	
		MH1C3	1,465	
CBS	Cystathionine beta-synthase	MH1C1	0,498	Patient level lower than control
		MH1C3	0,409	
TKT	Transketolase	MH1C1	0,643	
		MH1C3	0,564	
FABP5	Fatty acid-binding protein, epidermal	MH1C1	0,812	
		MH1C3	0,731	
SLC2A3; SLC2A14	Solute carrier family 2, facilitated glucose transporter member 3 and 14	MH1C1	0,563	
		MH1C3	0,509	

SILAC is a very powerful mass spectrometry-based technique, which allows proteome comparison in a quantitative and global approach. The change of light to labelled amino acid medium permits the access of protein turnover. We cannot, however, determine specifically in which extend synthesis and degradation rate contribute to the final turnover rate measured with this procedure.

To be able to compare control and patient cells, a slightly different method was chosen. In this procedure, control hiPSCs received medium labelled medium, and patient hiPSCs were fed with heavy labelled medium. At the end of the incubation time, a mixture containing 1:1 ratio of those samples was analyzed. The reverse labelling was also applied and analyzed, to exclude any effect that differently labelled amino acids could have on the results.

Since eIF2S3 is, so far, not described to participate in any protein degradation process, the experimental design described above excludes any influence of differences in degradation rate. Being the degradation rates similar for control

and patient cells, the observed turnover was considered as a result of the difference in translational efficiency.

Patient-derived iPSCs global protein analysis provided evidences for an imbalance in the translation of some interesting proteins, namely APOE, CRABP1, H2AFX, CBS, TKT and FABP5. Literature research indicates their association by direct and indirect means with two processes clearly affected in the patients: neurogenesis and adipogenesis. Moreover, diverse lines of evidence underscore their diverse role in survival/proliferative and apoptotic pathways.

4.7. Differentiation of patient iPS cells into neurons

Aiming to compare gene expression during early stages of neuronal development, control and patient iPSCs were subject of a neuronal undirected differentiation (Figure 19). Samples from four stages resembling singular embryonic neurogenesis moments were collected, and expression pattern of genes that could be affected by *EIF2S3* mutation were analyzed.

The selection of genes was based on literature research and SILAC experiment results (Table 18). Besides, genes directly involved in initiation translation paths were selected, as well as pan-neuronal markers, which were used to show the successful differentiation of both control and patient cells.

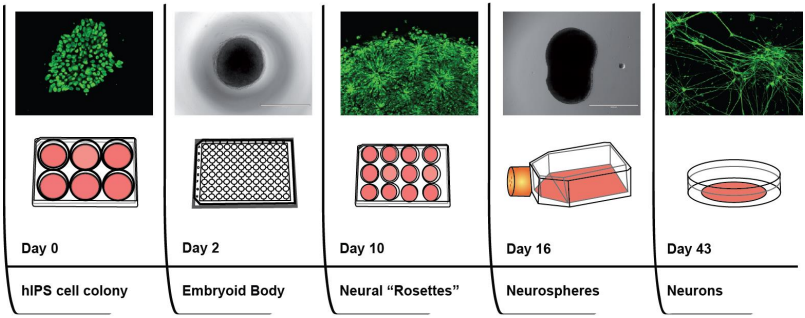

Figure 19. Scheme illustrating the culture steps of neuronal undirected differentiation. Immunofluorescence analysis showing staining against OCT4 (Day0), Nestin (Day 10) and TUBB3 (Day 43) (20X objective).

Primarily, no gross morphological differences were observed between control and patient lines in the different stages analyzed (Appendix – Figure A). Embryoid Bodies are hiPSCs aggregates that recapitulate, *in vitro,* the human pluripotent stage during embryogenesis, or blastocyst. Neural "rosettes" are epithelial cell structures possessing developmental parallel with the neural tube epithelium and a share very similar gene expression profiles. Neural stem cells (NSC) are multipotent cells capable of deriving as much neurons as glia cells and were present in the so called neurospheres.

4.7.1. Gene expression analysis throughout patient neuronal differentiation

To address the question of how the neuronal activity is impaired in the affected individuals, different stages of neuronal differentiation was analyzed via expression of neuronal markers and other selected candidates that might be MEHMO relevant. As undirected neuronal differentiation protocols yield a very heterogeneous neuronal population, Day 43 of differentiation was only stained using the neuronal marker TUBB3 (Appendix A - Figure A). Although hiPSCs, or Day 0, was already addressed in section 4.3., the data is shown once more to give an overview of expression fluctuation over the differentiation process. Thus, Days 0, 5, 11 and 22 were chosen for gene expression analysis and pattern of expression of the different target genes are shown below.

The first set of genes (Figure 20) are those selected due to their close relation to eukaryotic translation initiation factor 2 and the translation initiation process itself. In addition to the already observed change in *EIF2S2*, *EIF2S3*, *EIF2B4*, *EIF2B5* and *EIF4G1* expression on hiPSCs (Figure 11), no other significant discrepancy was detected during the course of neuronal differentiation, and all considered genes presented a very similar pattern of expression in both groups (patient and control).

As already described, among the SILAC candidates analyzed, APOE, CRABP1 and CBS hiPSCs mRNA levels confirmed the patient specific differentially expression that was seen in protein quantification (Table 18). Unlikely expected, patient TKT showed increased levels of mRNA. Besides that, CRABP1 and CBS exhibited same trend throughout neuronal differentiation significant at Day 5 of differentiation, for *CRABP1*, and at Day 11 for *CBS* expression (Figure 21).

The third group of genes (Figure 22) covered *MTOR*, a master translation regulator and two genes known to directly control special neuronal mRNA translation - *FMR1* and *CYFIP1*- (Figure 4). In addition, other genes which seem to be increased upon general translation suppression were selected, namely: *PPP1R15A* (Lee et al., 2009), *PPP1R15B* (Han et al., 2013), *ATF4* (Vattem and Wek, 2004) and *ATF5*. The latter being chosen due to its role in regulating neuronal progenitors proliferation and differentiation (Greene et al., 2009).

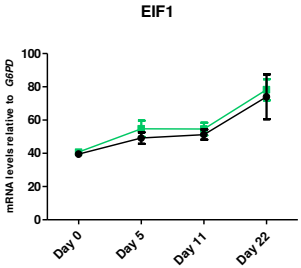
EIF1
mRNA levels relative to G6PD
100
80
60
40
20
0
Day 0
Day 5
Day 11
Day 22

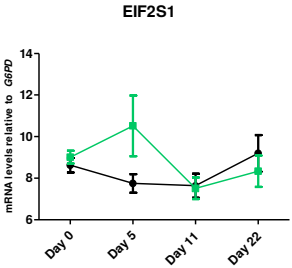
EIF2S1
mRNA levels relative to G6PD
14
12
10
8
6
Day 0
Day 5
Day 11
Day 22

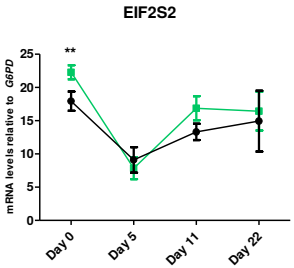
EIF2S2
**
mRNA levels relative to G6PD
25
20
15
10
5
0
Day 0
Day 5
Day 11
Day 22

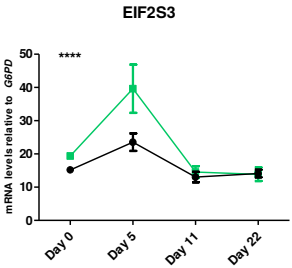
EIF2S3
****
mRNA levels relative to G6PD
50
40
30
20
10
0
Day 0
Day 5
Day 11
Day 22

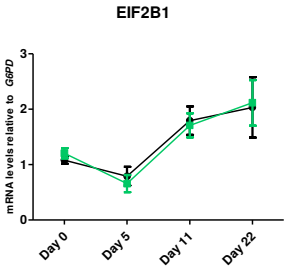
EIF2B1
mRNA levels relative to G6PD
3
2
1
0
Day 0
Day 5
Day 11
Day 22

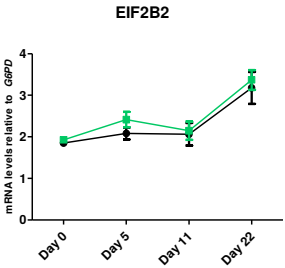
EIF2B2
mRNA levels relative to G6PD
4
3
2
1
0
Day 0
Day 5
Day 11
Day 22

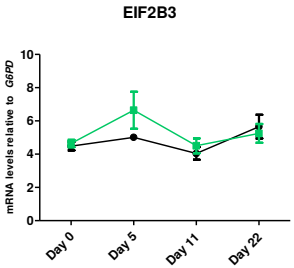
EIF2B3
mRNA levels relative to G6PD
10
8
6
4
2
0
Day 0
Day 5
Day 11
Day 22

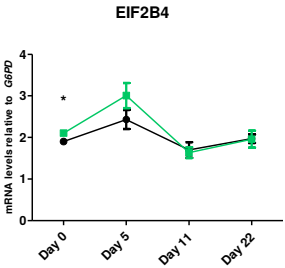
EIF2B4
*
mRNA levels relative to G6PD
4
3
2
1
0
Day 0
Day 5
Day 11
Day 22

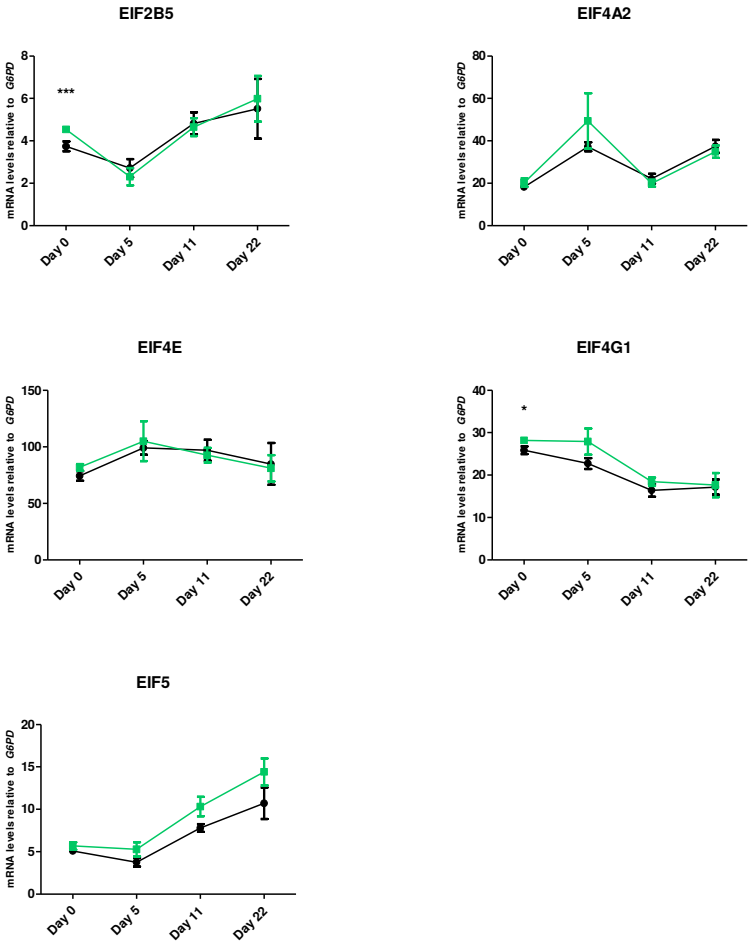

Figure 20. eIF2S3-related gene expression in patient (green) and control (black) early neuronal differentiation. The graph shows expression levels of hiPSCs (Day 0); embryoid body (Day 5); neuronal "rosettes" (Day 11); neural stem cells (Day 22). mRNA levels are relative to *G6PD* expression (Error bar = S.E.M.; P≤0.001****; P≤0.01***; P≤0.03**; P≤0.05*; P≤0.1 (*)).

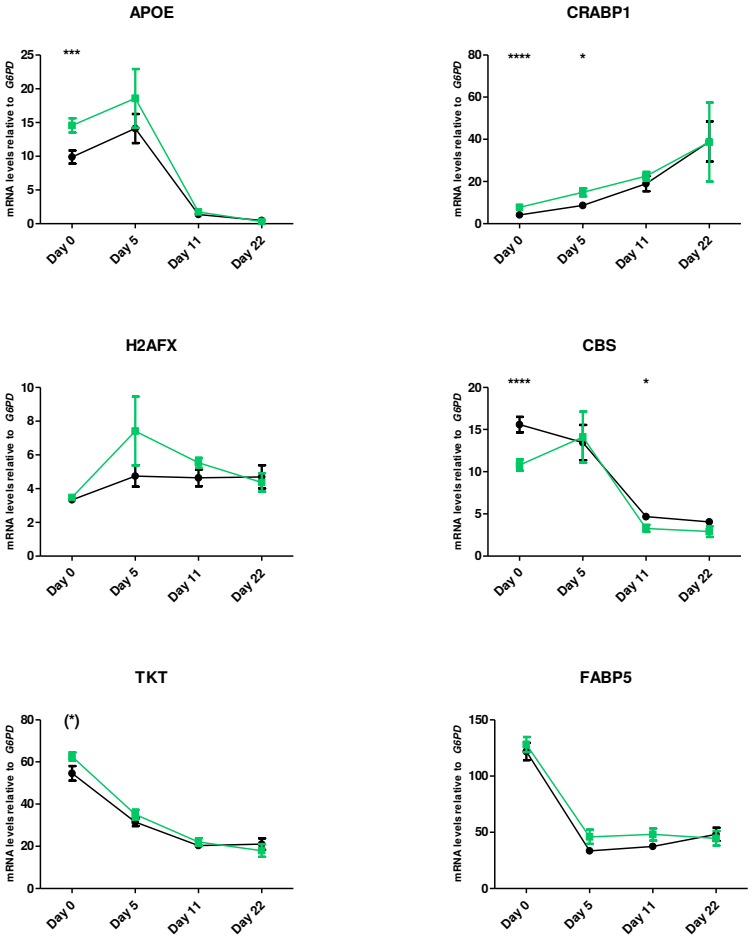

Figure 21. SILAC candidate gene expression in patient (green) and control (black) early neuronal differentiation. The graph shows expression levels of hiPSCs (Day 0); embryoid body (Day 5); neuronal "rosettes" (Day 11); neural stem cells (Day 22). mRNA levels are relative to *G6PD* expression (Error bar = S.E.M.; P≤0.001****; P≤0.01***; P≤0.03**; P≤0.05*; P≤0.1 (*)).

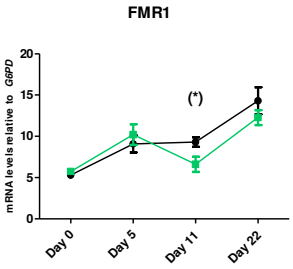
FMR1
mRNA levels relative to G6PD
20
15
10
5
0
(*)
Day 0
Day 5
Day 11
Day 22

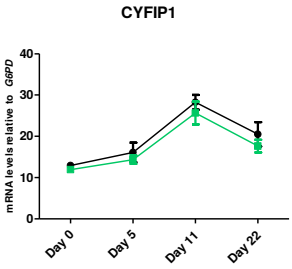
CYFIP1
mRNA levels relative to G6PD
40
30
20
10
0
Day 0
Day 5
Day 11
Day 22

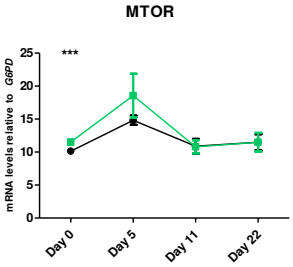
MTOR
mRNA levels relative to G6PD
25
20
15
10
5
0
***
Day 0
Day 5
Day 11
Day 22

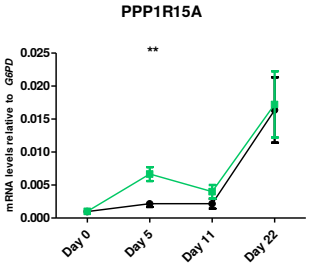
PPP1R15A
mRNA levels relative to G6PD
0.025
0.020
0.015
0.010
0.005
0.000
**
Day 0
Day 5
Day 11
Day 22

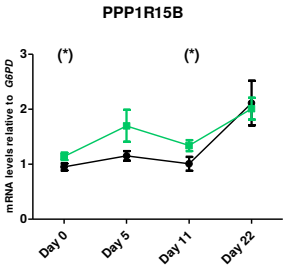
PPP1R15B
mRNA levels relative to G6PD
3
2
1
0
(*)
(*)
Day 0
Day 5
Day 11
Day 22

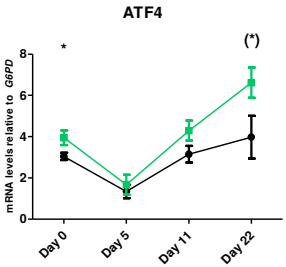
ATF4
mRNA levels relative to G6PD
8
6
4
2
0
*
(*)
Day 0
Day 5
Day 11
Day 22

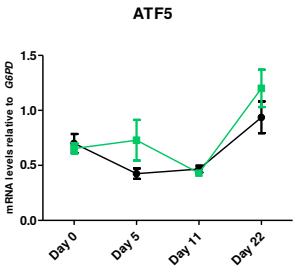
ATF5
mRNA levels relative to G6PD
1.5
1.0
0.5
0.0
Day 0
Day 5
Day 11
Day 22

Figure 22. Other translation-related gene expression in patient (green) and control (black) early neuronal differentiation. The graph shows expression levels of hiPSCs (Day 0); embryoid body (Day 5); neuronal "rosettes" (Day 11); neural stem cells (Day 22). mRNA levels are relative to *G6PD* expression (Error bar = S.E.M.; P≤0.001****; P≤0.01***; P≤0.03**; P≤0.05*; P≤0.1 (*)).

Besides CRABP1 and FABP5, other genes related to different RA homeostasis and signaling aspects were investigated. Among the selected: PPARD, RARB, STRA6, RBP1, CYP26A1, RDH10 and LRAT were differently expressed in at least one moment of neuronal differentiation (Figure 23).

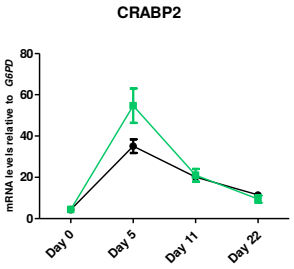
CRABP2
mRNA levels relative to G6PD
80
60
40
20
0
Day 0
Day 5
Day 11
Day 22

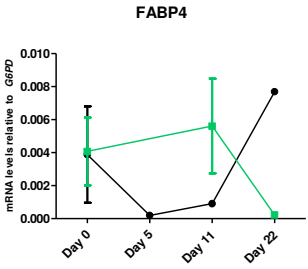
FABP4
mRNA levels relative to G6PD
0.010
0.008
0.006
0.004
0.002
0.000
Day 0
Day 5
Day 11
Day 22

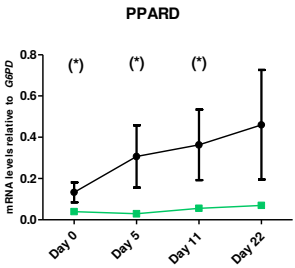
PPARD
mRNA levels relative to G6PD
(*)
(*)
(*)
0.8
0.6
0.4
0.2
0.0
Day 0
Day 5
Day 11
Day 22

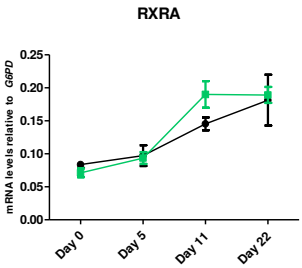
RXRA
mRNA levels relative to G6PD
0.25
0.20
0.15
0.10
0.05
0.00
Day 0
Day 5
Day 11
Day 22

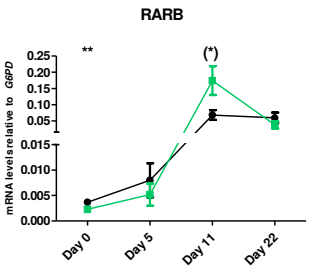
RARB
mRNA levels relative to G6PD
**
(*)
0.25
0.20
0.15
0.10
0.05
0.015
0.010
0.005
0.000
Day 0
Day 5
Day 11
Day 22

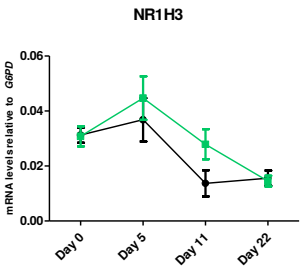
NR1H3
mRNA levels relative to G6PD
0.06
0.04
0.02
0.00
Day 0
Day 5
Day 11
Day 22

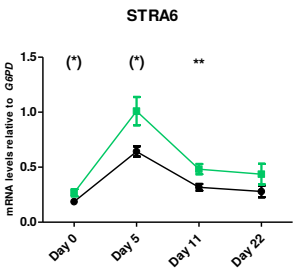
STRA6
mRNA levels relative to G6PD
(*)
(*)
**
1.5
1.0
0.5
0.0
Day 0
Day 5
Day 11
Day 22

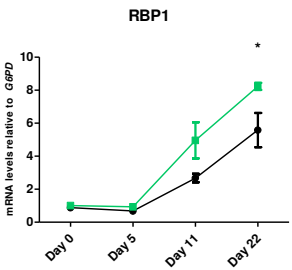
RBP1
mRNA levels relative to G6PD
*
10
8
6
4
2
0
Day 0
Day 5
Day 11
Day 22

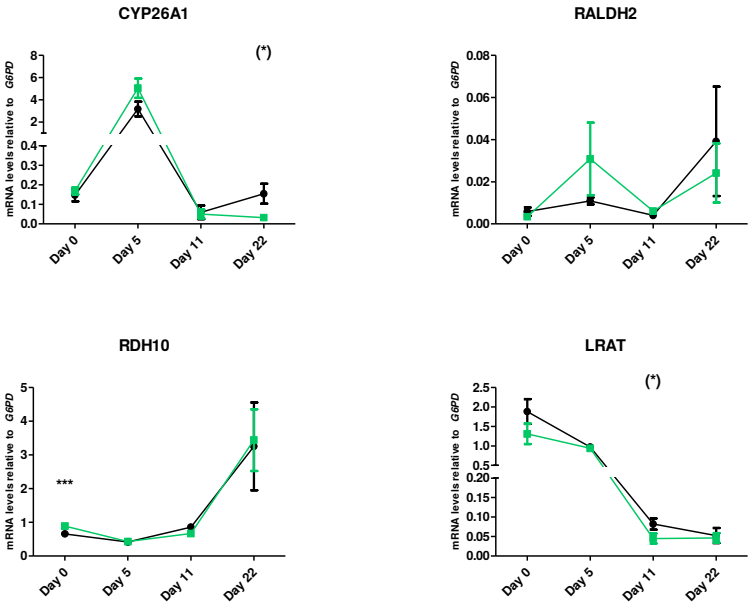

Figure 23. Retinoic acid-related gene expression in patient (green) and control (black) early neuronal differentiation. The graph shows expression levels of hiPSCs (Day 0); embryoid body (Day 5); neuronal "rosettes" (Day 11); neural stem cells (Day 22). mRNA levels are relative to *G6PD* expression (Error bar = S.E.M.; P≤0.001****; P≤0.01***; P≤0.03**; P≤0.05*; P≤0.1 (*)).

Based on the actions of CRABP1 (non-canonical) could have on apoptotic pathways, apoptosis-related gene expression of *DDIT3* and *BCL2* was investigated, but no changes were observed along neuronal differentiation (Figure 24).

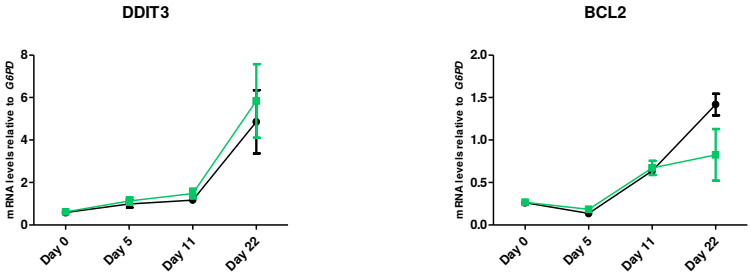

Figure 24. Apoptosis-related gene expression in patient (green) and control (black) early neuronal differentiation. The graph shows expression levels of hiPSCs (Day 0); embryoid body (Day 5); neuronal "rosettes" (Day 11); neural stem cells (Day 22). mRNA levels are relative to *G6PD* expression (Error bar = S.E.M.; P≤0.001****; P≤0.01***; P≤0.03**; P≤0.05*; P≤0.1 (*)).

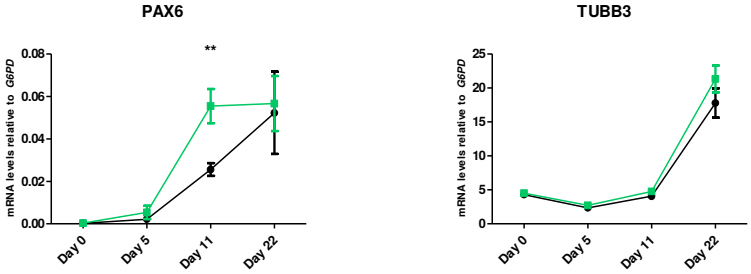

Figure 25. Pan-neuronal markers gene expression in patient (green) and control (black) early neuronal differentiation. The graph shows expression levels of hiPSCs (Day 0); embryoid body (Day 5); neuronal "rosettes" (Day 11); neural stem cells (Day 22). mRNA levels are relative to *G6PD* expression (Error bar = S.E.M.; P≤0.001****; P≤0.01***; P≤0.03**; P≤0.05*; P≤0.1 (*)).

Finally, despite the absence of significant differences in most of the genes analyzed, it is possible to note that patient and control groups present, overall, a very similar trend of expression during the course of differentiation. Furthermore, similar patterns of neuronal marker expression- TUBB3 and PAX6 (Figure 25) indicates for the robustness of the differentiation protocol used.

5. Discussion

Although transcription and translation rates frequently correlate, higher expression of a particular gene does not necessarily mean subsequent and proportional increased functional protein synthesis (Vogel and Marcotte, 2012). Thus, it is relevant to emphasize that effective gene expression can be followed by reduced levels of the relative protein via different mechanisms, such as direct degradation of mRNA/protein, or even selective translation, favoring certain mRNA compositions.

Aiming a more comprehensive view about how gene expression is affected in patients and to further assess whether SILAC candidate proteins (Table 18) presented comparable regulation on mRNA levels, RNA from patient and control iPS cells were extracted and analyzed by qRT-PCR (Figure 11 and Figure 12).

Concerning *EIF2S3* and *EIF2S2* increase in expression in patient-derived iPSCs (Figure 11), it is noteworthy to mention that an overexpression of *EIF2S2* in *EIF2S3* mutated yeast restored cellular growth (Borck et al., 2012). This study also showed that human eIF2S3 is interacting with both eIF2S1 and eIF2S2, and that *EIF2S3* mutation compromises eIF2S2 – eIF2S3 binding. Thus, an increase in *EIF2S2* expression could compensate for this interaction inefficiency, also in human cells. Furthermore, both EIF2B4 (δ subunit) and EIF2B5 (ε subunit), also significantly increased in patient cells (Figure 11) are interacting with eIF2S2 (Kimball et al., 1998) and the interface eIF2S2 –eIF2S3 contact with eIF2B5 has been reported as critical for the nucleotide exchanging role of eIF2B complex (Mohammad-Qureshi et al., 2007). By that line of reasoning, a slight increase in *EIF4G1* could also be related to the improve of translational machinery efficiency, since eIF4G1 is participating in the activation of eIF4E and in the formation of eIF4F complex to bind the cap- structure (Shveygert et al., 2010). Moreover, *EIF4G1* overexpression is associated to tumor progression, as its knock-down causes a decline in cell proliferation (Tu et al., 2010).

Patient aberrant expression correlated with SILAC candidate genes *APOE*, *CRABP1* and *CBS*, while *TKT* presented a significant inverse correlation (Figure 12). Moreover, significant higher expression of genes correlated to cell response

to global translation rates (*MTOR*, *PPP1R15B*, *ATF4*) were detected along with an enhance in key genes of retinoic acid metabolism (*STRA6*, *RDH1*0)*.*

Patient and control iPSC lines were subjected to an undirected neuronal differentiation. The continuously increasing expression of neuronal markers (Figure 25) indicates successful differentiation towards neuronal lineages. Besides this, all genes considered MEHMO-candidates were scrutinized along the differentiation process (section 4.7.1), and in the following sections their possible pathophysiological roles will be addressed.

5.1. Eukaryotic translation initiation factor 2 subunit 3 and retinoic acid

The patient significant and orchestrated increase in mRNA and protein levels of APOE and CRABP1 combined with lower FABP5 protein levels suggest a possible involvement of a common factor in the disease mechanism, namely retinoic acid (RA). Intriguingly, extensive literature research provides numerous cases of neurodevelopment impairment attributed to deregulated RA metabolism (Berry et al., 2012; Berry and Noy, 2009; Berry et al., 2010; Choi et al., 2014; Cohen et al., 1999; Corcoran et al., 2002; Huang et al., 2011; Jacobs et al., 2006; Krezel et al., 1998; Latasa and Cosgaya, 2011; Olson and Mello, 2010; Sandell et al., 2007; Shenefelt, 1972; Yu et al., 2012). The tightly regulated cellular response to RA gives a hint about the importance of such signaling, and lack of some important RA metabolic enzymes, receptors, or transporter proteins could irretrievably affect RA physiological homeostasis. How *EIF2S3* mutation favors translation of those proteins and whether RA is in center of this process remains unknown.

5.1.1. Cellular retinoic acid binding proteins

The control of the intracellular concentrations of RA is regulated at several levels of its metabolism. Vitamin A, the RA precursor, is mainly stored in the liver as retinyl esters, which are metabolized by hepatic enzymes to retinol and transported via blood stream bound to RBP4. Retinol is internalized by cells and further metabolized to RA in a process involving several enzymes and transporter proteins. Besides, reversible catalysis in RA synthesis, the control of gene

expression and generation of RA metabolites are of extreme importance in regulating cytoplasmic and nuclear RA levels.

Among the regulatory systems, maintenance of plasma steady levels is possibly the most relevant, since changes in vitamin A intake affect mainly hepatic retinyl esters storage, while retinol levels are maintained steady, allowing therefore a constant concentration of cellular available RA (Batres and Olson, 1987).

A special class of binding proteins, the cellular retinoic acid binding proteins (CRABP) belong to the very last steps of RA metabolism in the cytoplasm. CRABP proteins are essential in RA signaling pathways, but despite their shared RA binding feature and their common role in diminishing cytoplasmic concentration of RA, CRABP family members (CRABP1 and CRABP2) present singularities that have been studied in the past decades.

The aforementioned decrease in RA cytoplasmic levels by CRABP proteins is caused via two different mechanisms: transport into the nucleus by CRABP2, activating diverse receptors, or catabolism, due to the action of two proteins, the enzyme *CYP26* (Hernandez et al., 2007) and the carrier CRABP1 (Won et al., 2004).

CRABP1 (Canonical role)

Although no activation of retinoid receptors (RARs and RXRs) by direct function of CRABP1 has been reported (Venepally et al., 1996), its role in controlling RA intracellular concentrations has been shown (Napoli, 1993; Wei et al., 1999). Others also demonstrated a direct correlation of higher CRABP1 expression and higher levels of RA metabolites in carcinoma cells (Boylan and Gudas, 1992; Won et al., 2004). In accordance with the idea that CRABP1 is controlling cytoplasmic concentrations of RA, and therefore the amounts of available nuclear RA, CRABP1 overexpression produced a reduced cellular response to RA in F9 stem cells and head carcinoma (Boylan and Gudas, 1991; Won et al., 2004). To assess whether CRABP1 is also able to facilitate RA signaling, Wei and colleagues (Wei et al., 1999) generated lower RA-affinity CRABP1 to compare with the wild type protein. The experiment detected a biphasic effect of CRABP1, in which higher levels of wild type CRABP1 would increase RA nuclear receptor induction in a first phase, while in a posterior moment a decrease in this induction was reported.

This report raised the question whether CRABP1 would have other functions aside from mediating RA catabolism.

RA roles in stem cell fate was investigated and, differently from F9 cell line, which is induced by RA to form endodermal tissue (Strickland and Mahdavi, 1978), exposure of P19 to RA resulted in different cell types, including some of neuronal origin (Kanungo, 2016). Thus, the sensitivity to RA seems to differ among cell types. Also contrarily to F9, P19 presents augment of CRABP1 levels following RA treatment (Means et al., 2000), illustrating again CRABP1 function in regulating RA nuclear levels.

Since RA bound to CRABP1 has a more significant increase in catabolism than free-RA (Napoli, 1993), cells expressing this binding protein might do so, as a protection measurement in order to bring RA levels to physiological concentrations. Taking this into consideration, it is possible that higher levels of CRABP1 in patient iPSCs (Figure 12 and Table 18) is causing a slight deregulation on retinoid levels, as other genes related to increase of cellular RA precursors levels were up-regulated in patient (Figure 12). Therefore deregulated levels of RA, due to increased CRABP1, could produce deleterious effects during patient early development, as e.g. STRA6, a cellular retinol uptake protein is maintained elevated along neuronal differentiation (Figure 23).

A possible CRABP1 role in neurogenesis is supported by the unquestionable RA activity in neuronal development (Janesick et al., 2015), and by the observation that both CRABP1 and CRABP2 transcripts distribution in embryogenesis exhibited a strong increase in expression during neural crest cells migration and in neural epithelium in mice (Leonard et al., 1995; Ruberte et al., 1991). Therefore, the neurodevelopmental aspect of MEHMO syndrome reveals that CRABP1 might be an interesting study target to unveil unexplored paths of neurogenesis.

Despite CRABP1 and CRABP2 being highly conserved, both CRABP1- and CRABP1/CRABP2 null mutant mice did not present overt malformations (Gorry et al., 1994; Lampron et al., 1995). However, it is important to note that besides the difficulties in evaluating mouse phenotype, which are sometimes only evident under special conditions, the absence of several genes can be compensated in some species, while are disease causative, or even lethal in others (Barbaric et

al., 2007). Furthermore, a severe intellectual disability syndrome in the *CRABP1* chromosomal region (15q24) was reported in members of a consanguinity Pakistani family (Mitchell et al., 1998) which seems to inherit the condition in a recessive manner. Finally, differently from null mutations where the protein, if present, does not accomplish its function, gene overexpression may result in a completely different phenotype. In contrast to the previously mentioned absence of phenotype in CRABP1 null mice, and resembling what is observed in patients regarding enhanced CRABP1 expression, a transgenic mice overexpressing bovine CRABP1 produced only sterile female offspring that presented severe development phenotype in a variety of organs where the protein was expressed (Wei et al., 1992).

CRABP1 (Non-canonical role)

Apart from CRABP1 canonical function, a very recent role has been described for this molecule, in which its intriguing association to protein synthesis is noticeable. Instead of controlling intracellular levels of RA, via RA delivery to catalytic enzymes from cytochrome P-450 family, CRABP1 was shown to exhibit an ERK1/2 phosphorylation activity via binding of RA when examining embryonic stem cells (Persaud et al., 2016). With a high level of complexity, ERK1/2 signaling possesses opposing effects depending on its localization and strength of activation signal (Wortzel and Seger, 2011), so it can act promoting both proliferative and apoptotic responses. During CRABP1-mediated ERK1/2 phosphorylation, an increase in Bax/Bcl-2 protein ratio was observed, resulting in an apoptotic increment, also perceived by the growth of protein phosphatase 2A (PP2A) activity, a tumor suppressor protein.

Knowing that PP2A negatively regulates eIF4E phosphorylation (Li et al., 2010b), an activation of PP2A would ultimately produce a decrease in cap-dependent translation initiation. In this scenario, MEHMO patient cells translation would certainly be aggravated.

Cells exposed to extreme situations require an immediate response, as for example due to nutrient deprivation. Thus, it is natural to assume that translation might be coupled with apoptotic mechanisms, responding to sudden changes in cell physiology. In fact, diverse translation inhibitors have been long associated

to cell death by activation of Bcl-2 family apoptotic pathways (Lindqvist et al., 2012; Narayanan et al., 2005). Thus, a global translation decrease, as hypothesized here for MEHMO syndrome, is likely leading to activation of apoptotic pathways, which are not necessarily executed, since the apoptosis-triggering signal could be counterbalanced by other regulatory mechanisms, considering that even late stage apoptosis can be reversible (Tang et al., 2012). Thereupon, future apoptosis assay would be interesting to assess whether patient cells are prone to suffer apoptosis, due to CRABP1 higher levels of expression. A slight glance on it was done through the analysis of two apoptosis-related gene expression (*BCL2* and *DDIT3*). Although patient BCL2 and DDIT3 (CHOP) mRNA levels were comparable to control in all stages (Figure 24), it would be interesting to check for protein levels, since CRABP1 was described to decrease protein levels of BCL2, while its transcription was unaffected (Persaud et al., 2016).

Finally, it is possible that CRABP1/RA exerts particular roles in different tissues and/or embryo development stages, as *CRABP1* was reported to have two enhancers, one upstream of the gene, regulating its expression in the neural region, and another one responsible for mesenchymal and neural crest expression, located downstream from exon II (Kleinjan et al., 1997). Studies in different cancer cells produced conflicting data. Tanaka *et al.* (Tanaka et al., 2007) found the gene to be silenced in carcinoma cells and restoration of its expression led to a decrease in growth, by inducing cell cycle arrest. The gene knock-down, on the other hand, induced the opposite effect, supporting CRABP1 non-canonical role. Contrarily, the gene was found to be up-regulated in ovarian cancer (Banz et al., 2010) and responsible for increasing metastatic activity in mesenchymal and neuroendocrine tumors (Kainov et al., 2014).

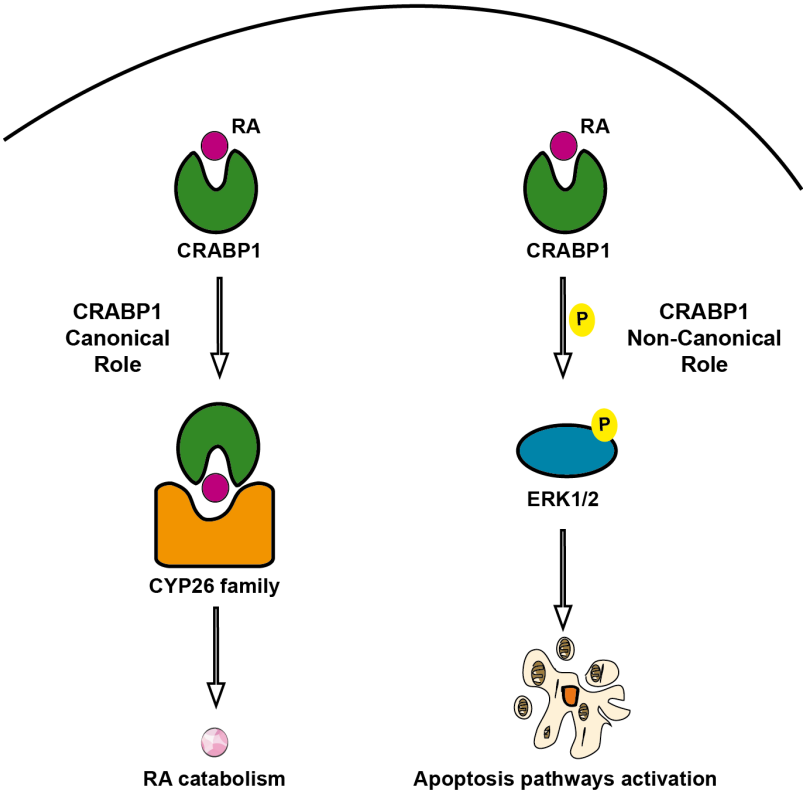

Figure 26. Simplified schema of CRABP1 roles demonstrating the activation of retinoic acid (RA) catabolic reaction (canonical) and the mediation of apoptosis via ERK1/2 phosphorylation (non-canonical) by binding of RA.

5.1.2. CRABP2 and FABP5 (Lipid binding proteins)

Both cellular retinoic acid binding protein 2 (CRABP2) and fatty acid binding protein type 5 (FABP5) are lipid binding proteins known to present RA to specific nuclear receptors, enabling the regulation of distinct cohort of target genes. Thus, according to the abundances of these molecules RA can mediate different effects. A sophisticated control mechanism of cell apoptosis and survival was proposed when investigating the targeting of different nuclear receptors by RA in skin tissue (Schug et al., 2007). In contrast to the catabolic effects caused by RA activation of retinoic acid receptors (RAR), the activation of peroxisome proliferator-activated receptor β/δ (PPARβ/δ) by RA produces an anti-apoptotic cellular response. The RA receptor selection was described as depending on the balance of the two early mentioned RA delivery proteins, CRABP2 and FABP5. These transporter proteins have the ability to bind RA and deliver it specifically to RAR and PPARβ/δ, respectively. Thereby, being CRABP2/FABP5 ratio high, RAR activation path is favored, while a low ratio supports PPARβ/δ activation and therefore, anti-apoptotic effects. A binding assay still revealed that the association of RA to CRABP2/RAR in comparison to FABP5/PPARβ/δ is higher in most cells, meaning that for a relevant PPARβ/δ activation to occur, a low CRABP2/FABP5 is needed (Schug et al., 2007).

In addition to its anabolic effect on skin, FABP5 was reported as an essential factor on neurite growth (Allen et al., 2000). Analysis of rat FABP5 (E-FABP) mRNA and protein expression patterns showed high expression levels during the whole process of brain development (Liu et al., 2000). Recent work associated FABP5 and CRABP2 with RA signaling in neurogenesis by investigating their expression pattern and correspondent pathways activation throughout neuronal differentiation (Yu et al., 2012).

Furthermore, PPARβ/δ is the most abundant isotype expressed during nervous system development (Braissant et al., 1996). Its in vitro selective activation caused significant increase in late maturation of mice oligodendrocytes, produced anti-apoptotic effects (Saluja et al., 2001) and, along with FABP5, PPARβ/δ seems to be important for neurite outgrowth (Benedetti et al., 2015).

Although not highly significant, our control group presented a constant increase in PPARβ/δ expression throughout neuronal differentiation, while patient cells

showed a relatively constant low expression (Figure 23). In this regard, it is worth mentioning that down-regulation of FABP5 reduced PPARβ/δ expression (Yu et al., 2012), and that MEHMO FABP5 protein levels were lower in comparison to control cells, at least at the hiPSCs stage. However, it remains elusive whether or not the patient low levels of FABP5 protein is maintained throughout neuronal development.

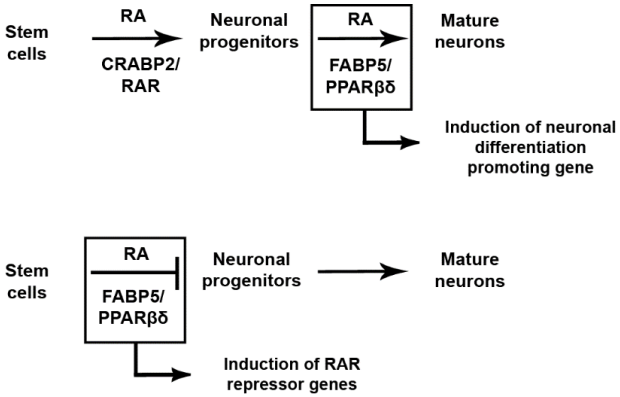

Figure 27. Retinoic acid (RA) activation and repression roles in neuronal differentiation gene regulatory network. Balance between RA-binding proteins CRABP2 and FABP5 determine to which nuclear receptor (RAR and PPARβ/δ, respectively) RA is being delivered. CRABP2/FABP5 ratio is therefore determining whether to induce neuronal progenitor formation or neuronal maturation. The two highlighted boxes might be under-activated in MEHMO patients, when FABP5 protein are kept under normal levels, in comparison to CRABP2.

Based on Yu et al., 2012, the scheme above (Figure 27) shows the effects caused by RA delivery and activation of RAR and PPARβ/δ in different time points of neuronal differentiation. Similarly to CRABP2, a transient up-regulation of RARβ is also observed during the early phase of neurogenesis, and this effect was also observed in the course of our differentiation (Figure 23).

A mechanism to control differentiation rate is operating by the increase of FABP5/CRABP2 ratio, which impairs neuronal progenitor formation and consequently neurogenesis. In a late phase of the differentiation process the down-regulation of CRABP2 is stimulating neuronal maturation, by allowing

FABP5 induction of *PDK1* expression, a gene which promotes neuronal maturation. Interestingly, FABP5 knock-out mice displayed expansion of progenitor markers, while presenting lower levels of mature neurons in comparison to wild-type mice (Yu et al., 2012). Thus, in case the correspondent FABP5 protein deficiency in MEHMO patient iPSCs is maintained throughout development, the two highlighted steps (Figure 27) might be kept suppressed during patient neuronal differentiation, causing CRABP2/FABP5 ratio imbalance with expected increase in patients neuronal progenitors population and poor maturation.

Finally, we found it interesting that RARβ presented higher expression levels in patient (Figure 23). This could also characterize an increased number of progenitors, fitting to the elevated levels of PAX6 at the same stage of differentiation - Day 11 - (Figure 25), once PAX6 is known for promoting neural stem cell self-renewal in a dose-dependent way (Sansom et al., 2009).

Anandamide signaling

Another pathway stimulating neurogenesis and, in which FABP5 could be involved with, is that of anandamide. Anandamide was first identified as a cannabinoid receptor agonist in porcine brain (Devane et al., 1992) and its metabolites (ethanolamine and arachnoid acid) were described as hydrolytic degradation products (Di Marzo et al., 1994). Findings on anandamide carriers, namely FABP5 and FABP7, explained how the molecule is able to move within the hydrophilic cytosol, since it is presenting a lipophilic character. In addition to transport anandamide, the carries were found to increase the hydrolysis rate of the molecule (Kaczocha et al., 2009).

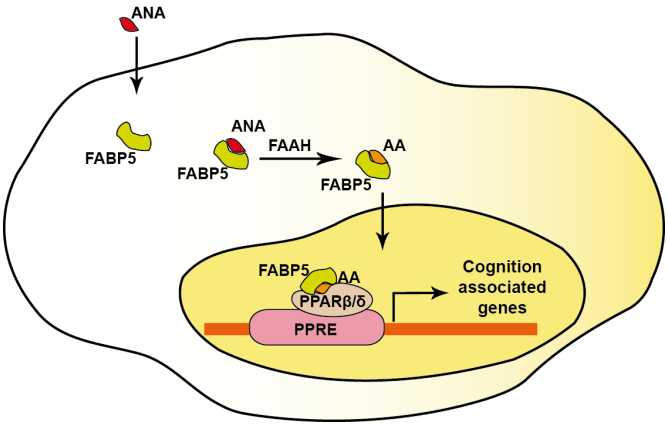

Figure 28. Anandamine signaling highlighting the action of FABP5 transport protein in anandamine metabolism and cognition associated genes activation, via delivery of arachidonic acid to PPARβ/δ nuclear receptor. Legend: ANA: Anandamine; FABP5: Fatty Acid-Binding Protein 5; FAAH: Fatty Acid Amide Hydrolase; AA: Arachidonic Acid; PPARβ/δ: Peroxisome Proliferator-Activated Receptor; PPRE: PPRA responsive element. (Adapted from (Yu et al., 2014)).

Besides activating cannabinoid receptors itself, anandamide metabolic product, arachnoid acid, presents an agonistic activity in relation to PPARβ/δ nuclear receptor in brain, up-regulating cognition associated genes (Yu et al., 2014). FABP5 transporter directly delivers arachnoid acid to PPARβ/δ nuclear receptor, being ultimately responsible for regulation of receptor activity, and consequently its cognition associated target genes expression (Yu, et al., 2014). Furthermore, the transcriptome of a cell line expressing high levels of FABP5 and treated with a selective PPARβ/δ agonist generated a list of possible target up-regulated genes, many of those involved in neuronal functions, including learning and memory processes (Yu et al., 2014) (Figure 28).

Thus, being FABP5 decreased in patient-derived iPSCs (Table 18), and PPARβ/δ expression reduced during neurogenesis (Figure 23), the maintenance of lower levels of these factors in mature neurons may compromise regulatory downstream process.

5.1.3. Apolipoprotein E, retinoic acid and lipids metabolism

Apolipoprotein E (APOE) functions as a binding protein carrying hydrophobic molecules, such as cholesterol and retinyl esters, throughout the circulatory system. Being a ligand of membrane receptors, such as low density lipoprotein receptor (Havel, 1998), APOE mediates uptake of chylomicron remnants and other lipoprotein particles by hepatocytes and regulates their traffic in diverse tissues.

Nervous system

Cholesterol, essential for membrane integrity, myelin production and proper neuronal development, is highly enriched in brain, where its binding protein APOE is also greatly expressed. Thus, it is logical to assume that APOE plays a role in cholesterol homeostasis, and that disruptions in this homeostasis caused by APOE could affect brain health and development (Dietschy, 2009). Therefore, APOE has been subject to extensive analysis and its different isoforms proved to influence the onset and progress of cardiac, Alzheimer´s and other neurological diseases in different ways (Mahley, 2016).

Along with cholesterol, RA is a fundamental substance for brain development and its precursor is likewise transported by APOE. Exclusively obtained via diet, vitamin A is absorbed as retinyl esters in the intestinal mucosa and incorporated into chylomicron remnants, which also consist of APOE. APOE mediates chylomicron remnants uptake in hepatocytes and retinyl esters are stored in its major storage, the stellate cells. As RA precursors cannot be synthetized, their uptake and transfer is of utmost importance to life (D'Ambrosio et al., 2011).

As earlier noted, APOE high expression in brain, mostly in glia cells, is long known (Boyles et al., 1985). The development of a transgenic mice expressing fluorescent tag enabled a sensitive description of APOE pattern of expression in CNS, and detected hippocampal neurons expression upon injury, in addition to high expression in cells belonging to choroid plexus and smooth muscle from the CNS vessels (Xu et al., 2006).

Membrane composition and other associated features, as fluidity and permeability are highly influenced by the amount of cholesterol. In brain, this

essential component is mainly glial-derived and, as before mentioned, transported by APOE. Notably, cholesterol and APOE are playing a role in synaptic maturation and activity (Dietschy, 2009; Mauch et al., 2001; Oh et al., 2010). Regardless of numerous studies indicating the negative influence of APOE4 isoform on spine formation and dendritic complexity (Dumanis et al., 2013; Dumanis et al., 2009; Jain et al., 2013; Ji et al., 2003; Klein et al., 2010; Nwabuisi-Heath et al., 2014; Rodriguez et al., 2013), a report of APOE absence in patient questions whether lack of APOE could have any neurological effect, since excepting dyslipidemia, patient presented no obvious CNS abnormality. Normal neurogenesis might indicate that another mechanism could replace the role of APOE during development, but as also highlighted by the authors, a progressive neurodegeneration is not excluded, and therefore a patient follow up is imperative (Mak et al., 2014).

In addition to membrane composition, equally important is the role of cholesterol in myelin production, where it is required in higher concentrations (Saher et al., 2005). Herein, the demonstrated up-regulation of APOE upon neuron injury is also interesting, since APOE is believed to assist myelin production following injury by increasing myelin debris clearance and Schwann cholesterol uptake in the PNS (Fagan et al., 1998; Goodrum, 1991; Li et al., 2010a). Besides that, APOE polymorphism is associated to differences in myelin content (Bartzokis et al., 2006; Dean et al., 2014).

Due to its interesting roles in the homeostasis of both retinoic acid and cholesterol, APOE expression has been widely studied. The gene presents multiple and complex regulatory elements, that can be specialized for different tissues. Several transcription factors, including nuclear receptors have been unveiled, but a lot of specificities are still uncovered (Allan et al., 1995; Berg et al., 1995; Garcia et al., 1996; Grehan et al., 2001; Liang et al., 2004; Paik et al., 1988; Shih et al., 2000; Smith et al., 1988; Yue and Mazzone, 2009; Yue et al., 2004; Zhao et al., 2014a; Zheng et al., 2004).

Different studies identified APOE among RA responsive genes, when analyzing both neural stem cells and astrocytes cultures (Cedazo-Minguez et al., 2001; Jacobs et al., 2006; Zhao et al., 2014a). Additionally, a neuronal specific cholesterol metabolite induced astrocytes APOE protein synthesis in a dose-

dependent manner, suggesting a link between neuronal metabolism and glial cholesterol supply that could perfectly influence neuronal synaptic plasticity (Abildayeva et al., 2006). But, as observed by Göritz and colleagues, an exorbitant secretion of APOE could deplete the cholesterol availability, impairing both synaptic function and nerve regeneration (Goritz et al., 2002).

Considering the apparent lack of phenotype in the absence of APOE, the gene induction upon brain injury, and the different synaptic plasticity modelling caused by each APOE isoform, we could hypothesize that more than its absence, APOE abnormal up-regulation could bring deleterious developmental and neuronal effects.

As mentioned earlier, APOE can have tissue-specialized regulatory elements, thus it is difficult to know how APOE protein levels are being controlled along differentiation. In one hand, it could be that the lack of differential expression between patient and control during neuronal differentiation (Figure 21) reflects what is also seen at protein level in these stages. On the other hand, an uncoupled transcription and translation control of APOE levels could take place and, as consequence, APOE protein could be increased during patient neurogenesis, as a result of a preferred translation mechanism, for example.

As delayed myelination and ataxia gait can be found on MEHMO patients, it would be interesting to investigate the effects that up-regulation of APOE, in its three genotypes, could have on white matter formation, by examining myelinating oligodendrocytes and Schwann cells differentiation.

To conclude, a direct link between APOE and translational mechanism in neurons is presented by Segev and colleagues in two studies where they observed human APOE4 inducing growth of eIF2S1 phosphorylation rates in mice brain and also increasing levels of ATF4, when compared with APOE3 (Segev et al., 2015; Segev et al., 2013).

Cardiovascular system and obesity

Apart from patient neurological dysfunction, obesity, diabetes and dyslipidemia might be considered in the context of patient iPSCs high levels of APOE (Figure 12 and Table 18).

Interestingly, besides development of hypercholesterolemia, APOE -/- mice

hallmarks are their lower propensity to gain weight and smaller adipocytes, probably due to their inability to take up fat via APOE. APOE adipogenic induction was long addressed in mice and human studies demonstrating a specific role of APOE in internalization of lipoproteins and differentiation of preadipocytes (Chiba et al., 2003; Huang et al., 2006; Lasrich et al., 2015). Although Chiba et al. 2003 showed an increase in adipogenesis via APOE bound to VLDL, Huang et al., 2006 questioned this finding, showing that adipocytes devoid of APOE are unable to increase their lipid content in presence of APOE bound to lipoproteins. In order to investigate a possible and specific role that adipocyte APOE expression could have on adipogenesis and obesity development, a tissue-target experiment model was applied and revealed that adipose tissue APOE deficiency was not sufficient to reduce lipid content and avoid adipogenesis (Wagner et al., 2015), demonstrating that other APOE sources, rather than adipocyte expressing cells, might compensate this lack of tissue endogenous APOE expression.

Besides APOE fat accumulation role, investigations on glucose metabolism indicated that lack of APOE improve glucose tolerance and insulin sensitivity (Gao et al., 2007; Hofmann et al., 2008; Karagiannides et al., 2008).

In line with these observations, mouse expressing human APOE became obese and exhibited hyperglycemia and glucose intolerance (Karagiannides et al., 2008). Additionally, overexpression of human APOE in mice and rabbits resulted in increased plasma levels of cholesterol and triglycerides (Huang et al., 1999; Huang et al., 1998). This could indicate a stronger predisposition of human APOE to induce these symptoms in comparison to its rat orthologue (Shimano et al., 1992; Yamamoto et al., 1995), and that APOE effects are highly dose-dependent, as also demonstrated by Huang and colleagues (Huang et al., 1998).

Unexpectedly, however, results from an investigation on APOE overexpression showed that high levels of APOE expression in human adipocytes was not correlated to increase in cell lipid accumulation. In spite of that, the aberrant overexpression, producing large amounts of APOE, converted adipocytes into cells more resistant to serum deprivation and increased their proliferative capacity (Carmel et al., 2009). This acquired cell characteristic could be examined from the perspective of translation impairment in MEHMO syndrome, in which a mutation in a key translation machinery factor leads to APOE increased

transcription and translation. Furthermore, nutrition/serum deprivation was associated to increase in APOE levels in different cell types (Do Carmo et al., 2002; Huang et al., 2007), showing again a correlation between decreased translation cell state and higher amounts of APOE. Added to starvation-induced growth arrest, apoptosis activation also promoted APOE up-regulation in mRNA and protein levels (Quinn et al., 2004).

In line with all these evidences, ovarian, breast and prostate cancer cells studies revealed an overexpression APOE, while APOE increased plasma concentrations was shown to associate with metastasis in lung cancer patients (Chen et al., 2005; Luo et al., 2016; Papi et al., 2012; Venanzoni et al., 2003).

Thus, it is tempting to speculate that the APOE increment observed in MEHMO patient could be a coping mechanism to increase cell division capacity, against the translation impairment imposed by *EIF2S3* mutation. Herein, it is also interesting to consider APOE previously mentioned role in acting upon brain injury. This could be another indication of a cell response connecting APOE to translation. Whether neurons may activate pro-survival pathways via APOE expression, and whether APOE isoforms and dose-dependence play relevant roles remain open questions.

Also regarding MEHMO patient phenotype, it is plausible to question whether hyperglycemia, dyslipidemia and obesity observed are correlated to the detected higher APOE levels, and whether an increase in cell proliferation during adipogenesis is the major contributor for obesity, being hypertrophy of adipocytes a less prominent factor.

Still in agreement with the idea of APOE being related to translation and, as seen for APOE4 genotype in brain (Segev et al., 2015; Segev et al., 2013), APOE deficient lipoproteins were also shown to induce phosphorylation of eIF2S1, decrease global translation and up-regulate ATF4 in macrophages (Wu et al., 2008). This difference in APOE isoforms could be one of the reasons why MEHMO syndrome displays variable expressivity. Therefore, it would be interesting to investigate which APOE alleles patient and control individuals inherited.

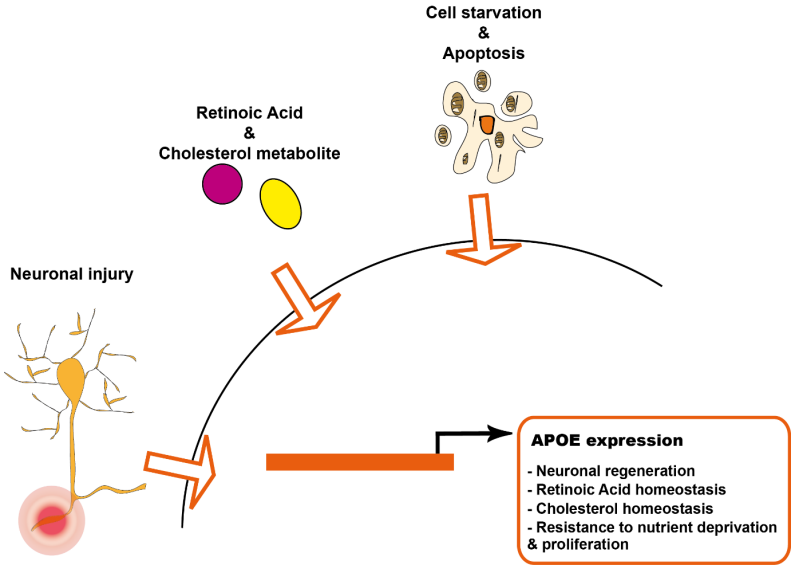

Figure 29. Summary schema of APOE expression inducers and the postulated consequences of APOE expression.

EIF2S3 misexpression and APOE

We could observe a successful overexpression of *EIF2S3* already after 24h of DOX treatment; however, a correlation with protein increase was detected after 48h DOX treatment, with higher levels of WT protein being translated in comparison to the mutated form (Figure 14 and Figure 15). Between transcription and translation of a gene, there are multiple levels of regulation, which will ultimately determine whether or not these two processes are coordinated. Among these regulatory mechanisms, mRNA and protein stability could perfectly differ between WT and MUT forms. Another point to be considered is that eIF2S3 is itself part of a protein complex, directly controlling translation initiation and therefore, its mutation might implicate in differential protein translation of mRNA strictly dependent on ternary complexes, including its own synthesis. APOE transcription was only increased upon overexpression of the MUT *EIF2S3* (Figure 14). This interesting effect resembles what is seen in MEHMO patient, once the patient eIF2S3 is causing enhanced levels of APOE transcripts. Nonetheless, the

expected increase in protein levels, such as observed in patient cells, was not apparent, at least not after 48h overexpression. On the contrary, the opposite response was seen, in which lower levels of APOE protein could be detected after 24 and 48h of DOX treatment. This very complex scenario can have different explanations. Firstly, overexpression is an artificial mean of studying dose-dependent cell response and it may disrupt other cellular processes producing unpredictable phenotypes. In the case studied here, *EIF2S3* overexpression might disturb the stoichiometry of eIF2 complex formation and consequently translational controlling mechanisms that cannot be traced. Another possibility is that unphysiological higher levels of eIF2S3 could activated new, previously non-related pathways. Very intriguing, and still open is the fact that even before eIF2S3 protein overexpression can be detected, changes in APOE transcription and translation are already observed (Prelich, 2012).

Whether this down-regulation in APOE translation is a direct cause of an increase in translation efficiency and whether MUT eIF2S3 cannot compete with the endogenous protein are still to be unveiled. We could, nevertheless, hypothesize that an increase in ternary complexes availability, even when not fully functional, as in the case of MUT eIF2S3, is repressing APOE translation. Insofar as, diminished levels of eIF2S3, produced by the gene knock-down, presented the exact opposite effect on APOE mRNA and protein levels (Figure 16 and Figure 17), when compared to the MUT overexpression experiment. Thus, corroborating with what discussed in the previous section, the continuous down-regulation of eIF2S3, such as in cases of nutrient starvation and apoptosis, resulted in increased APOE protein levels.

To conclude, differently from overexpression, which intends to disclose how the mutation itself is changing phenotype, the gene silencing experiment aimed to functionally characterize the endogenous gene by causing a reduction of its abundance. Even though these assays do not represent a faithful copy of the MEHMO pathology mechanism, they seek to unveil a possible dose-dependence relation between APOE and eIF2S3.

5.1.4. Other RA-related molecules

Considering the vast spectrum of RA activities in coordinating diverse

developmental process, and the indication of a possible deregulation RA levels in patients, some other RA-related molecules were chosen for mRNA levels measurement during early neuronal differentiation. These genes encode binding proteins (CRABP2, FABP4, FABP5, RBP1), a cellular retinol uptake protein (STRA6), nuclear receptors (RXRA, RARB, NR1H3, PPARβ/δ), a storage-related enzyme (LRAT), RA-synthesis enzymes (RDH10, RALDH2) and a RA-catabolic enzyme (CYP26A1).

Among those genes, CRABP2, FABP4, FABP5, RXRA, NR1H3 and RALDH2 did not show any significant difference in expression between control and patient groups when analyzing all stages of differentiation (Figure 21 and Figure 23).

A decrease in patient cytochrome P450 Family 26 Subfamily A Member 1 (CYP26A1) mRNA levels was observed at Day 22 of differentiation (Figure 23). This CYP26 family member is important in early stages of development and has been found to be in a negative feedback fashion up regulated by RA (Ross and Zolfaghari, 2011; White et al., 2007). Even though this gene was thought to be differently controlled in patient cells, as RA is delivered to this catabolic enzyme via CRABP1, the stages in which we observed simultaneously high levels of CRABP1 and low levels CYP26A1 were distinct, questioning CYP26A1 as a possible direct way to counter-balance differences in CRABP1 levels.

Retinol Binding Protein 1 (RBP1), presented higher levels of mRNA in patient lines (Day 22 of differentiation), as well as Retinol Dehydrogenase 10 (RDH10) (hiPSCs) and Stimulated by Retinoic Acid 6 (STRA6) (from Day 0 to Day 11 of differentiation) (Figure 23). All these proteins are indirectly involved in up-regulation of intracellular levels of RA precursors.

RBP1 is an important carrier of retinol and retinaldehyde that participates in the enzymatic conversions of retinol into retinaldehyde or retinyl esters and retinaldehyde into RA (Napoli, 2012). Intriguingly, likewise CRABP1, RBP1 is also described to have a retinoid-mediated anti-proliferative activity, this time by inhibiting the PI3K/Akt survival pathway (Doldo et al., 2014; Farias et al., 2005a; Farias et al., 2005b).

In the RA biosynthesis, RDH enzymes convert retinol into retinal by oxidation, which in turn is further oxidized into RA by RALDH (ALDH) family members. The ubiquitous expression of RDH (Duester et al., 2003) led to the interpretation that

the controlling point of RA synthesis would be just in the second step of oxidation from retinal to RA. Nevertheless, the finding of craniofacial malformation phenotype for mice RDH10 mutant (Sandell et al., 2007) clarified the topic, showing the importance of this step in RA control for normal embryogenesis. Like RBP1, overexpression of RDH10 has been linked to anti-proliferative effects (Rossi et al., 2007).

STRA6 is a membrane receptor with classical described function in mediating cellular retinol uptake by binding to a serum retinol binding protein (RBP4), and, similarly to RDH10 and RBP1, its silencing is increasing proliferation (Skazik et al., 2014) and its expression is associated to apoptosis (Carrera et al., 2013; Pavone et al., 2016)

To conclude, all three RA-related genes that were up-regulated in patient-derived cells in different stages of neuronal differentiation (Figure 23), including CRABP1 (non-canonical role), present anti-proliferative, apoptotic tendency common cell response.

On the contrary, Lecithin retinol acyltransferase (LRAT) that are producing the storage form of RA (retinyl esters), showed decreased levels of expression in patient cells, particularly at Day 11 of neuronal differentiation (Figure 23) and its overexpression is correlated with regulation of cell cycle and malignancy (Hassel et al., 2013; Shirakami et al., 2012).

5.2. eIF2S3 and other translation-related molecules

5.2.1. Fragile X mental retardation 1

As mentioned in the introductory section (1.2.2), both Fragile X syndrome, caused by silencing of *FMR1*, and Prader-Willi syndrome, produced by *CYFIP1* deletion, possess characteristics that very much resemble those found on MEHMO patients.

Due to this similarity in disease phenotype and the fact that FMR1, together with CYFIP1 present a relevant role in specific neuronal translation control, inhibiting the classic cap-binding translation of special FMR1 target mRNAs (Figure 4), we imagined that it would be interesting to check levels of FMR1 and CYIFP1 along early neuronal differentiation. Curiously, hiPSCs and EB´s patients exhibited a

slightly higher expression levels of FMR1, but from neuronal epithelium-like stage on, this pattern reversed and a small significance was observed for this time point. Although not significant, the patient group also showed reduced expression for CYFIP1, which was consistent along the whole differentiation (Figure 22). The confirmation of a down-regulation of FMR1 would open new avenues for investigation of possible common affected pathways in MEHMO and these other syndromes.

5.2.2. Protein Phosphatase 1 Regulatory Subunit 15B

Protein Phosphatase 1 Regulatory Subunit 15B (PPP1R15B) is part of a phosphatase complex functioning on eIF2S1 dephosphorylation, thus activating protein synthesis. Curiously, *PPP1R15B* mutation leads to a syndromic intellectual disability very similar to MEHMO, suggesting that increase in the phosphorylated status of eIF2S1 is associated with MEHMO pathomechanism or that, alternatively, a shared downstream effect is responsible by the common phenotype (Abdulkarim et al., 2015; Harding et al., 2009; Kernohan et al., 2015). Supporting this idea, increase in phospho-eIF2S1 by *RAX* (eIF2S1 kinase regulator) knock-out also causes symptoms related to MEHMO syndrome, such as reduced body size and anterior pituitary hypoplasia (Dickerman et al., 2015).

Conversely, decreased phospho-eIF2S1 availability has been linked to problems with glucose homeostasis (Harding et al., 2001; Julier and Nicolino, 2010; Scheuner et al., 2001; Scheuner et al., 2005). However, *PPP1R15B* mutation (Abdulkarim et al., 2015) also causes diabetes, meaning that both increase as decrease of phospho-eIF2S1 might result in the development of this particular pancreas-related symptom. In line with this observation, the MEHMO patient considered in this study is insulin dependent and presented hypoglycemia in its first six months of life, suggesting that the common PPP1R15B and eIF2S3 downstream deregulated translation rates might affect islets of Langerhans hormones production.

Being lower levels of functional ternary complexes an important effect of eIF2S1 phosphorylation, the increased PPP1R15B expression observed in MEHMO patient iPSCs and Day 11 of neuronal differentiation (Figure 22) might be seen

as an attempt to equilibrate ternary complexes formation and therefore translation, by decreasing phospho-eIF2S1 levels.

To conclude, another syndromes (see section 1.2.2) (Armistead et al., 2015; Brooks et al., 2014; Favaro et al., 2014; Wang et al., 2013a) which are indirectly affecting translation rates also present MEHMO characteristics, such as slow growth, microcephaly and craniofacial anomalies.

5.2.3. Activating Transcription Factor 4

Even if MEHMO patient cells do not present higher levels of phospho-eIF2S1, primary cause of Activating Transcription Factor 4 (ATF4) translation, it is reasonable to imagine that *EIF2S3* mutation could cause a reduction in ternary complexes, hence delayed ribosomal reinitiation, favoring ATF4 translation (Vattem and Wek, 2004). Although we could not see any significant difference in ATF4 protein levels, it was possible to detect higher levels of its mRNA along neuronal differentiation, with some significance at Days 0 and 22 (Figure 22).

ATF4 is a relevant transcription factor, known to be synthetized under different stress circumstances, and up-regulated in both mRNA and protein levels to circumvent cellular stress (Dey et al., 2010; Dey et al., 2012). Induction of ATF4 and CHOP (or DDIT3) by ER-stress in MEF cells increased protein synthesis, leading to the production of reactive oxygen species that trigger apoptosis (Han et al., 2013).

Interestingly, two eIF2S1 dephosphorylating factors, PPP1R15A and PPP1R15B, seems to be targets of both ATF4 and CHOP, but contrarily to PPP1R15A, which was up-regulated upon ER stress, PPP1R15B did not show differential expression (Han et al., 2013; Novoa et al., 2001). In fact, PPP1R15B factor exhibited significant increased mRNA levels in patient iPSCs and Day 11 of neuronal differentiation, while PPP1R15A, a significant increase at Day 5 of differentiation (Figure 22). Mutation on *PPP1R15B*, as mentioned previously, causes a syndrome very similar to MEHMO. And its overexpression definitely contribute to an increase in protein synthesis.

Other genes likewise regulated by ATF4 and CHOP are RBP4 and RDH10, retinoic acid related genes that, when increased, raise retinoic acid precursors cell internalization and synthesis, suggesting a possible RA role in the interface

translation/apoptosis. It is worth remembering that RDH10 was one of the RA-related genes analyzed and that it presented increased levels of expression also at hiPSCs stage (Figure 23).

5.2.4. Mechanistic Target Of Rapamycin

Functioning as part of a sensing mechanism, Mechanistic Target Of Rapamycin (MTOR) activation is regulated by factors such as nutrients and growth factors availability, and plays a central role in intermediating cell survival/growth/proliferative response to environmental conditions. These MTOR regulatory pathways are therefore adjusting anabolic processes performance such as translation to cell energetic nutrient state (Efeyan et al., 2015; Hay and Sonenberg, 2004). Besides the aforementioned (section 1.2.2) eIF4E binding protein (4E-BP) phosphorylation via MTORC activation, translation is activated also by MTOR mediated S6 kinase (S6K1) phosphorylation which stimulates a range of other translation effectors involved in ribosomal protein synthesis and in eIF4F complex mediated cap-dependent initiation (Hara et al., 1998; Ma and Blenis, 2009).

The hypothesized MEHMO patient decrease in global translation might lead to a general increase in amino acid availability. Continuously high amino acid content may exacerbate MTOR activation and, in line with this idea, we observed elevated levels of MTOR mRNA (Figure 12). Furthermore, the absence of uncharged tRNA that maintains general control nonderepressible 2 (GCN2) inactivated might decrease phospho-eIF2S1 levels in patient. The reducing phospho-eIF2S1 effect is probably a MEHMO cell aim, since increase in levels of PPP1R15B expression is also observed. Curiously though, ATF4 transcripts are also elevated in patient cells. But, as mentioned earlier, despite possible absence of higher levels of phospho-eIF2S1, *EIF2S3* mutation might reduce active ternary complexes, thus favoring ATF4 translation.

As nutrient deprivation increases APOE mRNA and protein levels, it would not be surprising if *EIF2S3* mutation could cause, in long term, reduction of amino acid abundance, producing APOE overexpression. On the other hand, considering that APOE up-regulation is also detected during apoptosis (another process inhibiting general translation) (Lasfargues et al., 2012), we cannot exclude the

possibility that changes in gene expression/mRNA translation are not a direct consequence of nutrient deprivation, but rather an indirect result of poor translation rates due to *EIF2S3* mutation (Quinn et al., 2004).

Finally, as discussed in the introductory section (1.2.2), along with ERK, MTOR pathway activation has a function on synapsis plasticity with repercussions on memory and learning capacities (Bhakar et al., 2012) and its imbalanced stimulation is correlated to neurodevelopmental and neuropsychiatric disorders (Costa-Mattioli and Monteggia, 2013). Thus, although no significant differences are seen in the course of our neuronal differentiation (Figure 22), a difference in mature neurons is not excluded.

5.3. H2A Histone Family Member X

Up-regulated in MEHMO patient iPSCs (Table 18), the H2A Histone Family Member X (H2AFX or H2AX) is a histone protein phosphorylated (γH2AX) upon DNA damage, to recruit repair complexes (Paull et al., 2000; Rogakou et al., 1998). Although H2AX phosphorylation is happening during DNA damage response processes, some evidence have indicated that γH2AX is dispensable during initial recruiting repair factors, but it is probably important in holding DNA ends and factors together (Celeste et al., 2003; Yin et al., 2009). The absence of H2AX produced growth retarded mice with decreased mitosis and increased chromosomal aberrations (Celeste et al., 2002).

Although we could observe significant increase in patient H2AX protein levels, it is important to mention that it was not possible to apply cell cycle synchronization during SILAC experiment and, to minimize problems due to differences arising from distinct cell cycle stage, three different time points in two independent experiments were analyzed and their results were highly comparable. Furthermore, unlike core histones, variant H2AX presents steady levels across cell cycles phases (Bretherick et al., 2014).

It is also noteworthy that the analyzed iPSCs are reprogrammed somatic cells that similarly to zygote, also pass through a massive epigenetic reprogramming, in which many histones are modified to achieve a completely different transcription profile, characteristic of pluripotent cells (Huang et al., 2015). Although the exact mechanisms governing epigenetic features are still unknown,

it is accepted that iPSCs possess an epigenetic profile very similar to hESCs (Guenther et al., 2010; Mallon et al., 2014), but it is also recognized that the so called “epigenetic memory” can give rise to differences among iPSC lines, due to inheritance of epigenetic markers of the somatic cell of origin (Kim et al., 2010). As all iPSCs (control and patient) were generated from keratinocytes, we could exclude effects caused by different origin of somatic cells, however individual differences could be something revealed in the different iPSC lines.

Regardless from H2AX canonical role in responding to DNA damage, H2AX phosphorylation was described to be highly enriched during embryogenesis, and interestingly, also in neurogenic brain areas, such as the subventricular zone (Barral et al., 2014; Kafer et al., 2010; Ziegler-Birling et al., 2009). H2AX presence on those proliferative tissues is tied to its role in stem cells self-renewal and cell proliferative capacity (Andang et al., 2008; Fernando et al., 2011; Turinetto et al., 2012). Moreover reprogrammed cells having different γH2AX genome distribution and pluripotency capacities (assessed via tetraploid assay), presented no differences in H2AX protein levels (Wu et al., 2014). Accordingly, despite of any difference both patient and control derived iPSCs could have on pluripotency and reprogramming efficiency, H2AX protein levels would still remain similar. So, the probability of having an iPS cell line with increased H2AX protein levels due to varied reprogramming efficiency is minimal, and the observed patient phenotype could indeed be a result of *EIF2S3* mutation.

Intriguingly, besides repressing extra-embryonic genes (Wu et al., 2014), thus contributing to iPSCs stemness, γH2AX was found to be undirected activated by γ-aminobutyric acid (GABA) signaling in both stem cells and neural stem cells and negatively regulate their proliferation rates (Andang et al., 2008; Fernando et al., 2011). Higher amounts of H2AX does not necessarily mean higher quantities of γH2AX. Yet likewise it occurs for serum starvation and chemical induced integrative stress response that activates phosphorylation of H2AX (Lu et al., 2008; Sayers et al., 2013), MEHMO decrease in global translation levels could imply higher levels of γH2AX; ergo, restriction of neural stem cells proliferation.

Finally, it is interesting to consider the possible role that changes in translation could have in modulating apoptosis by H2AX phosphorylation, since among a variety of other cellular stress triggers, serum starvation is increasing H2AX

phosphorylation and inducing apoptosis via mitogen-activated protein kinase (MAPK) pathway (Lu et al., 2008), showing in this manner a link between H2AX and translation mechanisms (see introduction section 1.2.2).

5.4. Transketolase

Transketolase (TKT) is a thiamine-dependent enzyme acting in the pentose phosphate pathway of the glucose metabolism, contributing to the production of ribose-5-phosphate, nucleotides component, and of reduced nicotinamide-adenine dinucleotide phosphate (NADPH), important in detoxification and synthesis of fatty acids and cholesterol.

While the oxidative branch of the pentose phosphate pathway is highly active in cells like hepatocytes and adipocytes, since the requirement for NADPH in fatty acids synthesis is increased there, the non-oxidative branch is ensuring production of ribose-5-phosphate, essential for DNA and RNA synthesis, and it is required in all tissues, especially those highly proliferative. Therefore, it is not surprising that TKT activity is commonly elevated in tumors (Ricciardelli et al., 2015). TKT inhibition, in turn, showed cell cycle arrest in tumor cells (Comin-Anduix et al., 2001; Rais et al., 1999) and caused decrease in hippocampal progenitor cells proliferation (Zhao et al., 2014b).

Besides presenting a decrease in cell proliferation, chemical TKT inhibition promoted a reduction in levels of some translation factors, while TKT own translation was markedly increased (Wang et al., 2013b). Likewise related to translation, phosphatidylinositol 3-kinase (PI3K)/Akt pathway is orchestrating a metabolic mechanism in which amino acid cellular content is activating the pathway and determining TKT activity, thereby increasing DNA synthesis and cell proliferation (Saha et al., 2014).

Curiously, disagreeing with what is seen in quantitative proteomics (Table 18), patient TKT mRNA levels were significant higher in comparison to control (Figure 12). This result could be seen as a cell attempt to compensate for the lower TKT protein levels, for the protein increased degradation rate, or even for an PI3K/Akt exacerbated activation, due to increased cellular amino acid content caused by the *EIF2S3* mutation.

To conclude, a very recent report correlates different TKT mutations that lead to

lack of activity with a syndrome characterized by delay development, short stature and heart malformation (Boyle et al., 2016), features also characteristic of MEHMO syndrome.

5.5. Cystathionine-Beta-Synthase

Cysteine is considered an essential amino acid, as its synthesis requires the uptake of another essential amino acid, the methionine, of which it receives the sulfur atom. Among several enzymes catalyzing this process, the cystathionine-beta-synthase (CBS) is condensing serine with homocysteine to synthetize the direct cysteine precursor: the cystathionine.

Cysteine and methionine are the only amino acids containing sulfur, but differently from methionine, cysteine is capable of forming disulfide bonds, which play a crucial role in protein folding and, as consequence, in establishing correct protein function. This importance, added to the fact that cysteine is the least abundant amino acid, suggest a regulatory role for this amino acid, in which its availability determine translation rates. Actually, a cysteine and methionine availability sensing mechanism was described to integrate, in yeast, metabolic status with translation capacity of the cells (Laxman et al., 2013). Although described in yeast, the authors proposed a parallel mechanism in mammals due to the highly conserved pathway involved. Furthermore, amino acid availability is known to regulate levels of translation via MTOR pathway activation (Hara et al., 1998; Wang et al., 1998)

In line with these reports, *CBS* silencing reduced cancer cell and neural stem cells proliferation (Szabo et al., 2013; Wang et al., 2013c) and cysteine deficiency increased ATF4 levels and reduced mTORC1 activation in human hepatoma cells (that are not able to synthetize cysteine from methionine) (Yu and Long, 2016). Similarly, cysteine supplementation following proteasome inhibition decreased CHOP-mediated cell death and rescued translation via decrease of phospho-eIF2S1 levels (Suraweera et al., 2012). Thus, although it is impossible to determine at the present moment any causality relation for what is observe in MEHMO patient iPSCs (mRNA - Figure 12 and protein level - Table 18), CBS decline, as well as increase in ATF4 transcript (Figure 22), seems to be a direct

consequence of poor translation, as it is the case for serum/nutrient starvation in human and yeast cells (Maclean et al., 2002).

Likewise iPSCs, patient neuronal epithelium-like cells derived from differentiation also exhibited lower *CBS* gene expression in relation to control group (Figure 21). Indicating its importance in the CNS development, *CBS* is particularly highly expressed in early neural tube and primary brain vesicles (Quere et al., 1999) and its inhibition showed suppression of neural stem cells proliferation and differentiation. These proliferative and differentiation effects could be induced by cysteine supplementation (Wang et al., 2013c). Lastly, defective CBS activity with homocysteine accumulation and cysteine deficiency is related to cognitive impairment, seizures and white matter lesions (Barbaux et al., 2000; Kluijtmans et al., 1996; Sasai et al., 2015; Suri et al., 2014; Yap et al., 2001). Therefore, considering amino acids homeostasis effects in protein synthesis, it would be important to assess whether patient CBS lower protein levels effectively reduce cysteine synthesis and perhaps more important, if this is a developed patient feature and whether its possible effects can be reversed via pyridoxine (vitamin B_6) treatment, a cofactor required for CBS activity.

Closing remarks

MEHMO is long described as an X-linked intellectual disability syndrome (DeLozier-Blanchet et al., 1999). Exome sequencing in a patient diagnosed with MEHMO syndrome allowed to conclude that the mutation responsible for the observed symptoms is located in the *EIF2S3* gene (G.Borck, personal communication). Eukaryotic translation initiation factors are known for their ability to orchestrate very fine mechanisms of translation control. Among these factors, eIF2S3 is an essential subunit of the heteromeric eIF2 factor that binds to GTP, enabling tRNA delivery.

Generation of patient-derived iPSCs and global protein analysis provided evidences for the imbalance in translation of some interesting candidates. Gene expression analysis confirmed their differential expression, reinforcing a possible relevance for disease pathophysiology. Literature research also indicated the differentially expressed genes association, by direct and indirect means, with a process clearly affected in patients: neurogenesis.

Certainly it is impossible to exclude the hypothesis that *EIF2S3* mutations produce a gain of function phenotype, however the fact that women carrying the mutation, although presenting out of range occipital measurements, do not present any other major symptom indicate that patient's phenotype (Borck et al., 2012) might be related to absence of entirely functional protein and lower levels of working ternary complexes rather than due to a gain of function problem. Furthermore, mutations in different protein sites produce the same syndrome, called MEHMO. On the basis of the results presented here, we propose a response mechanism (Figure 30) that differently regulates genes specifically acting on apoptotic and survival/proliferative pathways, in order to restore the disrupted cellular homeostasis created by translation impairment.

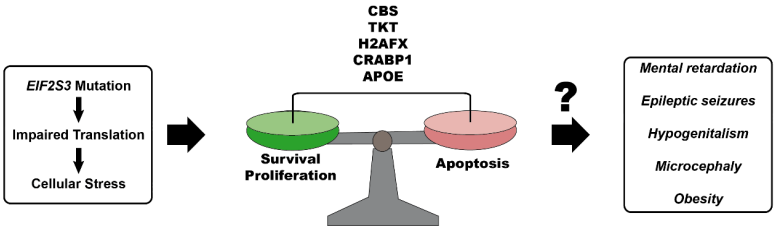

Figure 30. Proposed hypothesis for differential protein translation of specific genes in MEHMO patients. *EIF2S3* mutation would drive impaired translation and subsequently cellular stress activating response mechanisms to re-establish cellular homeostasis, via modulation of survival/apoptotic pathways. Whether patient presents an exaggerated activation of either survival/proliferation or apoptosis pathways has to be further evaluated.

Altogether, this study is a preliminary view of what *EIF2S3* disruption is causing and, undoubtedly, the use of other patient lines together with the generation of isogenic controls by using genetic targeting techniques, such as CRISPR/Cas9 system (Dow, 2015) will be necessary to validate the data found here. These invaluable controls would help to exclude any influences that genetic background could have on the changes observed in patient lines and could even elucidate if *APOE* polymorphism is indeed a source of phenotypic variability among patients. Moreover, as another possible control line, patient cells could be repaired for *EIF2S3* mutation. In order to confirm data produced here and explore other aspects of the disease, use of other differentiation protocols replicating, for example, stages of specific neuronal type and adipocytes development will be obviously advantageous.

Our intention here was to provide an overview about which genes, especially which proteins were differently expressed, giving a little contribution towards revealing possible altered pathways. Subsequent studies, more deeply investigating facts such as the presented increasing levels of APOE upon *EIF2S3* knock-down, might generate insights about the role of each candidate protein and their altered expression implications on MEHMO pathophysiology. Ultimately, further experiments such as synaptogenesis evaluation and electrophysiology will hopefully provide the yet uncovered eIF2 function in nervous system development, and in other regulatory pathways, so far not described.

Bibliography

Aasen, T., and Izpisua Belmonte, J.C. (2010). Isolation and cultivation of human keratinocytes from skin or plucked hair for the generation of induced pluripotent stem cells. Nature protocols *5*, 371-382.

Abdulkarim, B., Nicolino, M., Igoillo-Esteve, M., Daures, M., Romero, S., Philippi, A., Senee, V., Lopes, M., Cunha, D.A., Harding, H.P*., et al.* (2015). A Missense Mutation in PPP1R15B Causes a Syndrome Including Diabetes, Short Stature, and Microcephaly. Diabetes *64*, 3951-3962.

Abeyta, M.J., Clark, A.T., Rodriguez, R.T., Bodnar, M.S., Pera, R.A., and Firpo, M.T. (2004). Unique gene expression signatures of independently-derived human embryonic stem cell lines. Human molecular genetics *13*, 601-608.

Abildayeva, K., Jansen, P.J., Hirsch-Reinshagen, V., Bloks, V.W., Bakker, A.H., Ramaekers, F.C., de Vente, J., Groen, A.K., Wellington, C.L., Kuipers, F*., et al.* (2006). 24(S)-hydroxycholesterol participates in a liver X receptor-controlled pathway in astrocytes that regulates apolipoprotein E-mediated cholesterol efflux. The Journal of biological chemistry *281*, 12799-12808.

Allan, C.M., Walker, D., and Taylor, J.M. (1995). Evolutionary duplication of a hepatic control region in the human apolipoprotein E gene locus. Identification of a second region that confers high level and liver-specific expression of the human apolipoprotein E gene in transgenic mice. The Journal of biological chemistry *270*, 26278-26281.

Allen, G.W., Liu, J.W., and De Leon, M. (2000). Depletion of a fatty acid-binding protein impairs neurite outgrowth in PC12 cells. Brain research Molecular brain research *76*, 315-324.

Andang, M., Hjerling-Leffler, J., Moliner, A., Lundgren, T.K., Castelo-Branco, G., Nanou, E., Pozas, E., Bryja, V., Halliez, S., Nishimaru, H*., et al.* (2008). Histone H2AX-dependent GABA(A) receptor regulation of stem cell proliferation. Nature *451*, 460-464.

Andersen, J.S., Lyon, C.E., Fox, A.H., Leung, A.K., Lam, Y.W., Steen, H., Mann, M., and Lamond, A.I. (2002). Directed proteomic analysis of the human nucleolus. Curr Biol *12*, 1-11.

Armistead, J., Patel, N., Wu, X., Hemming, R., Chowdhury, B., Basra, G.S., Del Bigio, M.R., Ding, H., and Triggs-Raine, B. (2015). Growth arrest in the ribosomopathy, Bowen-Conradi syndrome, is due to dramatically reduced cell proliferation and a defect in mitotic progression. Biochimica et biophysica acta *1852*, 1029-1037.

Asano, K., Krishnamoorthy, T., Phan, L., Pavitt, G.D., and Hinnebusch, A.G. (1999). Conserved bipartite motifs in yeast eIF5 and eIF2Bepsilon, GTPase-activating and GDP-GTP exchange factors in translation initiation, mediate binding to their common substrate eIF2. The EMBO journal *18*, 1673-1688.

Ashley, C.T., Jr., Wilkinson, K.D., Reines, D., and Warren, S.T. (1993). FMR1 protein: conserved RNP family domains and selective RNA binding. Science *262*, 563-566.

Azevedo, F.A., Carvalho, L.R., Grinberg, L.T., Farfel, J.M., Ferretti, R.E., Leite, R.E., Jacob Filho, W., Lent, R., and Herculano-Houzel, S. (2009). Equal numbers of neuronal and nonneuronal cells make the human brain an isometrically scaled-up primate brain. J Comp Neurol *513*, 532-541.

Banz, C., Ungethuem, U., Kuban, R.J., Diedrich, K., Lengyel, E., and Hornung, D. (2010). The molecular signature of endometriosis-associated endometrioid ovarian cancer differs significantly from endometriosis-independent endometrioid ovarian cancer. Fertility and sterility *94*, 1212-1217.

Barbaric, I., Miller, G., and Dear, T.N. (2007). Appearances can be deceiving: phenotypes of knockout mice. Brief Funct Genomic Proteomic *6*, 91-103.

Barbaux, S., Plomin, R., and Whitehead, A.S. (2000). Polymorphisms of genes controlling homocysteine/folate metabolism and cognitive function. Neuroreport *11*, 1133-1136.

Barral, S., Beltramo, R., Salio, C., Aimar, P., Lossi, L., and Merighi, A. (2014). Phosphorylation of histone H2AX in the mouse brain from development to senescence. Int J Mol Sci *15*, 1554-1573.
Bartzokis, G., Lu, P.H., Geschwind, D.H., Edwards, N., Mintz, J., and Cummings, J.L. (2006). Apolipoprotein E genotype and age-related myelin breakdown in healthy individuals: implications for cognitive decline and dementia. Arch Gen Psychiatry *63*, 63-72.
Bassell, G.J., and Warren, S.T. (2008). Fragile X syndrome: loss of local mRNA regulation alters synaptic development and function. Neuron *60*, 201-214.
Batres, R.O., and Olson, J.A. (1987). Relative amount and ester composition of vitamin A in rat hepatocytes as a function of the method of cell preparation and of total liver stores. The Journal of nutrition *117*, 77-82.
Beilsten-Edmands, V., Gordiyenko, Y., Kung, J.C.K., Mohammed, S., Schmidt, C., and Robinson, C.V. (2015). eIF2 interactions with initiator tRNA and eIF2B are regulated by post-translational modifications and conformational dynamics. Cell Discovery *1*, 15020.
Benedetti, E., Di Loreto, S., D'Angelo, B., Cristiano, L., d'Angelo, M., Antonosante, A., Fidoamore, A., Raffaella, G., Cinque, B., Cifone, M.G.*, et al.* (2015). The PPARbeta/delta Agonist GW0742 Induces Early Neuronal Maturation of Cortical Post-Mitotic Neurons: Role of PPARbeta/delta in Neuronal Maturation. Journal of cellular physiology.
Berg, D.T., Calnek, D.S., and Grinnell, B.W. (1995). The human apolipoprotein E gene is negatively regulated in human liver HepG2 cells by the transcription factor BEF-1. The Journal of biological chemistry *270*, 15447-15450.
Berry, D.C., DeSantis, D., Soltanian, H., Croniger, C.M., and Noy, N. (2012). Retinoic acid upregulates preadipocyte genes to block adipogenesis and suppress diet-induced obesity. Diabetes *61*, 1112-1121.
Berry, D.C., and Noy, N. (2009). All-trans-retinoic acid represses obesity and insulin resistance by activating both peroxisome proliferation-activated receptor beta/delta and retinoic acid receptor. Molecular and cellular biology *29*, 3286-3296.
Berry, D.C., Soltanian, H., and Noy, N. (2010). Repression of cellular retinoic acid-binding protein II during adipocyte differentiation. The Journal of biological chemistry *285*, 15324-15332.
Bhakar, A.L., Dolen, G., and Bear, M.F. (2012). The pathophysiology of fragile X (and what it teaches us about synapses). Annual review of neuroscience *35*, 417-443.
Bielen, H., and Houart, C. (2014). The Wnt cries many: Wnt regulation of neurogenesis through tissue patterning, proliferation, and asymmetric cell division. Dev Neurobiol *74*, 772-780.
Bittel, D.C., Kibiryeva, N., and Butler, M.G. (2006). Expression of 4 genes between chromosome 15 breakpoints 1 and 2 and behavioral outcomes in Prader-Willi syndrome. Pediatrics *118*, e1276-1283.
Bogdan, S., Grewe, O., Strunk, M., Mertens, A., and Klambt, C. (2004). Sra-1 interacts with Kette and Wasp and is required for neuronal and bristle development in Drosophila. Development *131*, 3981-3989.
Bohnsack, M.T., Regener, K., Schwappach, B., Saffrich, R., Paraskeva, E., Hartmann, E., and Gorlich, D. (2002). Exp5 exports eEF1A via tRNA from nuclei and synergizes with other transport pathways to confine translation to the cytoplasm. The EMBO journal *21*, 6205-6215.
Bommer, U.A., and Kurzchalia, T.V. (1989). GTP interacts through its ribose and phosphate moieties with different subunits of the eukaryotic initiation factor eIF-2. FEBS letters *244*, 323-327.
Borck, G., Shin, B.S., Stiller, B., Mimouni-Bloch, A., Thiele, H., Kim, J.R., Thakur, M., Skinner, C., Aschenbach, L., Smirin-Yosef, P.*, et al.* (2012). eIF2gamma mutation that disrupts eIF2 complex integrity links intellectual disability to impaired translation initiation. Mol Cell *48*, 641-646.
Boylan, J.F., and Gudas, L.J. (1991). Overexpression of the cellular retinoic acid binding

protein-I (CRABP-I) results in a reduction in differentiation-specific gene expression in F9 teratocarcinoma cells. The Journal of cell biology *112*, 965-979.
Boylan, J.F., and Gudas, L.J. (1992). The level of CRABP-I expression influences the amounts and types of all-trans-retinoic acid metabolites in F9 teratocarcinoma stem cells. The Journal of biological chemistry *267*, 21486-21491.
Boyle, L., Wamelink, M.M., Salomons, G.S., Roos, B., Pop, A., Dauber, A., Hwa, V., Andrew, M., Douglas, J., Feingold, M.*, et al.* (2016). Mutations in TKT Are the Cause of a Syndrome Including Short Stature, Developmental Delay, and Congenital Heart Defects. American journal of human genetics *98*, 1235-1242.
Boyles, J.K., Pitas, R.E., Wilson, E., Mahley, R.W., and Taylor, J.M. (1985). Apolipoprotein E associated with astrocytic glia of the central nervous system and with nonmyelinating glia of the peripheral nervous system. The Journal of clinical investigation *76*, 1501-1513.
Braissant, O., Foufelle, F., Scotto, C., Dauca, M., and Wahli, W. (1996). Differential expression of peroxisome proliferator-activated receptors (PPARs): tissue distribution of PPAR-alpha, -beta, and -gamma in the adult rat. Endocrinology *137*, 354-366.
Bretherick, K.L., Leach, S., and Brooks-Wilson, A.R. (2014). Functional characterization of genetic polymorphisms in the H2AFX distal promoter. Mutat Res *766-767*, 37-43.
Brooks, S.S., Wall, A.L., Golzio, C., Reid, D.W., Kondyles, A., Willer, J.R., Botti, C., Nicchitta, C.V., Katsanis, N., and Davis, E.E. (2014). A novel ribosomopathy caused by dysfunction of RPL10 disrupts neurodevelopment and causes X-linked microcephaly in humans. Genetics *198*, 723-733.
Bugiani, M., Boor, I., Powers, J.M., Scheper, G.C., and van der Knaap, M.S. (2010). Leukoencephalopathy with vanishing white matter: a review. J Neuropathol Exp Neurol *69*, 987-996.
Carmel, J.F., Tarnus, E., Cohn, J.S., Bourdon, E., Davignon, J., and Bernier, L. (2009). High expression of apolipoprotein E impairs lipid storage and promotes cell proliferation in human adipocytes. J Cell Biochem *106*, 608-617.
Carrera, S., Cuadrado-Castano, S., Samuel, J., Jones, G.D., Villar, E., Lee, S.W., and Macip, S. (2013). Stra6, a retinoic acid-responsive gene, participates in p53-induced apoptosis after DNA damage. Cell Death Differ *20*, 910-919.
Cedazo-Minguez, A., Hamker, U., Meske, V., Veh, R.W., Hellweg, R., Jacobi, C., Albert, F., Cowburn, R.F., and Ohm, T.G. (2001). Regulation of apolipoprotein E secretion in rat primary hippocampal astrocyte cultures. Neuroscience *105*, 651-661.
Celeste, A., Fernandez-Capetillo, O., Kruhlak, M.J., Pilch, D.R., Staudt, D.W., Lee, A., Bonner, R.F., Bonner, W.M., and Nussenzweig, A. (2003). Histone H2AX phosphorylation is dispensable for the initial recognition of DNA breaks. Nat Cell Biol *5*, 675-679.
Celeste, A., Petersen, S., Romanienko, P.J., Fernandez-Capetillo, O., Chen, H.T., Sedelnikova, O.A., Reina-San-Martin, B., Coppola, V., Meffre, E., Difilippantonio, M.J.*, et al.* (2002). Genomic instability in mice lacking histone H2AX. Science *296*, 922-927.
Chakrabarti, A., and Maitra, U. (1992). Release and recycling of eukaryotic initiation factor 2 in the formation of an 80 S ribosomal polypeptide chain initiation complex. The Journal of biological chemistry *267*, 12964-12972.
Chen, Y.C., Pohl, G., Wang, T.L., Morin, P.J., Risberg, B., Kristensen, G.B., Yu, A., Davidson, B., and Shih Ie, M. (2005). Apolipoprotein E is required for cell proliferation and survival in ovarian cancer. Cancer Res *65*, 331-337.
Chen, Z., Borek, D., Padrick, S.B., Gomez, T.S., Metlagel, Z., Ismail, A.M., Umetani, J., Billadeau, D.D., Otwinowski, Z., and Rosen, M.K. (2010). Structure and control of the actin regulatory WAVE complex. Nature *468*, 533-538.
Chiba, T., Nakazawa, T., Yui, K., Kaneko, E., and Shimokado, K. (2003). VLDL induces adipocyte differentiation in ApoE-dependent manner. Arterioscler Thromb Vasc Biol *23*, 1423-1429.
Choi, J., Park, S., and Sockanathan, S. (2014). Activated retinoid receptors are required for the migration and fate maintenance of subsets of cortical neurons. Development *141*,

1151-1160.
Chung, L., Wang, X., Zhu, L., Towers, A.J., Cao, X., Kim, I.H., and Jiang, Y.H. (2015). Parental origin impairment of synaptic functions and behaviors in cytoplasmic FMRP interacting protein 1 (Cyfip1) deficient mice. Brain research *1629*, 340-350.
Cohen, L.E., Zanger, K., Brue, T., Wondisford, F.E., and Radovick, S. (1999). Defective retinoic acid regulation of the Pit-1 gene enhancer: a novel mechanism of combined pituitary hormone deficiency. Molecular endocrinology *13*, 476-484.
Comin-Anduix, B., Boren, J., Martinez, S., Moro, C., Centelles, J.J., Trebukhina, R., Petushok, N., Lee, W.N., Boros, L.G., and Cascante, M. (2001). The effect of thiamine supplementation on tumour proliferation. A metabolic control analysis study. Eur J Biochem *268*, 4177-4182.
Corcoran, J., So, P.L., and Maden, M. (2002). Absence of retinoids can induce motoneuron disease in the adult rat and a retinoid defect is present in motoneuron disease patients. Journal of cell science *115*, 4735-4741.
Costa-Mattioli, M., Gobert, D., Harding, H., Herdy, B., Azzi, M., Bruno, M., Bidinosti, M., Ben Mamou, C., Marcinkiewicz, E., Yoshida, M.*, et al.* (2005). Translational control of hippocampal synaptic plasticity and memory by the eIF2alpha kinase GCN2. Nature *436*, 1166-1173.
Costa-Mattioli, M., Gobert, D., Stern, E., Gamache, K., Colina, R., Cuello, C., Sossin, W., Kaufman, R., Pelletier, J., Rosenblum, K.*, et al.* (2007). eIF2alpha phosphorylation bidirectionally regulates the switch from short- to long-term synaptic plasticity and memory. Cell *129*, 195-206.
Costa-Mattioli, M., and Monteggia, L.M. (2013). mTOR complexes in neurodevelopmental and neuropsychiatric disorders. Nature neuroscience *16*, 1537-1543.
Cox, J., and Mann, M. (2008). MaxQuant enables high peptide identification rates, individualized p.p.b.-range mass accuracies and proteome-wide protein quantification. Nature biotechnology *26*, 1367-1372.
Culjkovic, B., Topisirovic, I., and Borden, K.L. (2007). Controlling gene expression through RNA regulons: the role of the eukaryotic translation initiation factor eIF4E. Cell cycle *6*, 65-69.
D'Ambrosio, D.N., Clugston, R.D., and Blaner, W.S. (2011). Vitamin A metabolism: an update. Nutrients *3*, 63-103.
De Rubeis, S., Pasciuto, E., Li, K.W., Fernandez, E., Di Marino, D., Buzzi, A., Ostroff, L.E., Klann, E., Zwartkruis, F.J., Komiyama, N.H.*, et al.* (2013). CYFIP1 coordinates mRNA translation and cytoskeleton remodeling to ensure proper dendritic spine formation. Neuron *79*, 1169-1182.
Dean, D.C., 3rd, Jerskey, B.A., Chen, K., Protas, H., Thiyyagura, P., Roontiva, A., O'Muircheartaigh, J., Dirks, H., Waskiewicz, N., Lehman, K.*, et al.* (2014). Brain differences in infants at differential genetic risk for late-onset Alzheimer disease: a cross-sectional imaging study. JAMA neurology *71*, 11-22.
Del Re, E.C., Konishi, J., Bouix, S., Blokland, G.A., Mesholam-Gately, R.I., Goldstein, J., Kubicki, M., Wojcik, J., Pasternak, O., Seidman, L.J.*, et al.* (2015). Enlarged lateral ventricles inversely correlate with reduced corpus callosum central volume in first episode schizophrenia: association with functional measures. Brain Imaging Behav.
DeLozier-Blanchet, C.D., Haenggeli, C.A., and Bottani, A. (1999). MEHMO, a novel syndrome: assignment of disease locus to Xp21.1-p22.13. Mental retardation, epileptic seizures, hypogonadism and genitalism, microcephaly, obesity. European journal of human genetics : EJHG *7*, 621-622.
Delozier-Blanchet, C.D., Haenggeli, C.A., and Engel, E. (1989). [Microencephalic nanism, severe retardation, hypertonia, obesity, and hypogonadism in two brothers: a new syndrome?]. J Genet Hum *37*, 353-365.
Devane, W.A., Hanus, L., Breuer, A., Pertwee, R.G., Stevenson, L.A., Griffin, G., Gibson, D., Mandelbaum, A., Etinger, A., and Mechoulam, R. (1992). Isolation and structure of a

brain constituent that binds to the cannabinoid receptor. Science *258*, 1946-1949.
Dever, T.E., and Green, R. (2012). The elongation, termination, and recycling phases of translation in eukaryotes. Cold Spring Harb Perspect Biol *4*, a013706.
Dey, S., Baird, T.D., Zhou, D., Palam, L.R., Spandau, D.F., and Wek, R.C. (2010). Both transcriptional regulation and translational control of ATF4 are central to the integrated stress response. The Journal of biological chemistry *285*, 33165-33174.
Dey, S., Savant, S., Teske, B.F., Hatzoglou, M., Calkhoven, C.F., and Wek, R.C. (2012). Transcriptional repression of ATF4 gene by CCAAT/enhancer-binding protein beta (C/EBPbeta) differentially regulates integrated stress response. The Journal of biological chemistry *287*, 21936-21949.
Di Marzo, V., Fontana, A., Cadas, H., Schinelli, S., Cimino, G., Schwartz, J.C., and Piomelli, D. (1994). Formation and inactivation of endogenous cannabinoid anandamide in central neurons. Nature *372*, 686-691.
Dickerman, B.K., White, C.L., Kessler, P.M., Sadler, A.J., Williams, B.R., and Sen, G.C. (2015). The protein activator of protein kinase R, PACT/RAX, negatively regulates protein kinase R during mouse anterior pituitary development. FEBS J *282*, 4766-4781.
Dietschy, J.M. (2009). Central nervous system: cholesterol turnover, brain development and neurodegeneration. Biol Chem *390*, 287-293.
Do Carmo, S., Seguin, D., Milne, R., and Rassart, E. (2002). Modulation of apolipoprotein D and apolipoprotein E mRNA expression by growth arrest and identification of key elements in the promoter. The Journal of biological chemistry *277*, 5514-5523.
Doldo, E., Costanza, G., Ferlosio, A., Passeri, D., Bernardini, S., Scioli, M.G., Mazzaglia, D., Agostinelli, S., Del Bufalo, D., Czernobilsky, B.*, et al.* (2014). CRBP-1 expression in ovarian cancer: a potential therapeutic target. Anticancer Res *34*, 3303-3312.
Donnelly, N., Gorman, A.M., Gupta, S., and Samali, A. (2013). The eIF2alpha kinases: their structures and functions. Cell Mol Life Sci *70*, 3493-3511.
Dow, L.E. (2015). Modeling Disease In Vivo With CRISPR/Cas9. Trends Mol Med *21*, 609-621.
Du, F., Zhu, X.H., Zhang, Y., Friedman, M., Zhang, N., Ugurbil, K., and Chen, W. (2008). Tightly coupled brain activity and cerebral ATP metabolic rate. Proceedings of the National Academy of Sciences of the United States of America *105*, 6409-6414.
Duester, G., Mic, F.A., and Molotkov, A. (2003). Cytosolic retinoid dehydrogenases govern ubiquitous metabolism of retinol to retinaldehyde followed by tissue-specific metabolism to retinoic acid. Chemico-biological interactions *143-144*, 201-210.
Dumanis, S.B., DiBattista, A.M., Miessau, M., Moussa, C.E., and Rebeck, G.W. (2013). APOE genotype affects the pre-synaptic compartment of glutamatergic nerve terminals. Journal of neurochemistry *124*, 4-14.
Dumanis, S.B., Tesoriero, J.A., Babus, L.W., Nguyen, M.T., Trotter, J.H., Ladu, M.J., Weeber, E.J., Turner, R.S., Xu, B., Rebeck, G.W.*, et al.* (2009). ApoE4 decreases spine density and dendritic complexity in cortical neurons in vivo. The Journal of neuroscience : the official journal of the Society for Neuroscience *29*, 15317-15322.
Efeyan, A., Comb, W.C., and Sabatini, D.M. (2015). Nutrient-sensing mechanisms and pathways. Nature *517*, 302-310.
Engl, E., and Attwell, D. (2015). Non-signalling energy use in the brain. J Physiol *593*, 3417-3429.
Fagan, A.M., Murphy, B.A., Patel, S.N., Kilbridge, J.F., Mobley, W.C., Bu, G., and Holtzman, D.M. (1998). Evidence for normal aging of the septo-hippocampal cholinergic system in apoE (-/-) mice but impaired clearance of axonal degeneration products following injury. Experimental neurology *151*, 314-325.
Farias, E.F., Marzan, C., and Mira-y-Lopez, R. (2005a). Cellular retinol-binding protein-I inhibits PI3K/Akt signaling through a retinoic acid receptor-dependent mechanism that regulates p85-p110 heterodimerization. Oncogene *24*, 1598-1606.
Farias, E.F., Ong, D.E., Ghyselinck, N.B., Nakajo, S., Kuppumbatti, Y.S., and Mira y Lopez, R. (2005b). Cellular retinol-binding protein I, a regulator of breast epithelial

retinoic acid receptor activity, cell differentiation, and tumorigenicity. J Natl Cancer Inst *97*, 21-29.
Favaro, F.P., Alvizi, L., Zechi-Ceide, R.M., Bertola, D., Felix, T.M., de Souza, J., Raskin, S., Twigg, S.R., Weiner, A.M., Armas, P.*, et al.* (2014). A noncoding expansion in EIF4A3 causes Richieri-Costa-Pereira syndrome, a craniofacial disorder associated with limb defects. American journal of human genetics *94*, 120-128.
Fernando, R.N., Eleuteri, B., Abdelhady, S., Nussenzweig, A., Andang, M., and Ernfors, P. (2011). Cell cycle restriction by histone H2AX limits proliferation of adult neural stem cells. Proceedings of the National Academy of Sciences of the United States of America *108*, 5837-5842.
Flynn, A., Shatsky, I.N., Proud, C.G., and Kaminski, A. (1994). The RNA-binding properties of protein synthesis initiation factor eIF-2. Biochimica et biophysica acta *1219*, 293-301.
Frank, S., Zhang, M., Scholer, H.R., and Greber, B. (2012). Small molecule-assisted, line-independent maintenance of human pluripotent stem cells in defined conditions. PloS one *7*, e41958.
Fu, X., Shah, A., and Baraban, J.M. (2016). Rapid reversal of translational silencing: Emerging role of microRNA degradation pathways in neuronal plasticity. Neurobiol Learn Mem.
Fuccillo, M., Joyner, A.L., and Fishell, G. (2006). Morphogen to mitogen: the multiple roles of hedgehog signalling in vertebrate neural development. Nature reviews Neuroscience *7*, 772-783.
Fuentealba, L.C., Obernier, K., and Alvarez-Buylla, A. (2012). Adult neural stem cells bridge their niche. Cell stem cell *10*, 698-708.
Galan, A., Diaz-Gimeno, P., Poo, M.E., Valbuena, D., Sanchez, E., Ruiz, V., Dopazo, J., Montaner, D., Conesa, A., and Simon, C. (2013). Defining the genomic signature of totipotency and pluripotency during early human development. PloS one *8*, e62135.
Gao, J., Katagiri, H., Ishigaki, Y., Yamada, T., Ogihara, T., Imai, J., Uno, K., Hasegawa, Y., Kanzaki, M., Yamamoto, T.T.*, et al.* (2007). Involvement of apolipoprotein E in excess fat accumulation and insulin resistance. Diabetes *56*, 24-33.
Garcia, M.A., Vazquez, J., Gimenez, C., Valdivieso, F., and Zafra, F. (1996). Transcription factor AP-2 regulates human apolipoprotein E gene expression in astrocytoma cells. The Journal of neuroscience : the official journal of the Society for Neuroscience *16*, 7550-7556.
Gaspar, N.J., Kinzy, T.G., Scherer, B.J., Humbelin, M., Hershey, J.W., and Merrick, W.C. (1994). Translation initiation factor eIF-2. Cloning and expression of the human cDNA encoding the gamma-subunit. The Journal of biological chemistry *269*, 3415-3422.
Gaur, S., Mandelbaum, M., Herold, M., Majumdar, H.D., Neilson, K.M., Maynard, T.M., Mood, K., Daar, I.O., and Moody, S.A. (2016). Neural transcription factors bias cleavage stage blastomeres to give rise to neural ectoderm. Genesis.
Gonsky, R., Itamar, D., Harary, R., and Kaempfer, R. (1992). Binding of ATP and messenger RNA by the beta-subunit of eukaryotic initiation factor 2. Biochimie *74*, 427-434.
Goodrum, J.F. (1991). Cholesterol from degenerating nerve myelin becomes associated with lipoproteins containing apolipoprotein E. Journal of neurochemistry *56*, 2082-2086.
Goritz, C., Mauch, D.H., Nagler, K., and Pfrieger, F.W. (2002). Role of glia-derived cholesterol in synaptogenesis: new revelations in the synapse-glia affair. Journal of physiology, Paris *96*, 257-263.
Gorry, P., Lufkin, T., Dierich, A., Rochette-Egly, C., Decimo, D., Dolle, P., Mark, M., Durand, B., and Chambon, P. (1994). The cellular retinoic acid binding protein I is dispensable. Proceedings of the National Academy of Sciences of the United States of America *91*, 9032-9036.
Greene, L.A., Lee, H.Y., and Angelastro, J.M. (2009). The transcription factor ATF5: role in neurodevelopment and neural tumors. Journal of neurochemistry *108*, 11-22.

Grehan, S., Allan, C., Tse, E., Walker, D., and Taylor, J.M. (2001). Expression of the apolipoprotein E gene in the skin is controlled by a unique downstream enhancer. J Invest Dermatol *116*, 77-84.
Guenther, M.G., Frampton, G.M., Soldner, F., Hockemeyer, D., Mitalipova, M., Jaenisch, R., and Young, R.A. (2010). Chromatin structure and gene expression programs of human embryonic and induced pluripotent stem cells. Cell stem cell *7*, 249-257.
Guo, H., Zhu, P., Yan, L., Li, R., Hu, B., Lian, Y., Yan, J., Ren, X., Lin, S., Li, J.*, et al.* (2014). The DNA methylation landscape of human early embryos. Nature *511*, 606-610.
Gupta, N.K., Woodley, C.L., Chen, Y.C., and Bose, K.K. (1973). Protein synthesis in rabbit reticulocytes. Assays, purification, and properties of different ribosomal factors and their roles in peptide chain initiation. The Journal of biological chemistry *248*, 4500-4511.
Han, J., Back, S.H., Hur, J., Lin, Y.H., Gildersleeve, R., Shan, J., Yuan, C.L., Krokowski, D., Wang, S., Hatzoglou, M.*, et al.* (2013). ER-stress-induced transcriptional regulation increases protein synthesis leading to cell death. Nat Cell Biol *15*, 481-490.
Hanahan, D. (1983). Studies on transformation of Escherichia coli with plasmids. J Mol Biol *166*, 557-580.
Hara, K., Yonezawa, K., Weng, Q.P., Kozlowski, M.T., Belham, C., and Avruch, J. (1998). Amino acid sufficiency and mTOR regulate p70 S6 kinase and eIF-4E BP1 through a common effector mechanism. The Journal of biological chemistry *273*, 14484-14494.
Harding, H.P., Zeng, H., Zhang, Y., Jungries, R., Chung, P., Plesken, H., Sabatini, D.D., and Ron, D. (2001). Diabetes mellitus and exocrine pancreatic dysfunction in perk-/- mice reveals a role for translational control in secretory cell survival. Mol Cell *7*, 1153-1163.
Harding, H.P., Zhang, Y., Scheuner, D., Chen, J.J., Kaufman, R.J., and Ron, D. (2009). Ppp1r15 gene knockout reveals an essential role for translation initiation factor 2 alpha (eIF2alpha) dephosphorylation in mammalian development. Proceedings of the National Academy of Sciences of the United States of America *106*, 1832-1837.
Hassel, J.C., Amann, P.M., Schadendorf, D., Eichmuller, S.B., Nagler, M., and Bazhin, A.V. (2013). Lecithin retinol acyltransferase as a potential prognostic marker for malignant melanoma. Exp Dermatol *22*, 757-759.
Havel, R.J. (1998). Receptor and non-receptor mediated uptake of chylomicron remnants by the liver. Atherosclerosis *141 Suppl 1*, S1-7.
Hay, N., and Sonenberg, N. (2004). Upstream and downstream of mTOR. Genes & development *18*, 1926-1945.
Heaney, J.D., Michelson, M.V., Youngren, K.K., Lam, M.Y., and Nadeau, J.H. (2009). Deletion of eIF2beta suppresses testicular cancer incidence and causes recessive lethality in agouti-yellow mice. Human molecular genetics *18*, 1395-1404.
Hernandez, R.E., Putzke, A.P., Myers, J.P., Margaretha, L., and Moens, C.B. (2007). Cyp26 enzymes generate the retinoic acid response pattern necessary for hindbrain development. Development *134*, 177-187.
Hinds, H.L., Ashley, C.T., Sutcliffe, J.S., Nelson, D.L., Warren, S.T., Housman, D.E., and Schalling, M. (1993). Tissue specific expression of FMR-1 provides evidence for a functional role in fragile X syndrome. Nature genetics *3*, 36-43.
Hofmann, S.M., Perez-Tilve, D., Greer, T.M., Coburn, B.A., Grant, E., Basford, J.E., Tschop, M.H., and Hui, D.Y. (2008). Defective lipid delivery modulates glucose tolerance and metabolic response to diet in apolipoprotein E-deficient mice. Diabetes *57*, 5-12.
Huang, F.J., Hsu, Y.C., Kang, H.Y., Chang, S.Y., Hsuuw, Y.D., and Huang, K.E. (2005). Effects of retinoic acid on the inner cell mass in mouse blastocysts. Fertility and sterility *83*, 238-242.
Huang, J.K., Jarjour, A.A., Nait Oumesmar, B., Kerninon, C., Williams, A., Krezel, W., Kagechika, H., Bauer, J., Zhao, C., Baron-Van Evercooren, A.*, et al.* (2011). Retinoid X receptor gamma signaling accelerates CNS remyelination. Nature neuroscience *14*, 45-53.
Huang, K., Zhang, X., Shi, J., Yao, M., Lin, J., Li, J., Liu, H., Li, H., Shi, G., Wang, Z.*, et al.* (2015). Dynamically reorganized chromatin is the key for the reprogramming of

somatic cells to pluripotent cells. Sci Rep *5*, 17691.
Huang, Y., Ji, Z.S., Brecht, W.J., Rall, S.C., Jr., Taylor, J.M., and Mahley, R.W. (1999). Overexpression of apolipoprotein E3 in transgenic rabbits causes combined hyperlipidemia by stimulating hepatic VLDL production and impairing VLDL lipolysis. Arterioscler Thromb Vasc Biol *19*, 2952-2959.
Huang, Y., Liu, X.Q., Rall, S.C., Jr., Taylor, J.M., von Eckardstein, A., Assmann, G., and Mahley, R.W. (1998). Overexpression and accumulation of apolipoprotein E as a cause of hypertriglyceridemia. The Journal of biological chemistry *273*, 26388-26393.
Huang, Z.H., Luque, R.M., Kineman, R.D., and Mazzone, T. (2007). Nutritional regulation of adipose tissue apolipoprotein E expression. Am J Physiol Endocrinol Metab *293*, E203-209.
Huang, Z.H., Reardon, C.A., and Mazzone, T. (2006). Endogenous ApoE expression modulates adipocyte triglyceride content and turnover. Diabetes *55*, 3394-3402.
Iborra, F.J., Jackson, D.A., and Cook, P.R. (2001). Coupled transcription and translation within nuclei of mammalian cells. Science *293*, 1139-1142.
Jackson, R.J., Hellen, C.U., and Pestova, T.V. (2010). The mechanism of eukaryotic translation initiation and principles of its regulation. Nat Rev Mol Cell Biol *11*, 113-127.
Jacobs, S., Lie, D.C., DeCicco, K.L., Shi, Y., DeLuca, L.M., Gage, F.H., and Evans, R.M. (2006). Retinoic acid is required early during adult neurogenesis in the dentate gyrus. Proceedings of the National Academy of Sciences of the United States of America *103*, 3902-3907.
Jain, S., Yoon, S.Y., Leung, L., Knoferle, J., and Huang, Y. (2013). Cellular source-specific effects of apolipoprotein (apo) E4 on dendrite arborization and dendritic spine development. PloS one *8*, e59478.
Janesick, A., Wu, S.C., and Blumberg, B. (2015). Retinoic acid signaling and neuronal differentiation. Cell Mol Life Sci *72*, 1559-1576.
Ji, Y., Gong, Y., Gan, W., Beach, T., Holtzman, D.M., and Wisniewski, T. (2003). Apolipoprotein E isoform-specific regulation of dendritic spine morphology in apolipoprotein E transgenic mice and Alzheimer's disease patients. Neuroscience *122*, 305-315.
Johannes, G., Carter, M.S., Eisen, M.B., Brown, P.O., and Sarnow, P. (1999). Identification of eukaryotic mRNAs that are translated at reduced cap binding complex eIF4F concentrations using a cDNA microarray. Proceedings of the National Academy of Sciences of the United States of America *96*, 13118-13123.
Julier, C., and Nicolino, M. (2010). Wolcott-Rallison syndrome. Orphanet J Rare Dis *5*, 29.
Jung, H., Gkogkas, C.G., Sonenberg, N., and Holt, C.E. (2014). Remote control of gene function by local translation. Cell *157*, 26-40.
Jung, H., Yoon, B.C., and Holt, C.E. (2012). Axonal mRNA localization and local protein synthesis in nervous system assembly, maintenance and repair. Nature reviews Neuroscience *13*, 308-324.
Kaczocha, M., Glaser, S.T., and Deutsch, D.G. (2009). Identification of intracellular carriers for the endocannabinoid anandamide. Proceedings of the National Academy of Sciences of the United States of America *106*, 6375-6380.
Kafer, G.R., Lehnert, S.A., Pantaleon, M., Kaye, P.L., and Moser, R.J. (2010). Expression of genes coding for histone variants and histone-associated proteins in pluripotent stem cells and mouse preimplantation embryos. Gene Expr Patterns *10*, 299-305.
Kainov, Y., Favorskaya, I., Delektorskaya, V., Chemeris, G., Komelkov, A., Zhuravskaya, A., Trukhanova, L., Zueva, E., Tavitian, B., Dyakova, N.*, et al.* (2014). CRABP1 provides high malignancy of transformed mesenchymal cells and contributes to the pathogenesis of mesenchymal and neuroendocrine tumors. Cell cycle *13*, 1530-1539.
Kantor, L., Harding, H.P., Ron, D., Schiffmann, R., Kaneski, C.R., Kimball, S.R., and Elroy-Stein, O. (2005). Heightened stress response in primary fibroblasts expressing mutant eIF2B genes from CACH/VWM leukodystrophy patients. Hum Genet *118*, 99-

106.
Kanungo, J. (2016). Retinoic acid Signaling in P19 Stem Cell Differentiation. Anticancer Agents Med Chem.
Kapp, L.D., and Lorsch, J.R. (2004). GTP-dependent recognition of the methionine moiety on initiator tRNA by translation factor eIF2. J Mol Biol *335*, 923-936.
Karagiannides, I., Abdou, R., Tzortzopoulou, A., Voshol, P.J., and Kypreos, K.E. (2008). Apolipoprotein E predisposes to obesity and related metabolic dysfunctions in mice. FEBS J *275*, 4796-4809.
Kernohan, K.D., Tetreault, M., Liwak-Muir, U., Geraghty, M.T., Qin, W., Venkateswaran, S., Davila, J., Care4Rare Canada, C., Holcik, M., Majewski, J.*, et al.* (2015). Homozygous mutation in the eukaryotic translation initiation factor 2alpha phosphatase gene, PPP1R15B, is associated with severe microcephaly, short stature and intellectual disability. Human molecular genetics *24*, 6293-6300.
Kim, J.E., O'Sullivan, M.L., Sanchez, C.A., Hwang, M., Israel, M.A., Brennand, K., Deerinck, T.J., Goldstein, L.S., Gage, F.H., Ellisman, M.H.*, et al.* (2011). Investigating synapse formation and function using human pluripotent stem cell-derived neurons. Proceedings of the National Academy of Sciences of the United States of America *108*, 3005-3010.
Kim, K., Doi, A., Wen, B., Ng, K., Zhao, R., Cahan, P., Kim, J., Aryee, M.J., Ji, H., Ehrlich, L.I.*, et al.* (2010). Epigenetic memory in induced pluripotent stem cells. Nature *467*, 285-290.
Kimball, S.R., Heinzinger, N.K., Horetsky, R.L., and Jefferson, L.S. (1998). Identification of interprotein interactions between the subunits of eukaryotic initiation factors eIF2 and eIF2B. The Journal of biological chemistry *273*, 3039-3044.
Klein, R.C., Mace, B.E., Moore, S.D., and Sullivan, P.M. (2010). Progressive loss of synaptic integrity in human apolipoprotein E4 targeted replacement mice and attenuation by apolipoprotein E2. Neuroscience *171*, 1265-1272.
Kleinjan, D.A., Dekker, S., Vaessen, M.J., and Grosveld, F. (1997). Regulation of the CRABP-I gene during mouse embryogenesis. Mech Dev *67*, 157-169.
Kluijtmans, L.A., Boers, G.H., Stevens, E.M., Renier, W.O., Kraus, J.P., Trijbels, F.J., van den Heuvel, L.P., and Blom, H.J. (1996). Defective cystathionine beta-synthase regulation by S-adenosylmethionine in a partially pyridoxine responsive homocystinuria patient. The Journal of clinical investigation *98*, 285-289.
Komada, M. (2012). Sonic hedgehog signaling coordinates the proliferation and differentiation of neural stem/progenitor cells by regulating cell cycle kinetics during development of the neocortex. Congenit Anom (Kyoto) *52*, 72-77.
Kozak, M. (1978). How do eucaryotic ribosomes select initiation regions in messenger RNA? Cell *15*, 1109-1123.
Kozak, M. (2002). Pushing the limits of the scanning mechanism for initiation of translation. Gene *299*, 1-34.
Krezel, W., Ghyselinck, N., Samad, T.A., Dupe, V., Kastner, P., Borrelli, E., and Chambon, P. (1998). Impaired locomotion and dopamine signaling in retinoid receptor mutant mice. Science *279*, 863-867.
Krishnamoorthy, T., Pavitt, G.D., Zhang, F., Dever, T.E., and Hinnebusch, A.G. (2001). Tight binding of the phosphorylated alpha subunit of initiation factor 2 (eIF2alpha) to the regulatory subunits of guanine nucleotide exchange factor eIF2B is required for inhibition of translation initiation. Molecular and cellular biology *21*, 5018-5030.
Kunda, P., Craig, G., Dominguez, V., and Baum, B. (2003). Abi, Sra1, and Kette control the stability and localization of SCAR/WAVE to regulate the formation of actin-based protrusions. Curr Biol *13*, 1867-1875.
Lampron, C., Rochette-Egly, C., Gorry, P., Dolle, P., Mark, M., Lufkin, T., LeMeur, M., and Chambon, P. (1995). Mice deficient in cellular retinoic acid binding protein II (CRABPII) or in both CRABPI and CRABPII are essentially normal. Development *121*, 539-548.
Lasfargues, C., Martineau, Y., Bousquet, C., and Pyronnet, S. (2012). Changes in

translational control after pro-apoptotic stress. Int J Mol Sci *14*, 177-190.
Lasrich, D., Bartelt, A., Grewal, T., and Heeren, J. (2015). Apolipoprotein E promotes lipid accumulation and differentiation in human adipocytes. Experimental cell research *337*, 94-102.
Latasa, M.J., and Cosgaya, J.M. (2011). Regulation of retinoid receptors by retinoic acid and axonal contact in Schwann cells. PloS one *6*, e17023.
Laurino, J.P., Thompson, G.M., Pacheco, E., and Castilho, B.A. (1999). The beta subunit of eukaryotic translation initiation factor 2 binds mRNA through the lysine repeats and a region comprising the C2-C2 motif. Molecular and cellular biology *19*, 173-181.
Laxman, S., Sutter, B.M., Wu, X., Kumar, S., Guo, X., Trudgian, D.C., Mirzaei, H., and Tu, B.P. (2013). Sulfur amino acids regulate translational capacity and metabolic homeostasis through modulation of tRNA thiolation. Cell *154*, 416-429.
Lee, Y.Y., Cevallos, R.C., and Jan, E. (2009). An upstream open reading frame regulates translation of GADD34 during cellular stresses that induce eIF2alpha phosphorylation. The Journal of biological chemistry *284*, 6661-6673.
Leegwater, P.A., Vermeulen, G., Konst, A.A., Naidu, S., Mulders, J., Visser, A., Kersbergen, P., Mobach, D., Fonds, D., van Berkel, C.G.*, et al.* (2001). Subunits of the translation initiation factor eIF2B are mutant in leukoencephalopathy with vanishing white matter. Nature genetics *29*, 383-388.
Leonard, L., Horton, C., Maden, M., and Pizzey, J.A. (1995). Anteriorization of CRABP-I expression by retinoic acid in the developing mouse central nervous system and its relationship to teratogenesis. Developmental biology *168*, 514-528.
Levin, D.H., Kyner, D., and Acs, G. (1973). Protein initiation in eukaryotes: formation and function of a ternary complex composed of a partially purified ribosomal factor, methionyl transfer RNA, and guanosine triphosphate. Proceedings of the National Academy of Sciences of the United States of America *70*, 41-45.
Li, F.Q., Fowler, K.A., Neil, J.E., Colton, C.A., and Vitek, M.P. (2010a). An apolipoprotein E-mimetic stimulates axonal regeneration and remyelination after peripheral nerve injury. J Pharmacol Exp Ther *334*, 106-115.
Li, Y., Yue, P., Deng, X., Ueda, T., Fukunaga, R., Khuri, F.R., and Sun, S.Y. (2010b). Protein phosphatase 2A negatively regulates eukaryotic initiation factor 4E phosphorylation and eIF4F assembly through direct dephosphorylation of Mnk and eIF4E. Neoplasia *12*, 848-855.
Liang, Y., Lin, S., Beyer, T.P., Zhang, Y., Wu, X., Bales, K.R., DeMattos, R.B., May, P.C., Li, S.D., Jiang, X.C.*, et al.* (2004). A liver X receptor and retinoid X receptor heterodimer mediates apolipoprotein E expression, secretion and cholesterol homeostasis in astrocytes. Journal of neurochemistry *88*, 623-634.
Lindqvist, L.M., Vikstrom, I., Chambers, J.M., McArthur, K., Ann Anderson, M., Henley, K.J., Happo, L., Cluse, L., Johnstone, R.W., Roberts, A.W.*, et al.* (2012). Translation inhibitors induce cell death by multiple mechanisms and Mcl-1 reduction is only a minor contributor. Cell Death Dis *3*, e409.
Liu, A., and Niswander, L.A. (2005). Bone morphogenetic protein signalling and vertebrate nervous system development. Nature reviews Neuroscience *6*, 945-954.
Liu, Y., Longo, L.D., and De Leon, M. (2000). In situ and immunocytochemical localization of E-FABP mRNA and protein during neuronal migration and differentiation in the rat brain. Brain research *852*, 16-27.
Livak, K.J., and Schmittgen, T.D. (2001). Analysis of relative gene expression data using real-time quantitative PCR and the 2(-Delta Delta C(T)) Method. Methods *25*, 402-408.
Lobo, M.V., Alonso, F.J., Rodriguez, S., Alcazar, A., Martin, E., Munoz, F., R, G.S., Salinas, M., and Fando, J.L. (1997). Localization of eukaryotic initiation factor 2 in neuron primary cultures and established cell lines. The Histochemical journal *29*, 453-468.
Lossner, C., Warnken, U., Pscherer, A., and Schnolzer, M. (2011). Preventing arginine-to-proline conversion in a cell-line-independent manner during cell cultivation under stable isotope labeling by amino acids in cell culture (SILAC) conditions. Analytical

biochemistry *412*, 123-125.
Louvi, A., and Artavanis-Tsakonas, S. (2006). Notch signalling in vertebrate neural development. Nature reviews Neuroscience *7*, 93-102.
Lowery, L.A., and Sive, H. (2009). Totally tubular: the mystery behind function and origin of the brain ventricular system. Bioessays *31*, 446-458.
Lu, C., Shi, Y., Wang, Z., Song, Z., Zhu, M., Cai, Q., and Chen, T. (2008). Serum starvation induces H2AX phosphorylation to regulate apoptosis via p38 MAPK pathway. FEBS letters *582*, 2703-2708.
Lun, M.P., Monuki, E.S., and Lehtinen, M.K. (2015). Development and functions of the choroid plexus-cerebrospinal fluid system. Nature reviews Neuroscience *16*, 445-457.
Luo, J., Song, J., Feng, P., Wang, Y., Long, W., Liu, M., and Li, L. (2016). Elevated serum apolipoprotein E is associated with metastasis and poor prognosis of non-small cell lung cancer. Tumour Biol.
Lyoo, I.K., Noam, G.G., Lee, C.K., Lee, H.K., Kennedy, B.P., and Renshaw, P.F. (1996). The corpus callosum and lateral ventricles in children with attention-deficit hyperactivity disorder: a brain magnetic resonance imaging study. Biol Psychiatry *40*, 1060-1063.
Ma, X.M., and Blenis, J. (2009). Molecular mechanisms of mTOR-mediated translational control. Nat Rev Mol Cell Biol *10*, 307-318.
Maag, D., Algire, M.A., and Lorsch, J.R. (2006). Communication between eukaryotic translation initiation factors 5 and 1A within the ribosomal pre-initiation complex plays a role in start site selection. J Mol Biol *356*, 724-737.
Maclean, K.N., Janosik, M., Kraus, E., Kozich, V., Allen, R.H., Raab, B.K., and Kraus, J.P. (2002). Cystathionine beta-synthase is coordinately regulated with proliferation through a redox-sensitive mechanism in cultured human cells and Saccharomyces cerevisiae. Journal of cellular physiology *192*, 81-92.
Mahley, R.W. (2016). Apolipoprotein E: from cardiovascular disease to neurodegenerative disorders. J Mol Med (Berl) *94*, 739-746.
Mak, A.C., Pullinger, C.R., Tang, L.F., Wong, J.S., Deo, R.C., Schwarz, J.M., Gugliucci, A., Movsesyan, I., Ishida, B.Y., Chu, C.*, et al.* (2014). Effects of the absence of apolipoprotein e on lipoproteins, neurocognitive function, and retinal function. JAMA neurology *71*, 1228-1236.
Mallon, B.S., Hamilton, R.S., Kozhich, O.A., Johnson, K.R., Fann, Y.C., Rao, M.S., and Robey, P.G. (2014). Comparison of the molecular profiles of human embryonic and induced pluripotent stem cells of isogenic origin. Stem Cell Res *12*, 376-386.
Martin, F., Barends, S., Jaeger, S., Schaeffer, L., Prongidi-Fix, L., and Eriani, G. (2011). Cap-assisted internal initiation of translation of histone H4. Mol Cell *41*, 197-209.
Marzluff, W.F. (2005). Metazoan replication-dependent histone mRNAs: a distinct set of RNA polymerase II transcripts. Curr Opin Cell Biol *17*, 274-280.
Matsubara, Y., Kato, T., Kashimada, K., Tanaka, H., Zhi, Z., Ichinose, S., Mizutani, S., Morio, T., Chiba, T., Ito, Y.*, et al.* (2015). TALEN-Mediated Gene Disruption on Y Chromosome Reveals Critical Role of EIF2S3Y in Mouse Spermatogenesis. Stem cells and development *24*, 1164-1170.
Mauch, D.H., Nagler, K., Schumacher, S., Goritz, C., Muller, E.C., Otto, A., and Pfrieger, F.W. (2001). CNS synaptogenesis promoted by glia-derived cholesterol. Science *294*, 1354-1357.
Means, A.L., Thompson, J.R., and Gudas, L.J. (2000). Transcriptional regulation of the cellular retinoic acid binding protein I gene in F9 teratocarcinoma cells. Cell growth & differentiation : the molecular biology journal of the American Association for Cancer Research *11*, 71-82.
Merrick, W.C. (2004). Cap-dependent and cap-independent translation in eukaryotic systems. Gene *332*, 1-11.
Mitchell, S.J., McHale, D.P., Campbell, D.A., Lench, N.J., Mueller, R.F., Bundey, S.E., and Markham, A.F. (1998). A syndrome of severe mental retardation, spasticity, and tapetoretinal degeneration linked to chromosome 15q24. American journal of human

genetics *62*, 1070-1076.
Mohammad-Qureshi, S.S., Haddad, R., Hemingway, E.J., Richardson, J.P., and Pavitt, G.D. (2007). Critical contacts between the eukaryotic initiation factor 2B (eIF2B) catalytic domain and both eIF2beta and -2gamma mediate guanine nucleotide exchange. Molecular and cellular biology *27*, 5225-5234.
Mouilleron, H., Delcourt, V., and Roucou, X. (2016). Death of a dogma: eukaryotic mRNAs can code for more than one protein. Nucleic Acids Res *44*, 14-23.
Nanda, J.S., Saini, A.K., Munoz, A.M., Hinnebusch, A.G., and Lorsch, J.R. (2013). Coordinated movements of eukaryotic translation initiation factors eIF1, eIF1A, and eIF5 trigger phosphate release from eIF2 in response to start codon recognition by the ribosomal preinitiation complex. The Journal of biological chemistry *288*, 5316-5329.
Napoli, I., Mercaldo, V., Boyl, P.P., Eleuteri, B., Zalfa, F., De Rubeis, S., Di Marino, D., Mohr, E., Massimi, M., Falconi, M*., et al.* (2008). The fragile X syndrome protein represses activity-dependent translation through CYFIP1, a new 4E-BP. Cell *134*, 1042-1054.
Napoli, J.L. (1993). Biosynthesis and metabolism of retinoic acid: roles of CRBP and CRABP in retinoic acid: roles of CRBP and CRABP in retinoic acid homeostasis. The Journal of nutrition *123*, 362-366.
Napoli, J.L. (2012). Physiological insights into all-trans-retinoic acid biosynthesis. Biochimica et biophysica acta *1821*, 152-167.
Narayanan, S., Surendranath, K., Bora, N., Surolia, A., and Karande, A.A. (2005). Ribosome inactivating proteins and apoptosis. FEBS letters *579*, 1324-1331.
Naveau, M., Lazennec-Schurdevin, C., Panvert, M., Dubiez, E., Mechulam, Y., and Schmitt, E. (2013). Roles of yeast eIF2alpha and eIF2beta subunits in the binding of the initiator methionyl-tRNA. Nucleic Acids Res *41*, 1047-1057.
Niederreither, K., Subbarayan, V., Dolle, P., and Chambon, P. (1999). Embryonic retinoic acid synthesis is essential for early mouse post-implantation development. Nature genetics *21*, 444-448.
Nika, J., Rippel, S., and Hannig, E.M. (2001). Biochemical analysis of the eIF2beta gamma complex reveals a structural function for eIF2alpha in catalyzed nucleotide exchange. The Journal of biological chemistry *276*, 1051-1056.
Novoa, I., Zeng, H., Harding, H.P., and Ron, D. (2001). Feedback inhibition of the unfolded protein response by GADD34-mediated dephosphorylation of eIF2alpha. The Journal of cell biology *153*, 1011-1022.
Nwabuisi-Heath, E., Rebeck, G.W., Ladu, M.J., and Yu, C. (2014). ApoE4 delays dendritic spine formation during neuron development and accelerates loss of mature spines in vitro. ASN neuro *6*, e00134.
Oh, J.Y., Nam, Y.J., Jo, A., Cheon, H.S., Rhee, S.M., Park, J.K., Lee, J.A., and Kim, H.K. (2010). Apolipoprotein E mRNA is transported to dendrites and may have a role in synaptic structural plasticity. Journal of neurochemistry *114*, 685-696.
Okada, Y., Shimazaki, T., Sobue, G., and Okano, H. (2004). Retinoic-acid-concentration-dependent acquisition of neural cell identity during in vitro differentiation of mouse embryonic stem cells. Developmental biology *275*, 124-142.
Olson, C.R., and Mello, C.V. (2010). Significance of vitamin A to brain function, behavior and learning. Mol Nutr Food Res *54*, 489-495.
Paik, Y.K., Chang, D.J., Reardon, C.A., Walker, M.D., Taxman, E., and Taylor, J.M. (1988). Identification and characterization of transcriptional regulatory regions associated with expression of the human apolipoprotein E gene. The Journal of biological chemistry *263*, 13340-13349.
Papi, A., Guarnieri, T., Storci, G., Santini, D., Ceccarelli, C., Taffurelli, M., De Carolis, S., Avenia, N., Sanguinetti, A., Sidoni, A*., et al.* (2012). Nuclear receptors agonists exert opposing effects on the inflammation dependent survival of breast cancer stem cells. Cell Death Differ *19*, 1208-1219.
Pathania, M., Davenport, E.C., Muir, J., Sheehan, D.F., Lopez-Domenech, G., and Kittler,

J.T. (2014). The autism and schizophrenia associated gene CYFIP1 is critical for the maintenance of dendritic complexity and the stabilization of mature spines. Transl Psychiatry *4*, e374.
Paull, T.T., Rogakou, E.P., Yamazaki, V., Kirchgessner, C.U., Gellert, M., and Bonner, W.M. (2000). A critical role for histone H2AX in recruitment of repair factors to nuclear foci after DNA damage. Curr Biol *10*, 886-895.
Pavitt, G.D., and Proud, C.G. (2009). Protein synthesis and its control in neuronal cells with a focus on vanishing white matter disease. Biochem Soc Trans *37*, 1298-1310.
Pavone, M.E., Malpani, S.S., Dyson, M., Kim, J.J., and Bulun, S.E. (2016). Fenretinide: A Potential Treatment for Endometriosis. Reprod Sci.
Persaud, S.D., Park, S.W., Ishigami-Yuasa, M., Koyano-Nakagawa, N., Kagechika, H., and Wei, L.N. (2016). All trans-retinoic acid analogs promote cancer cell apoptosis through non-genomic Crabp1 mediating ERK1/2 phosphorylation. Sci Rep *6*, 22396.
Prelich, G. (2012). Gene overexpression: uses, mechanisms, and interpretation. Genetics *190*, 841-854.
Quere, I., Paul, V., Rouillac, C., Janbon, C., London, J., Demaille, J., Kamoun, P., Dufier, J.L., Abitbol, M., and Chasse, J.F. (1999). Spatial and temporal expression of the cystathionine beta-synthase gene during early human development. Biochemical and biophysical research communications *254*, 127-137.
Quinn, C.M., Kagedal, K., Terman, A., Stroikin, U., Brunk, U.T., Jessup, W., and Garner, B. (2004). Induction of fibroblast apolipoprotein E expression during apoptosis, starvation-induced growth arrest and mitosis. Biochem J *378*, 753-761.
Raab, S., Klingenstein, M., Liebau, S., and Linta, L. (2014). A Comparative View on Human Somatic Cell Sources for iPSC Generation. Stem cells international *2014*, 768391.
Rais, B., Comin, B., Puigjaner, J., Brandes, J.L., Creppy, E., Saboureau, D., Ennamany, R., Lee, W.N., Boros, L.G., and Cascante, M. (1999). Oxythiamine and dehydroepiandrosterone induce a G1 phase cycle arrest in Ehrlich's tumor cells through inhibition of the pentose cycle. FEBS letters *456*, 113-118.
Rajesh, K., Iyer, A., Suragani, R.N., and Ramaiah, K.V. (2008). Intersubunit and interprotein interactions of alpha- and beta-subunits of human eIF2: Effect of phosphorylation. Biochemical and biophysical research communications *374*, 336-340.
Rhinn, M., and Dolle, P. (2012). Retinoic acid signalling during development. Development *139*, 843-858.
Ricciardelli, C., Lokman, N.A., Cheruvu, S., Tan, I.A., Ween, M.P., Pyragius, C.E., Ruszkiewicz, A., Hoffmann, P., and Oehler, M.K. (2015). Transketolase is upregulated in metastatic peritoneal implants and promotes ovarian cancer cell proliferation. Clin Exp Metastasis *32*, 441-455.
Richter, J.D., Bassell, G.J., and Klann, E. (2015). Dysregulation and restoration of translational homeostasis in fragile X syndrome. Nature reviews Neuroscience *16*, 595-605.
Rodriguez, G.A., Burns, M.P., Weeber, E.J., and Rebeck, G.W. (2013). Young APOE4 targeted replacement mice exhibit poor spatial learning and memory, with reduced dendritic spine density in the medial entorhinal cortex. Learn Mem *20*, 256-266.
Rogakou, E.P., Pilch, D.R., Orr, A.H., Ivanova, V.S., and Bonner, W.M. (1998). DNA double-stranded breaks induce histone H2AX phosphorylation on serine 139. The Journal of biological chemistry *273*, 5858-5868.
Roll-Mecak, A., Alone, P., Cao, C., Dever, T.E., and Burley, S.K. (2004). X-ray structure of translation initiation factor eIF2gamma: implications for tRNA and eIF2alpha binding. The Journal of biological chemistry *279*, 10634-10642.
Ross, A.C., and Zolfaghari, R. (2011). Cytochrome P450s in the regulation of cellular retinoic acid metabolism. Annu Rev Nutr *31*, 65-87.
Rossi, E., Picozzi, P., Bodega, B., Lavazza, C., Carlo-Stella, C., Marozzi, A., and Ginelli, E. (2007). Forced expression of RDH10 gene retards growth of HepG2 cells. Cancer Biol

Ther *6*, 238-244.
Ruberte, E., Dolle, P., Chambon, P., and Morriss-Kay, G. (1991). Retinoic acid receptors and cellular retinoid binding proteins. II. Their differential pattern of transcription during early morphogenesis in mouse embryos. Development *111*, 45-60.
Safer, B., Kemper, W., and Jagus, R. (1978). Identification of a 48 S preinitiation complex in reticulocyte lysate. The Journal of biological chemistry *253*, 3384-3386.
Saha, A., Connelly, S., Jiang, J., Zhuang, S., Amador, D.T., Phan, T., Pilz, R.B., and Boss, G.R. (2014). Akt phosphorylation and regulation of transketolase is a nodal point for amino acid control of purine synthesis. Mol Cell *55*, 264-276.
Saher, G., Brugger, B., Lappe-Siefke, C., Mobius, W., Tozawa, R., Wehr, M.C., Wieland, F., Ishibashi, S., and Nave, K.A. (2005). High cholesterol level is essential for myelin membrane growth. Nature neuroscience *8*, 468-475.
Saluja, I., Granneman, J.G., and Skoff, R.P. (2001). PPAR delta agonists stimulate oligodendrocyte differentiation in tissue culture. Glia *33*, 191-204.
Sandell, L.L., Sanderson, B.W., Moiseyev, G., Johnson, T., Mushegian, A., Young, K., Rey, J.P., Ma, J.X., Staehling-Hampton, K., and Trainor, P.A. (2007). RDH10 is essential for synthesis of embryonic retinoic acid and is required for limb, craniofacial, and organ development. Genes & development *21*, 1113-1124.
Sansom, S.N., Griffiths, D.S., Faedo, A., Kleinjan, D.J., Ruan, Y., Smith, J., van Heyningen, V., Rubenstein, J.L., and Livesey, F.J. (2009). The level of the transcription factor Pax6 is essential for controlling the balance between neural stem cell self-renewal and neurogenesis. PLoS Genet *5*, e1000511.
Sasai, H., Shimozawa, N., Asano, T., Kawamoto, N., Yamamoto, T., Kimura, T., Kawamoto, M., Matsui, E., and Fukao, T. (2015). Successive MRI Findings of Reversible Cerebral White Matter Lesions in a Patient with Cystathionine beta-Synthase Deficiency. Tohoku J Exp Med *237*, 323-327.
Sayers, C.M., Papandreou, I., Guttmann, D.M., Maas, N.L., Diehl, J.A., Witze, E.S., Koong, A.C., and Koumenis, C. (2013). Identification and characterization of a potent activator of p53-independent cellular senescence via a small-molecule screen for modifiers of the integrated stress response. Mol Pharmacol *83*, 594-604.
Schenck, A., Bardoni, B., Moro, A., Bagni, C., and Mandel, J.L. (2001). A highly conserved protein family interacting with the fragile X mental retardation protein (FMRP) and displaying selective interactions with FMRP-related proteins FXR1P and FXR2P. Proceedings of the National Academy of Sciences of the United States of America *98*, 8844-8849.
Scheuner, D., Song, B., McEwen, E., Liu, C., Laybutt, R., Gillespie, P., Saunders, T., Bonner-Weir, S., and Kaufman, R.J. (2001). Translational control is required for the unfolded protein response and in vivo glucose homeostasis. Mol Cell *7*, 1165-1176.
Scheuner, D., Vander Mierde, D., Song, B., Flamez, D., Creemers, J.W., Tsukamoto, K., Ribick, M., Schuit, F.C., and Kaufman, R.J. (2005). Control of mRNA translation preserves endoplasmic reticulum function in beta cells and maintains glucose homeostasis. Nature medicine *11*, 757-764.
Schmitt, E., Blanquet, S., and Mechulam, Y. (2002). The large subunit of initiation factor aIF2 is a close structural homologue of elongation factors. The EMBO journal *21*, 1821-1832.
Schmitt, E., Naveau, M., and Mechulam, Y. (2010). Eukaryotic and archaeal translation initiation factor 2: a heterotrimeric tRNA carrier. FEBS letters *584*, 405-412.
Schug, T.T., Berry, D.C., Shaw, N.S., Travis, S.N., and Noy, N. (2007). Opposing effects of retinoic acid on cell growth result from alternate activation of two different nuclear receptors. Cell *129*, 723-733.
Segev, Y., Barrera, I., Ounallah-Saad, H., Wibrand, K., Sporild, I., Livne, A., Rosenberg, T., David, O., Mints, M., Bramham, C.R*., et al.* (2015). PKR Inhibition Rescues Memory Deficit and ATF4 Overexpression in ApoE epsilon4 Human Replacement Mice. The Journal of neuroscience : the official journal of the Society for Neuroscience *35*, 12986-

12993.
Segev, Y., Michaelson, D.M., and Rosenblum, K. (2013). ApoE epsilon4 is associated with eIF2alpha phosphorylation and impaired learning in young mice. Neurobiol Aging *34*, 863-872.
Shenefelt, R.E. (1972). Morphogenesis of malformations in hamsters caused by retinoic acid: relation to dose and stage at treatment. Teratology *5*, 103-118.
Shih, S.J., Allan, C., Grehan, S., Tse, E., Moran, C., and Taylor, J.M. (2000). Duplicated downstream enhancers control expression of the human apolipoprotein E gene in macrophages and adipose tissue. The Journal of biological chemistry *275*, 31567-31572.
Shimano, H., Yamada, N., Katsuki, M., Shimada, M., Gotoda, T., Harada, K., Murase, T., Fukazawa, C., Takaku, F., and Yazaki, Y. (1992). Overexpression of apolipoprotein E in transgenic mice: marked reduction in plasma lipoproteins except high density lipoprotein and resistance against diet-induced hypercholesterolemia. Proceedings of the National Academy of Sciences of the United States of America *89*, 1750-1754.
Shin, B.S., Kim, J.R., Walker, S.E., Dong, J., Lorsch, J.R., and Dever, T.E. (2011). Initiation factor eIF2gamma promotes eIF2-GTP-Met-tRNAi(Met) ternary complex binding to the 40S ribosome. Nature structural & molecular biology *18*, 1227-1234.
Shirakami, Y., Gottesman, M.E., and Blaner, W.S. (2012). Diethylnitrosamine-induced hepatocarcinogenesis is suppressed in lecithin:retinol acyltransferase-deficient mice primarily through retinoid actions immediately after carcinogen administration. Carcinogenesis *33*, 268-274.
Shveygert, M., Kaiser, C., Bradrick, S.S., and Gromeier, M. (2010). Regulation of eukaryotic initiation factor 4E (eIF4E) phosphorylation by mitogen-activated protein kinase occurs through modulation of Mnk1-eIF4G interaction. Molecular and cellular biology *30*, 5160-5167.
Singh, C.R., Udagawa, T., Lee, B., Wassink, S., He, H., Yamamoto, Y., Anderson, J.T., Pavitt, G.D., and Asano, K. (2007). Change in nutritional status modulates the abundance of critical pre-initiation intermediate complexes during translation initiation in vivo. J Mol Biol *370*, 315-330.
Skazik, C., Amann, P.M., Heise, R., Marquardt, Y., Czaja, K., Kim, A., Ruhl, R., Kurschat, P., Merk, H.F., Bickers, D.R., *et al.* (2014). Downregulation of STRA6 expression in epidermal keratinocytes leads to hyperproliferation-associated differentiation in both in vitro and in vivo skin models. J Invest Dermatol *134*, 1579-1588.
Smith, J.D., Melian, A., Leff, T., and Breslow, J.L. (1988). Expression of the human apolipoprotein E gene is regulated by multiple positive and negative elements. The Journal of biological chemistry *263*, 8300-8308.
Smith, Z.D., Chan, M.M., Mikkelsen, T.S., Gu, H., Gnirke, A., Regev, A., and Meissner, A. (2012). A unique regulatory phase of DNA methylation in the early mammalian embryo. Nature *484*, 339-344.
Sokabe, M., and Fraser, C.S. (2014). Human eukaryotic initiation factor 2 (eIF2)-GTP-Met-tRNAi ternary complex and eIF3 stabilize the 43 S preinitiation complex. The Journal of biological chemistry *289*, 31827-31836.
Steinmuller, R., Steinberger, D., and Muller, U. (1998). MEHMO (mental retardation, epileptic seizures, hypogonadism and -genitalism, microcephaly, obesity), a novel syndrome: assignment of disease locus to xp21.1-p22.13. European journal of human genetics : EJHG *6*, 201-206.
Stolboushkina, E., Nikonov, S., Nikulin, A., Blasi, U., Manstein, D.J., Fedorov, R., Garber, M., and Nikonov, O. (2008). Crystal structure of the intact archaeal translation initiation factor 2 demonstrates very high conformational flexibility in the alpha- and beta-subunits. J Mol Biol *382*, 680-691.
Streit, A., Berliner, A.J., Papanayotou, C., Sirulnik, A., and Stern, C.D. (2000). Initiation of neural induction by FGF signalling before gastrulation. Nature *406*, 74-78.
Strickland, S., and Mahdavi, V. (1978). The induction of differentiation in teratocarcinoma stem cells by retinoic acid. Cell *15*, 393-403.

Sullivan, G.J., Bai, Y., Fletcher, J., and Wilmut, I. (2010). Induced pluripotent stem cells: epigenetic memories and practical implications. Molecular human reproduction *16*, 880-885.
Suragani, R.N., Kamindla, R., Ehtesham, N.Z., and Ramaiah, K.V. (2005). Interaction of recombinant human eIF2 subunits with eIF2B and eIF2alpha kinases. Biochemical and biophysical research communications *338*, 1766-1772.
Suraweera, A., Munch, C., Hanssum, A., and Bertolotti, A. (2012). Failure of amino acid homeostasis causes cell death following proteasome inhibition. Mol Cell *48*, 242-253.
Suri, F., Narooie-Nejad, M., Safari, I., Moazzeni, H., Rohani, M.R., Khajeh, A., Klotzle, B., Fan, J.B., and Elahi, E. (2014). Diagnosis of cystathionine beta-synthase deficiency by genetic analysis. J Neurol Sci *347*, 305-309.
Sutton, M.A., and Schuman, E.M. (2005). Local translational control in dendrites and its role in long-term synaptic plasticity. Journal of neurobiology *64*, 116-131.
Szabo, C., Coletta, C., Chao, C., Modis, K., Szczesny, B., Papapetropoulos, A., and Hellmich, M.R. (2013). Tumor-derived hydrogen sulfide, produced by cystathionine-beta-synthase, stimulates bioenergetics, cell proliferation, and angiogenesis in colon cancer. Proceedings of the National Academy of Sciences of the United States of America *110*, 12474-12479.
Takahashi, K., and Yamanaka, S. (2006). Induction of pluripotent stem cells from mouse embryonic and adult fibroblast cultures by defined factors. Cell *126*, 663-676.
Tanaka, K., Imoto, I., Inoue, J., Kozaki, K., Tsuda, H., Shimada, Y., Aiko, S., Yoshizumi, Y., Iwai, T., Kawano, T*., et al.* (2007). Frequent methylation-associated silencing of a candidate tumor-suppressor, CRABP1, in esophageal squamous-cell carcinoma. Oncogene *26*, 6456-6468.
Tanenbaum, M.E., Stern-Ginossar, N., Weissman, J.S., and Vale, R.D. (2015). Regulation of mRNA translation during mitosis. Elife *4*.
Tang, H.L., Tang, H.M., Mak, K.H., Hu, S., Wang, S.S., Wong, K.M., Wong, C.S., Wu, H.Y., Law, H.T., Liu, K*., et al.* (2012). Cell survival, DNA damage, and oncogenic transformation after a transient and reversible apoptotic response. Mol Biol Cell *23*, 2240-2252.
Tarpey, P.S., Smith, R., Pleasance, E., Whibley, A., Edkins, S., Hardy, C., O'Meara, S., Latimer, C., Dicks, E., Menzies, A*., et al.* (2009). A systematic, large-scale resequencing screen of X-chromosome coding exons in mental retardation. Nature genetics *41*, 535-543.
Tejada, S., Lobo, M.V., Garcia-Villanueva, M., Sacristan, S., Perez-Morgado, M.I., Salinas, M., and Martin, M.E. (2009). Eukaryotic initiation factors (eIF) 2alpha and 4E expression, localization, and phosphorylation in brain tumors. The journal of histochemistry and cytochemistry : official journal of the Histochemistry Society *57*, 503-512.
Todd, M.A., Huh, M.S., and Picketts, D.J. (2016). The sub-nucleolar localization of PHF6 defines its role in rDNA transcription and early processing events. European journal of human genetics : EJHG.
Tu, L., Liu, Z., He, X., He, Y., Yang, H., Jiang, Q., Xie, S., Xiao, G., Li, X., Yao, K*., et al.* (2010). Over-expression of eukaryotic translation initiation factor 4 gamma 1 correlates with tumor progression and poor prognosis in nasopharyngeal carcinoma. Mol Cancer *9*, 78.
Turinetto, V., Orlando, L., Sanchez-Ripoll, Y., Kumpfmueller, B., Storm, M.P., Porcedda, P., Minieri, V., Saviozzi, S., Accomasso, L., Cibrario Rocchietti, E*., et al.* (2012). High basal gammaH2AX levels sustain self-renewal of mouse embryonic and induced pluripotent stem cells. Stem cells *30*, 1414-1423.
Vattem, K.M., and Wek, R.C. (2004). Reinitiation involving upstream ORFs regulates ATF4 mRNA translation in mammalian cells. Proceedings of the National Academy of Sciences of the United States of America *101*, 11269-11274.
Venanzoni, M.C., Giunta, S., Muraro, G.B., Storari, L., Crescini, C., Mazzucchelli, R.,

Montironi, R., and Seth, A. (2003). Apolipoprotein E expression in localized prostate cancers. Int J Oncol *22*, 779-786.
Venepally, P., Reddy, L.G., and Sani, B.P. (1996). Analysis of the effects of CRABP I expression on the RA-induced transcription mediated by retinoid receptors. Biochemistry *35*, 9974-9982.
Vogel, C., and Marcotte, E.M. (2012). Insights into the regulation of protein abundance from proteomic and transcriptomic analyses. Nature reviews Genetics *13*, 227-232.
Wagner, T., Bartelt, A., Schlein, C., and Heeren, J. (2015). Genetic Dissection of Tissue-Specific Apolipoprotein E Function for Hypercholesterolemia and Diet-Induced Obesity. PloS one *10*, e0145102.
Wang, J., Leung, J.W., Gong, Z., Feng, L., Shi, X., and Chen, J. (2013a). PHF6 regulates cell cycle progression by suppressing ribosomal RNA synthesis. The Journal of biological chemistry *288*, 3174-3183.
Wang, J., Zhang, X., Ma, D., Lee, W.N., Xiao, J., Zhao, Y., Go, V.L., Wang, Q., Yen, Y., Recker, R.*, et al.* (2013b). Inhibition of transketolase by oxythiamine altered dynamics of protein signals in pancreatic cancer cells. Exp Hematol Oncol *2*, 18.
Wang, X., Campbell, L.E., Miller, C.M., and Proud, C.G. (1998). Amino acid availability regulates p70 S6 kinase and multiple translation factors. Biochem J *334 (Pt 1)*, 261-267.
Wang, Z., Liu, D.X., Wang, F.W., Zhang, Q., Du, Z.X., Zhan, J.M., Yuan, Q.H., Ling, E.A., and Hao, A.J. (2013c). L-Cysteine promotes the proliferation and differentiation of neural stem cells via the CBS/H(2)S pathway. Neuroscience *237*, 106-117.
Warlich, E., Kuehle, J., Cantz, T., Brugman, M.H., Maetzig, T., Galla, M., Filipczyk, A.A., Halle, S., Klump, H., Scholer, H.R.*, et al.* (2011). Lentiviral vector design and imaging approaches to visualize the early stages of cellular reprogramming. Mol Ther *19*, 782-789.
Wei, L.-N., Lee, C.-H., Chang, S.-L., and Chu, Y.-S. (1992). Pathogenesis in Transgenic Mice Expressing Bovine Cellular Retinoic Acid-Binding Protein. Development, growth & differentiation *34*, 479-488.
Wei, L.N., Chang, L., and Hu, X. (1999). Studies of the type I cellular retinoic acid-binding protein mutants and their biological activities. Molecular and cellular biochemistry *200*, 69-76.
Wethmar, K. (2014). The regulatory potential of upstream open reading frames in eukaryotic gene expression. Wiley Interdiscip Rev RNA *5*, 765-778.
White, R.J., Nie, Q., Lander, A.D., and Schilling, T.F. (2007). Complex regulation of cyp26a1 creates a robust retinoic acid gradient in the zebrafish embryo. PLoS biology *5*, e304.
Won, J.Y., Nam, E.C., Yoo, S.J., Kwon, H.J., Um, S.J., Han, H.S., Kim, S.H., Byun, Y., and Kim, S.Y. (2004). The effect of cellular retinoic acid binding protein-I expression on the CYP26-mediated catabolism of all-trans retinoic acid and cell proliferation in head and neck squamous cell carcinoma. Metabolism: clinical and experimental *53*, 1007-1012.
Wortzel, I., and Seger, R. (2011). The ERK Cascade: Distinct Functions within Various Subcellular Organelles. Genes Cancer *2*, 195-209.
Wu, D., Yang, H., Zhao, Y., Sharan, C., Goodwin, J.S., Zhou, L., Guo, Y., and Guo, Z. (2008). 2-Aminopurine inhibits lipid accumulation induced by apolipoprotein E-deficient lipoprotein in macrophages: potential role of eukaryotic initiation factor-2alpha phosphorylation in foam cell formation. J Pharmacol Exp Ther *326*, 395-405.
Wu, T., Liu, Y., Wen, D., Tseng, Z., Tahmasian, M., Zhong, M., Rafii, S., Stadtfeld, M., Hochedlinger, K., and Xiao, A. (2014). Histone variant H2A.X deposition pattern serves as a functional epigenetic mark for distinguishing the developmental potentials of iPSCs. Cell stem cell *15*, 281-294.
Xu, Q., Bernardo, A., Walker, D., Kanegawa, T., Mahley, R.W., and Huang, Y. (2006). Profile and regulation of apolipoprotein E (ApoE) expression in the CNS in mice with targeting of green fluorescent protein gene to the ApoE locus. The Journal of

neuroscience : the official journal of the Society for Neuroscience *26*, 4985-4994.
Yamamoto, K., Shimano, H., Shimada, M., Kawamura, M., Gotoda, T., Harada, K., Ohsuga, J., Yazaki, Y., and Yamada, N. (1995). Overexpression of apolipoprotein E prevents development of diabetic hyperlipidemia in transgenic mice. Diabetes *44*, 580-585.
Yamauchi, Y., Riel, J.M., Ruthig, V.A., Ortega, E.A., Mitchell, M.J., and Ward, M.A. (2016). Two genes substitute for the mouse Y chromosome for spermatogenesis and reproduction. Science *351*, 514-516.
Yan, L., Yang, M., Guo, H., Yang, L., Wu, J., Li, R., Liu, P., Lian, Y., Zheng, X., Yan, J.*, et al.* (2013). Single-cell RNA-Seq profiling of human preimplantation embryos and embryonic stem cells. Nature structural & molecular biology *20*, 1131-1139.
Yap, S., Rushe, H., Howard, P.M., and Naughten, E.R. (2001). The intellectual abilities of early-treated individuals with pyridoxine-nonresponsive homocystinuria due to cystathionine beta-synthase deficiency. J Inherit Metab Dis *24*, 437-447.
Yatime, L., Mechulam, Y., Blanquet, S., and Schmitt, E. (2006). Structural switch of the gamma subunit in an archaeal aIF2 alpha gamma heterodimer. Structure *14*, 119-128.
Yatime, L., Mechulam, Y., Blanquet, S., and Schmitt, E. (2007). Structure of an archaeal heterotrimeric initiation factor 2 reveals a nucleotide state between the GTP and the GDP states. Proceedings of the National Academy of Sciences of the United States of America *104*, 18445-18450.
Yin, B., Savic, V., Juntilla, M.M., Bredemeyer, A.L., Yang-Iott, K.S., Helmink, B.A., Koretzky, G.A., Sleckman, B.P., and Bassing, C.H. (2009). Histone H2AX stabilizes broken DNA strands to suppress chromosome breaks and translocations during V(D)J recombination. J Exp Med *206*, 2625-2639.
Yu, S., Levi, L., Casadesus, G., Kunos, G., and Noy, N. (2014). Fatty acid-binding protein 5 (FABP5) regulates cognitive function both by decreasing anandamide levels and by activating the nuclear receptor peroxisome proliferator-activated receptor beta/delta (PPARbeta/delta) in the brain. The Journal of biological chemistry *289*, 12748-12758.
Yu, S., Levi, L., Siegel, R., and Noy, N. (2012). Retinoic acid induces neurogenesis by activating both retinoic acid receptors (RARs) and peroxisome proliferator-activated receptor beta/delta (PPARbeta/delta). The Journal of biological chemistry *287*, 42195-42205.
Yu, X., and Long, Y.C. (2016). Crosstalk between cystine and glutathione is critical for the regulation of amino acid signaling pathways and ferroptosis. Sci Rep *6*, 30033.
Yue, L., and Mazzone, T. (2009). Peroxisome proliferator-activated receptor {gamma} stimulation of adipocyte ApoE gene transcription mediated by the liver receptor X pathway. The Journal of biological chemistry *284*, 10453-10461.
Yue, L., Rasouli, N., Ranganathan, G., Kern, P.A., and Mazzone, T. (2004). Divergent effects of peroxisome proliferator-activated receptor gamma agonists and tumor necrosis factor alpha on adipocyte ApoE expression. The Journal of biological chemistry *279*, 47626-47632.
Zhao, J., Fu, Y., Liu, C.C., Shinohara, M., Nielsen, H.M., Dong, Q., Kanekiyo, T., and Bu, G. (2014a). Retinoic acid isomers facilitate apolipoprotein E production and lipidation in astrocytes through the retinoid X receptor/retinoic acid receptor pathway. The Journal of biological chemistry *289*, 11282-11292.
Zhao, X.Y., Li, W., Lv, Z., Liu, L., Tong, M., Hai, T., Hao, J., Guo, C.L., Ma, Q.W., Wang, L.*, et al.* (2009). iPS cells produce viable mice through tetraploid complementation. Nature *461*, 86-90.
Zhao, Y., Wu, Y., Hu, H., Cai, J., Ning, M., Ni, X., and Zhong, C. (2014b). Downregulation of transketolase activity is related to inhibition of hippocampal progenitor cell proliferation induced by thiamine deficiency. Biomed Res Int *2014*, 572915.
Zheng, P., Pennacchio, L.A., Le Goff, W., Rubin, E.M., and Smith, J.D. (2004). Identification of a novel enhancer of brain expression near the apoE gene cluster by comparative genomics. Biochimica et biophysica acta *1676*, 41-50.

Zhu, P.J., Huang, W., Kalikulov, D., Yoo, J.W., Placzek, A.N., Stoica, L., Zhou, H., Bell, J.C., Friedlander, M.J., Krnjevic, K.*, et al.* (2011). Suppression of PKR promotes network excitability and enhanced cognition by interferon-gamma-mediated disinhibition. Cell *147*, 1384-1396.
Ziegler-Birling, C., Helmrich, A., Tora, L., and Torres-Padilla, M.E. (2009). Distribution of p53 binding protein 1 (53BP1) and phosphorylated H2A.X during mouse preimplantation development in the absence of DNA damage. The International journal of developmental biology *53*, 1003-1011.
Zukin, R.S., Richter, J.D., and Bagni, C. (2009). Signals, synapses, and synthesis: how new proteins control plasticity. Front Neural Circuits *3*, 14.

Prerequisites for carrying out the project

Control and patient plucked hair samples are/were requisite for the generation of iPS cell lines, and their use had to be approved by the institutional ethics committee (Eberhard Karls Universität Tübingen). All participants or their legally authorized representatives provided us with written informed consent for use of collected biological material. Since somatic cells reprogramming make use of mouse and rat embryonic fibroblasts, approval of the ethics committee was also needed for work with animals cells.

Appendix A

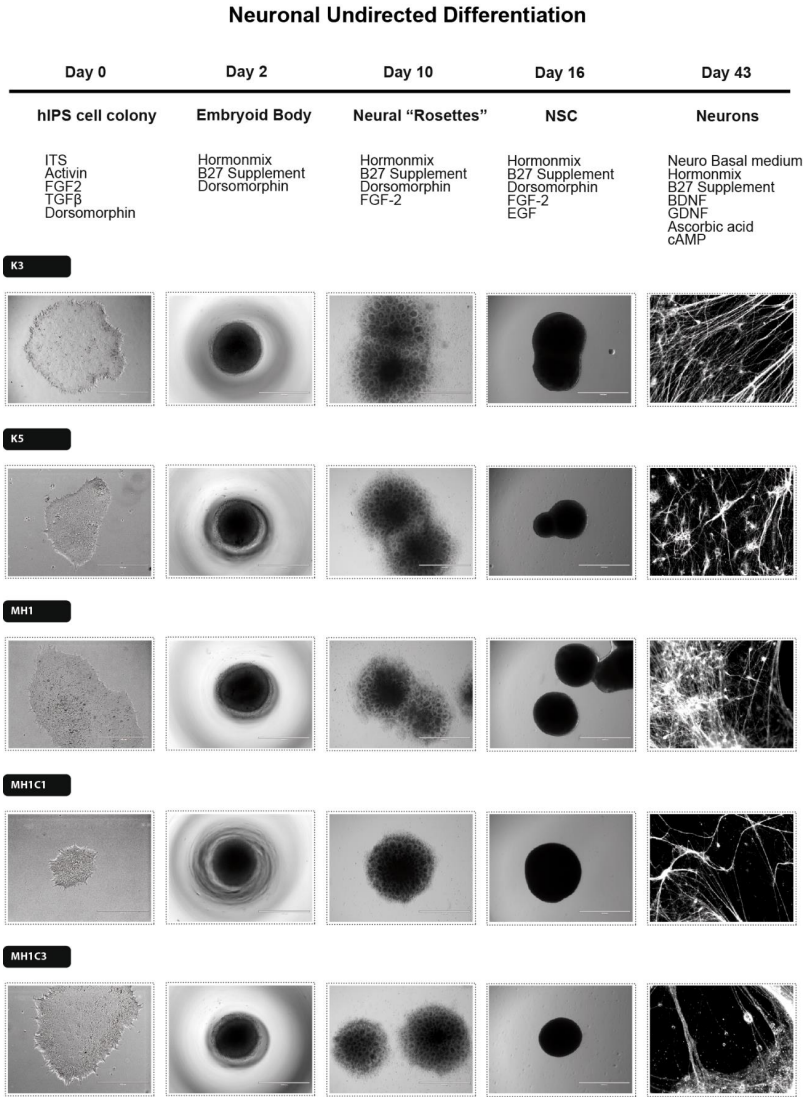

Figure A) Neuronal undirected differentiation. Representative light microscopy images of stages from Days 0, 2, 10 and 16. Immunostaining for TUBB3 are seen for neurons from Day43 of differentiation.

Appendix B

Table B) Experimental design of SILAC proteome analysis.

First experiment samples		Medium labelled			Time of incubation
		Light	Medium	Heavy	
a	K5	✓			6h
b	MH1C3	✓			6h
c	K5		✓		6h
	MH1C3			✓	
d	K5		✓		16h
	MH1C3			✓	
e	K5		✓		24h
	MH1C3			✓	
f	K5			✓	6h
	MH1C3		✓		
g	K5			✓	16h
	MH1C3		✓		
h	K5			✓	24h
	MH1C3		✓		

Second experiment samples		Medium labelled			Time of incubation
		Light	Medium	Heavy	
a	K5	✓			6h
b	MH1C1	✓			6h
c	K5		✓		6h
	MH1C1			✓	
d	K5		✓		16h
	MH1C1			✓	
e	K5		✓		24h
	MH1C1			✓	
f	K5			✓	6h
	MH1C1		✓		
g	K5			✓	16h
	MH1C1		✓		
h	K5			✓	24h
	MH1C1		✓		